



---

# **Response to Requests for Additional Information for the Review of the ARCADIA<sup>®</sup> Reactor Analysis System for PWRs Methodology Description and Benchmarking Results Topical Report**

ANP-10297Q1NP  
Revision 1

## **Topical Report**

May 2011

AREVA NP Inc.

---

(c) 2011 AREVA NP Inc.

**Copyright © 2011**

**AREVA NP Inc.  
All Rights Reserved**

### **Nature of Changes**

<b>Item</b>	<b>Section(s) or Page(s)</b>	<b>Description and Justification</b>
1	1-1, 2-2	Updated applicability of document to address the responses to all of the draft RAIs.
2	Section 2.0	Inserted responses for RAIs 2, 6, 7, 8, 9, 12, 13, 14, 15, 16, 17, 18, 19, 20, 30, 36, 38, 47, 53, 56, 57, 58, 59, 60

## Contents

	<u>Page</u>
1.0 INTRODUCTION .....	1-1
2.0 AREVA NP RESPONSES TO RAIS .....	2-2

## **1.0 INTRODUCTION**

The ARCADIA® Topical Report [1-1] was submitted to the US Nuclear Regulatory Commission for review in March 2010. A draft set of Requests for Additional Information (RAI) was released by the NRC in December 2010. This document addresses the AREVA NP Inc. responses to these RAIs.

### Reference

- 1-1 ANP-10297P, Revision 0, ARCADIA®: Reactor Analysis System for PWRs Methodology Description and Benchmarking

## **2.0 AREVA NP RESPONSES TO RAIs**

This section contains the AREVA NP Inc. Responses to the NRC RAIs. These responses address all of the RAIs.

**RAI 1** ARTEMIS uses a single cross section library to span the entire range of application temperatures (hot to cold). Please address the following points on page 1-2:

- The report does not directly address qualification at cold conditions, though most of the critical experiments are at cold conditions.
- No information is provided on how ARCADIA addresses the typical differences between hot and cold cross section libraries.
- Important differences can be the xenon treatment (cold lattice cases are usually run without xenon, while hot cases typically include equilibrium xenon), and the Doppler treatment (cold cases are typically run isothermal, while hot cases typically have independent fuel temperature branches).
- There is also no documented validation of the cold cross section library model to reinforce its applicability during cold transients.

### AREVA Response

*This response for bullet four pertains to cold temperatures not cold transients.*

The cross section libraries are functionalized continuously from hot conditions to cold conditions to handle both temperature changes and the corresponding density changes. The functional dependence of the library against all independent variables (such as xenon and fuel temperature) is available at all temperature conditions. Branch cases are used at a large variety of conditions (including cold states) to determine the functional dependence of the cross sections. The methodology of the cross section tables is described in Section 3.5. ARCADIA utilizes a cross section library structure similar to that employed by CASMO/NEMO [1] and SCIENCE [2] (both previously approved by USNRC).

The underlying cross sections calculated by APOLLO2-A are qualified at cold conditions based on the agreement of APOLLO2-A to measured criticality conditions for critical experiments at cold temperatures. Section 6.2 contains many APOLLO2-A calculations at cold conditions and shows the accuracy of the APOLLO2-A at these temperatures.

### References

1. BAW-10180-A, "NEMO – Nodal Expansion Method Optimized," Revision 1, March,, 1993
2. BAW-10228P-A, "SCIENCE", December, 2000.

**RAI 2** [Page 2-37] What is the purpose of including an equilibrium xenon model at zero exposure in APOLLO2-A?

**AREVA Response**

The equilibrium xenon model is used at zero exposure in order to reduce the effect of significant changes in xenon concentration at the beginning of the base depletion. However, to build cross-section libraries for downstream calculations, the xenon concentration is used as a physical parameter and is fixed (including a zero-concentration point) in APOLLO2-A branch calculations.



**RAI 3** [Page 3-13] The homogenized cross section case matrix used by ARTEMIS appears to be functionalized by only instantaneous perturbations. Spectral (energy) or geometric (shape) corrections induced by depletion at off-nominal conditions have been excluded from the discussion (such as moderator temperature history, fuel temperature history, boron history, and/or control rod history). Is ARCADIA using a pseudo-microscopic model? If so, justification for equation 3-38 should be provided to address omission of multi-dimensional combinatorial effects (i.e. the total homogenized worth in course-group  $g$  is not equivalent to the sum of the worths of the individual isotopes due to the combined effects on the flux spectrum (neutron competition)).

### AREVA Response

The ARTEMIS calculation uses a detailed microscopic cross section model with [ ] explicitly treated isotopes. The microscopic cross sections are functionalized by instantaneous perturbations. From experience with previous code systems, the reactivity effect of depletion at off-nominal conditions is known to be dominated by changes in the nuclide densities. The effect of the change in the microscopic cross sections is generally a secondary minor effect. This was confirmed by running the following calculations.

- A “base” depletion using the APOLLO2-A code. This depletion was performed at typical core average conditions for a reactor at hot full power.
- A “perturbed” depletion using the APOLLO2-A code. The perturbation was induced by an increase in the moderator temperature of 20 K and a corresponding change in the moderator density.
- Branch cases from the “perturbed” depletion in which the moderator temperature was decreased by 20 K along with the corresponding moderator density change. These branch cases are thus run at the instantaneous condition of the “base” depletion.

The differences in reactivity of these cases compared to those of the base depletion are due to the spectral effects of depletion at off-nominal conditions. These cases include changes in the nuclide densities due to the depletion at off-nominal conditions. They also include the effect of the modified nuclide vector on the corresponding microscopic cross sections.

For a typical fuel assembly with 40 GWD/MTU of burnup at the perturbed state, the above calculation yielded a reactivity effect of [ ] .

Then a cross section library was generated for ARTEMIS using the standard methods for this process. The ARTEMIS code was then used to run the same calculations;

- A “base” depletion at nominal conditions.

- A “perturbed” depletion with an increased moderator temperature of 20 K and the corresponding change in the moderator density.
- Branch cases from the “perturbed” depletion in which the moderator temperature was decreased by 20 K along with the corresponding moderator density change. These branch cases are thus run at the instantaneous condition of the “base” depletion.

The differences in reactivity of these cases compared to those of the base depletion are due to the spectral effects of depletion at off-nominal conditions. These cases include changes in the nuclide densities due to the depletion at off-nominal conditions. There are no changes in the microscopic cross sections since the cross section library was used to evaluate these values. For the same fuel assembly used in the APOLLO2-A calculations, the reactivity change due to depletion at the off-nominal conditions was calculated to be [                      ]. Thus, [                      ] of the spectral effect was obtained by the change in the nuclide densities that is treated by the detailed microscopic cross section model used in ARTEMIS.

**RAI 4** On page 3-18, ARTEMIS calculates the fuel rod exposures by integration of fuel rod powers over the nodal depletion.

- Are the fuel rod exposures maintained in the assembly repository throughout the life of the fuel (i.e. is the fuel rod exposures shuffled?).
- Does this also mean that the fuel rod exposures calculated by APOLLO2-A are essentially ignored?

**AREVA Response**

The fuel rod exposures are maintained in the assembly repository throughout the life of the fuel. These values include each axial level used in the core model. The fuel rod information is updated to reflect any assembly rotation during the shuffling process. The fuel rod exposures calculated by APOLLO2-A are essentially ignored.

**RAI 5** On page 3-19, ARTEMIS uses the infinite lattice detector flux form factor to calculate the neutron detector reaction rate in the instrument tube. This assumes that the reconstructed flux is relatively equal to the infinite lattice flux, for the regions near the instrument tube. Is this assumption also valid for peripheral fuel assemblies?

### **AREVA Response**

The detector flux form factor provides the ratio of the heterogeneous detector flux to the homogeneous flux at the detector location. The assumption is that the reconstructed homogeneous flux is accurately determined at the detector location. The group-wise homogeneous flux at the detector location is determined using the two dimensional flux within each node as determined by the dehomogenization (reconstruction) process. The flux is integrated over the corresponding local region (cell) that contains the detector. This takes into account the flux gradients that occur in peripheral fuel assemblies. The flux is then multiplied by the detector flux form factor to provide the heterogeneous group-wise flux in the detector.

**RAI 6** On page 13-1, the intended application range for the PWR lattices is not clear in Section 13.1. Is the intention to license the ARCADIA code system for only the benchmarked lattice geometries or any PWR lattice geometry with 4 cell water holes or less? If an approval for general pin lattice geometry is requested, please provide justification for the generalized application range. Summary plots or tables for the benchmark results over different lattice geometries, average enrichments, and core sizes would be helpful to discern any trends or biases.

### AREVA Response

Approval for the ARCADIA® code system is requested for any square lattice PWR geometry with 4 cell water holes or smaller. The justification is based on the accuracy seen for the critical experiments for 14x14, 15x15, 16x16, and 17x17 lattices and the operating plant benchmarks for 14x14, 15x15, 17x17 and 18x18 lattices. The lattice configuration (e.g., 14X14, 15X15 etc.) is not the only parameter considered for the applicability of the codes in PWR applications. In addition, the applicability is based on many parameters that affect neutronics. ARCADIA® is validated for these parameters throughout the Topical Report.

This variability in parameters accounts for a variety of global and local lattice geometry effects. These include pin pitch, water hole size within the lattice, fuel enrichment, discrete and integral poisons, control rod materials and boron concentrations. ARCADIA® is capable of predicting with accuracy both the reactivity and the fission rate distribution when considering the spectral differences observed with the critical experiments.

The validation also includes comparisons to operating cores. In this validation process a large range of core sizes and pin lattices were used. The range went from cores with 157 assemblies up a core with 217 assemblies. Core size is important because it establishes how well ARCADIA® handles leakage. These cores also contained fuel assemblies with different lattice geometries including assemblies with large water holes. Enrichments ranged from ~0.70 wt% U-235 (blanket enrichment) up to 4.95 wt% U-235 with a wide variety of absorbers and control rod materials used. Cycle lengths in the core validations cases run from ~15 month to ~24 month. All of these parameters are important because they can affect the neutronic solution and show that ARCADIA® is capable of accurately modeling these conditions and provides a reliable tool for analyzing PWR core and lattice geometries.

No specific trends in capability can be specified because each new core reload will have a unique number of fresh assemblies at a unique enrichment with unique locations in the core relative to previous cycles. Multiple enrichments and multiple poison loadings are commonly employed within each cycle and commonly changes in order to meet the cycle length which also may be different for each cycle. These aspects of the core design add sufficient variability that makes it difficult to categorize a trending variable.

Each cycle is verified through low power physics testing, Technical Specification Surveillance, and also post-evaluated to ensure that the cycle behavior is within what is expected.

Additionally, AREVA has committed to evaluate at least three cycles for existing plants against the criteria in Table 13.2-1 of the Topical Report prior to applying ARCADIA® (Section 13.3 of the Topical Report). For cores that have less than 3 cycles of available data (for example cycle 1 cores), three cycles of a similar plant and/or fuel type would be evaluated to show applicability.

**RAI 7** APOLLO2 gamma transport models and gamma detector modeling capability of the ARCADIA code system are mentioned briefly in the report, [Page 2-38], but only thermal detector methodology is described on Page 3-19. Is the requested application range limited to the fission detectors or an approval for gamma detectors also requested? Since the types of detectors are not included with the plant descriptions of the benchmark cases, all the plants are assumed to have fission detectors. If the intended application range includes gamma detectors please provide model details and benchmarks or revise the application range on Page 13-1 to include applicable detector types.

### AREVA Response

While the gamma detector modeling is a capability of APOLLO2-A, and therefore mentioned in the methodology description, AREVA does not intend to use gamma detectors for industrial applications in PWR UOX plants. In the same manner, as noted on page 2-6 of the Topical Report, a model is available for the gamma contribution to the neutron detector response; however, this model is also not used for the benchmark calculations nor proposed for UOX industrial applications.

It should be noted that the methodology described on Page 3-19 of the Topical Report covers all types of neutron detectors (e.g. Cobalt, Vanadium, and Rhodium detectors) not only fission detectors. Although the detector types are not included in the plant descriptions for the benchmark cases, the benchmarks in the Topical Report include fission chambers, Rhodium SPNDs and Aeroball (Vanadium) detectors. The plant descriptions will be updated in the approved version of the Topical Report to include the detector types.

The application range on Page 13-1 of the approved Topical Report will also be updated to specify the applicable detector types.

**RAI 8** On page 6-9, the APOLLO2-A critical experiment results state that “these results confirm the ability of APOLLO2-A to accurately calculate the reactivity and fission rate of fuel pin lattices.” This statement should be qualified with the range set by the critical experiments, which are performed without depletion, etc.. Furthermore, if certain types of fuel rods are neglected from the statistics (relative pin power), then those types of pins should be explicitly stated as not being validated for the code or system. (i.e. gad).

### AREVA Response

Fundamentally, the neutronic behavior of a critical system is dependent upon the materials and the configuration of the materials. The ability of APOLLO2-A to predict neutronic behavior depends upon the materials, the configuration of materials, the cross sections of the materials, and the ability of the method to approximate the transport of neutrons. The APOLLO2-A neutronic predictions are benchmarked at ranges of conditions shown in Table 8-1 for 0 burnup. The neutronic solution accuracy for pin powers and critical k-effective of APOLLO2-A for this diverse range of materials and configuration of materials is excellent. All the critical k-effectives are within [ ] delta k and the pin powers for the core are within [ ] RMS. These benchmarks validate the neutronic solution for APOLLO2-A for these materials in these configurations which validates the methodology for the materials, configuration of materials, cross sections of the materials, and the ability to transport neutrons. These benchmarks also validate that given the correct cross sections and composition of materials, the neutron solution is accurate. If all the cross sections for all the materials are generated in the same manner with the same accuracy, then APOLLO2-A will give similar results for those materials. The cross sections are taken from JEF3.1.1 for these benchmarks as are all the isotopes that APOLLO2-A uses. In the development of APOLLO2-A, there were no specific empirical treatments for any of the materials modeled in the critical experiments so APOLLO2-A is expected to perform with similar accuracy for any expected PWR configurations and materials. As explained in response to RAI 14, only pins with low powers are eliminated from the statistics in Section 6 because the relative deviations for low power pins can be dominated by the measurement error.

Although Table 8-1 contains clearly defined ranges for the critical experiments, the table does not define the range of applicability of APOLLO2-A. APOLLO2-A does not employ any empirical models to extrapolate beyond the ranges listed below and hence is not vulnerable to extrapolation errors. For example, the reactor benchmarks that use cross sections from APOLLO2-A include U235 contents from 0.7 w/o to 4.95 w/o and boron concentrations from ~0 to 2406 ppm without degradation of the results. Therefore, APOLLO2-A capabilities are not limited to the range of values in Table 8-1.



**Table 8-1. Range of Experimental Conditions**

Parameters	Low / High
U235, weight percent	2.46 / 4.02
Soluble Boron, ppm	16 / 1899
H/U	2.90 / 6.19
Materials	U, Al, H, O, Gd, B, Zr, SS, Inconel
Local Spectral effects - Discrete poisons	Boron, Gadolinia, AgInCd, Hf, SS
Local Spectral effects - Water Hole Size	1 cell / 4 cell
Local Spectral effects – voids in central 7x7 array	30-100%

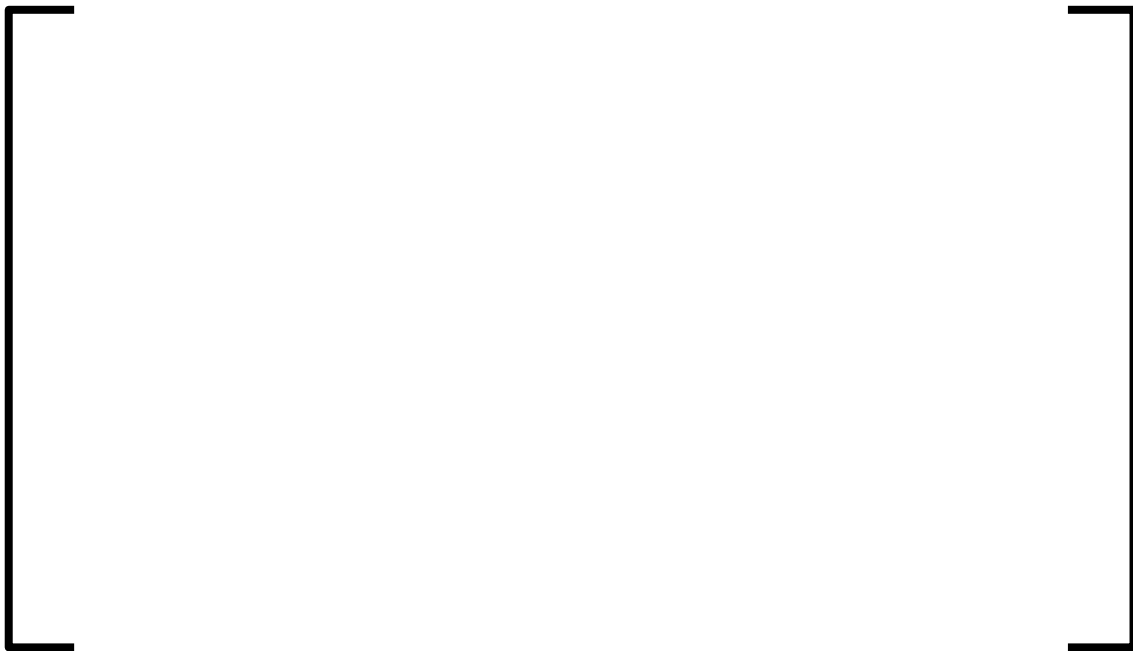
**RAI 9** On page 6-9, all presented criticals are for fresh fuel at cold conditions. APOLLO2 pin power uncertainties rely on the comparisons with these criticals. However, pin power uncertainties can change with depletion as the isotopics change. Not necessarily from the computational model itself but also from the nuclear data. APOLLO2 methodology and the group structure can exhibit different fidelity at different spectrums and isotopic concentrations. Although fresh MOX fuel criticals can capture spectrum of a spent fuel up to a degree, spent fuel is more challenging to model. Please justify that the pin power uncertainties calculated at zero burnup are conservative or provide additional benchmark cases.

### AREVA Response

If the flux and cross sections are correct, the evolution of the isotopic content is a non complex time integration problem. Since the flux and cross section errors of APOLLO2-A are addressed for zero burnup conditions, the errors due to depletion are expected to be similar to the errors at zero burnup.

To validate this assertion, measured to predicted activation rates from plant data, as a function of burnup, are used to demonstrate the applicability of the uncertainty method over the entire range of burnups. The total peaking uncertainty is composed of two components of uncertainty, local and global. These two components are estimated with calculations and measurements and are assumed to be independent. The local uncertainty component is estimated using critical experiments. These types of critical experiments are only available with burnup free fuel designs and have been historically used to validate local peaking uncertainties for PWR operations and methods. The global uncertainty component is estimated by a comparison of the measured reaction rates in the instrument tube compared to the predicted values for each detector. The reaction rate in the instrument location in a PWR is sensitive to both the average power in the entire assembly and the powers in the nearest pins around the instrument tube. In essence, this comparison will sense both global and local power swings if significant deviations between the predicted and measured pin or assembly power exist with burnup. The radial measured to predicted activation rates (relative difference) for all the cores presented in Section 12.4.1 are shown in Figure 9-1. The visual variation of the data with burnup remains relatively constant. The data does show some improvement with burnup between 0 and 20 GWd/MTU and after 20 GWd/MTU which corresponds to the approximate burnups of the fresh fuel and the burnup of the once burned fuel at the beginning of the plant cycle, respectively. It can be concluded that any error with burnup is within the variation seen with fresh fuel. In addition, the critical boron concentrations with cycle burnup shown in the Appendices for each plant in the Topical Report are within their expected ranges (+/- 500 pcm). This shows that the long term depletion of all the isotopes results in acceptable accuracy with burnup. Therefore, the overall method to estimate pin power errors provides a reasonable approach to include the effects of burnup.

**Figure 9-1. Relative Difference with Assembly Burnup**



**RAI 10** On page 4-2, the ARTEMIS/COBRA-FLX coupling accounts for cross flow effects. Have these effects been evaluated for PWR conditions undergoing two-phase flow (accident scenario)?

### AREVA Response

It is recognized that the quoted statement in Ref. [1] implies unintended data flow from the COBRA-FLX module to the rest of the ARCADIA package due to the use of the word “main” in the text, which is not further clarified in this section.

As stated on pg. 4-5 in Ref. [1], COBRA-FLX coupling with ARTEMIS is twofold.

- a. Generating the required information for the cross-section updates during the flux iteration process, and
- b. Thermal-hydraulic evaluation of the power density distribution resulting from a converged flux solution.

The data passed back to ARTEMIS from COBRA-FLX for the purpose of cross section updates (during the flux iteration process) are: node-average coolant temperatures, coolant densities, and void fractions [1, pp. 4-6, 3-21]. In order to calculate these coolant properties, COBRA-FLX obtains the data pertaining to the core power distribution from ARTEMIS [1, pp. 4-6]. Therefore, the calculations and the use of cross flows for determining the nodal coolant conditions are contained within the COBRA-FLX module, which in turn calculates the node specific coolant properties to be passed onto ARTEMIS.

Examples of COBRA-FLX Transient (accident) simulations involving two phase flow are provided in Section 5.7.2 in Ref. [2]. Section 5.5 in Ref. [2] provides comparisons of COBRA-FLX modeling the 4 pump coast down transient with varying model complexity that ranges from 12 channels where lumped channels are involved, to 7083 channels where all subchannels are individually modeled. Results provided in Table 5-6 in Ref. [2] show excellent agreement between varying degrees of modeling detail.

### References

1. ANP-10297P, Rev 0, The ARCADIA® Reactor Analysis System for PWRs Methodology Description and Benchmarking Results, March 2010.
2. ANP-10311P, Rev 0, COBRA-FLX: A Core Thermal-Hydraulic Analysis Code Topical Report, March 2010.

**RAI 11** On page 5-1, 5- 5, the ARTEMIS Fuel Rod Methodology (FRM) solves the one-dimensional heat conduction equations (static and time-dependent) for the average fuel rod in each node. The effective temperature is calculated for nodal cross section evaluation using equation 5-2, which is NOT a simple volume-average (VAFT). Please provide qualitative and quantitative technical Justification for this equation

### AREVA Response

The effective temperature evaluation as shown in equation 5-2 is the same as the equation used in ANP-10286P [1] (end of section 6.2.4) and in ANP-2788P [2] (end of section 6.2.4).

In a qualitative sense, [

]

The relationship for the effective temperature ( $T_{\text{eff}}$ ) has been validated with the computer code APOLLO2 described in BAW-10228PA, (Reference 3). The reactivity and U-238 capture rate of several snapshot fuel temperature distributions at steady state conditions and those temperatures expected during a Reactivity Initiated Accident (RIA) event were examined with APOLLO2. Calculations were repeated with a uniform fuel temperature until the reactivity and U-238 capture rates were equivalent to the nonuniform temperature distributions. This uniform temperature was defined as the effective temperature and compared to the values predicted by Rowland's formula and the new  $T_{\text{eff}}$  formula. Fifteen cases were run for each temperature distribution, which spanned burnups from 0 to 60 GWD/MTU and U-235 enrichments from [ ] weight percent (w/o). Results showed that Rowland's formula resulted in nearly the same temperature as the new  $T_{\text{eff}}$  formula for steady state cases, and that both agreed with the APOLLO2 effective temperature. For the transient fuel temperature cases, the new  $T_{\text{eff}}$  definition showed substantial improvement reducing the mean prediction error of  $T_{\text{eff}}$  from a range [ ] K for the Rowland's formula down to a range of [ ] K. Both models had about a [ ] K standard deviation. The APOLLO2 temperature solution was benchmarked to Monte Carlo N-Particle (MCNP) transport code calculations. In addition, the new  $T_{\text{eff}}$  method was compared in Table 7-5 of Reference 2 to an average temperature formulation and was found to yield slightly more limiting results than a simple average weighting.

### References

1. ANP-10286P, Revision 0, "U.S. EPR Rod Ejection Accident Methodology Topical Report," November 2007, AREVA NP, Inc.
2. ANP-2788P, Revision 0, "Crystal River 3 Rod Ejection Accident Methodology Report", February 2009, AREVA NP, Inc.
3. BAW-10228P-A, "SCIENCE", December, 2000.

**RAI 12** On page 6-5, please provide more detailed description of the critical experiments used in the APOLLO2 validation. There are eigenvalue swings as well as biases in different directions between different sets of the same criticals. Without knowing the difference between the configurations, it is not possible to draw a conclusion. (For instance, what is the difference between the WH1 and CR1 KRITZ experiments?). These results should be discussed in more detail.

### AREVA Response

A more detailed description of the critical experiment configurations used in the APOLLO2-A validation is provided in Tables 12-1 to 12-5. These descriptions supplement what is already provided in the Topical Report.

The comparisons of APOLLO2-A results to measurements are discussed in the response to RAI 13.

**Table 12-1: B&W-1970s Critical Experiment – Description**

Configuration.	Ref. Configuration.	Description
XI_2	XI_2	15x15, UO <sub>2</sub> pin configuration, 2.46 wt% U235
XI_6	XI_2	Ref. Configuration. with 8 Pyrex rods
XI_8	XI_2	Ref. Configuration. with 16 Pyrex rods
XI_11	XI_2	Ref. Configuration. with 16 Al <sub>2</sub> O <sub>3</sub> rods
XI_14	XI_2	Ref. Configuration. with 8 Al <sub>2</sub> O <sub>3</sub> rods
XII_1	XII_1	15x15, UO <sub>2</sub> pin configuration, 2.46 wt% U235 Instrumentation tubes
XII_2	XII_1	Ref. Configuration. with 16 AIC rods

**Table 12-2: B&W-1980s Critical Experiment – Description**

Configuration.	Ref. Configuration.	Description
1	1	15x15, UO <sub>2</sub> pin configuration, 2.46 wt% 235U Instrumentation tube
2	1	Ref. Configuration. with 16 AIC rods
3	1	Ref. Configuration with 8 Gd <sub>2</sub> O <sub>3</sub> rods (4 wt% / 1.94 wt% U235)
4	1	Ref. Configuration. with 8 Gd <sub>2</sub> O <sub>3</sub> rods (4 wt% / 1.94 wt% U235) + 16 AIC rods
5	1	Ref. Configuration. with 12 Gd <sub>2</sub> O <sub>3</sub> rods (4 wt% / 1.94 wt% U235)
6	1	Ref. Configuration. with 12 Gd <sub>2</sub> O <sub>3</sub> rods (4 wt% / 1.94 wt% U235)) + 16 AIC rods
7	1	Ref. Configuration. with 12 Gd <sub>2</sub> O <sub>3</sub> rods (4 wt% / 1.94 wt% U235) No instrumentation tube
12	12	15x15, UO <sub>2</sub> pin configuration, 2.46 wt% 235U outer zone and 4.02 wt% 235U inner zone
14	12	Ref. Configuration. with 12 Gd <sub>2</sub> O <sub>3</sub> rods (4 wt% / 1.94 wt% U235)
15	12	Ref. Configuration. with 12 Gd <sub>2</sub> O <sub>3</sub> rods (4 wt% / 1.94 wt% U235) + 16 B <sub>4</sub> C rods
16	12	Ref. Configuration. with 16 Gd <sub>2</sub> O <sub>3</sub> rods (4 wt% / 1.94 wt% U235)
17	12	Ref. Configuration. with 16 Gd <sub>2</sub> O <sub>3</sub> rods (4 wt% / 1.94 wt% U235) + 16 B <sub>4</sub> C rods
18	18	16x16 CE UO <sub>2</sub> pin configuration, 2.46 wt% 235U outer zone and 4.02 wt% 235U inner zone
20	18	Ref. Configuration. with 16 Gd <sub>2</sub> O <sub>3</sub> rods (4 wt% / 1.94 wt% U235)

**Table 12-3: KRITZ KWU Critical Experiment – Description**

Configuration	Absorbers	Temperature
U-WH1 22C	Empty Guide Tubes	22°C
U-WH1 55C		55°C
U-WH1 90C		90°C
U-WH1 200C		200°C
U-WH1 229C		229°C
U-WH1 241C		241°C
U-CR1 21C	16 AIC control rods	21°C
U-CR1 55C		55°C
U-CR1 91C		91°C
U-CR1 200C		200°C
U-CR1 225C		225°C
U-CR1 243C		243°C

**Table 12-4: EPICURE Critical Experiment – Description**

Configuration	Description
UH1.2	Homogeneous Lattice
UH1.2 - 30% Void	30% Void in the 7x7 central area
UH1.2 - 50% Void	50% Void in the 7x7 central area
UH1.2 - 100% Void	100% Void in the 7x7 central area
UH1.4	25 Guide Tubes
UH1.4 Pyrex	24 Pyrex rods
UH1.4 SS&AIC	12 Stainless Steel rods and 12 AIC rods



**Table 12-5: CAMELEON Critical Experiment – Description**

<b>Configuration</b>	<b>Guide Tubes</b>	<b>Absorbers</b>
25 Guide Tubes	25 Guide Tubes	-
25 Guide Tubes – 12 Gd <sub>2</sub> O <sub>3</sub> Pins	25 Guide Tubes	12 Gd <sub>2</sub> O <sub>3</sub> pins (7 wt% Gd <sub>2</sub> O <sub>3</sub> and 0.25% U235)
5 Gd <sub>2</sub> O <sub>3</sub> Pins	None	5 Gd <sub>2</sub> O <sub>3</sub> pins (3 wt% Gd <sub>2</sub> O <sub>3</sub> and 5.1% U235)
12 Gd <sub>2</sub> O <sub>3</sub> Pins	None	12 Gd <sub>2</sub> O <sub>3</sub> pins (3 wt% Gd <sub>2</sub> O <sub>3</sub> and 5.1% U235)
13 Gd <sub>2</sub> O <sub>3</sub> Pins	None	13 Gd <sub>2</sub> O <sub>3</sub> pins (7 wt% Gd <sub>2</sub> O <sub>3</sub> and 0.25% U235)
24 Hf Pins	25 Guide Tubes	24 Hf pins

**RAI 13** On page 6-5, the APOLLO2-A eigenvalue results of the critical experiment calculations are not presented in a manner that permits treading or bias identification over geometry, composition, temperature, etc. More in-line details in Tables 6.2-1 to 6.2-5 would be useful.

### AREVA Response

More details are included for the critical experiment reactivity comparisons in Tables 13-1 to 13-5.

The calculations of k-effective for all of the critical configurations show very good agreement with the measurements. All of the configurations fall within  $2\sigma$  of the estimated measurement uncertainty (see RAI 60).

Apart from the average overestimation of the reactivity which is well within the estimated measurement uncertainty, it is difficult to conclude that any specific trend exists that is related to the physical features of the configurations, such as the presence of absorbers, certain type of absorbers, the number of the absorber pins, the number of the water cells, the U235 enrichment, and the boron concentration.

It can be observed that B&W 1980's experiments with large CE-type water holes (Configurations 18 and 20) show an overestimation, on average, of about [ ] greater than the other experiments in the same experimental program. Although this shows a small bias in this type of configuration, the discrepancy between the calculation and measurement for these cores is well within the estimated measurement uncertainty so it is impossible to conclude that the APOLLO2-A calculation is biased based on the size of water holes.

Regarding the KRITZ program, the KRITZ U-WH1 cases show an underestimation of the reactivity while the KRITZ U-CR1 cases present an overestimation. Essentially, this only represents two configurations since each configuration of a set is only different in the temperature at which the experiment was conducted. The other experimental configuration which includes AIC, EPICURE 1.4 SS and AIC does not show the same overestimation of reactivity, therefore, it is concluded that APOLLO2-A correctly calculates the reactivity of critical experiments which contain AIC.

Note : In revisiting the calculations of the critical experiments presented in the Topical Report, while responding to the RAIs, some errors were found in the modeling of two EPICURE UH1.4 configurations and a typographical error was found in the reporting of the KRITZ-KWU results. These results have been updated in the tables presented in this response and will be updated in the approved version of the Topical Report. The value of the overall average overprediction [ ] of k-effective changed slightly and the standard deviation was slightly improved [ ] .

**Table 13-1: B&W-1970s Critical Experiment - Reactivity Comparisons**

Configuration	Ref. Configuration	Description	Boron Conc. (ppm)	Target k-eff	Calc. k-eff	C-M (pcm)
XI_2	XI_2	15x15, UO2 pin configuration, 2.46 wt% U235	1334	1.00000		
XI_6	XI_2	Ref Configuration with 8 Pyrex rods	1034	1.00000		
XI_8	XI_2	Ref Configuration with 16 Pyrex rods	794	1.00000		
XI_11	XI_2	Ref Configuration with 16 Al <sub>2</sub> O <sub>3</sub> rods	1384	1.00000		
XI_14	XI_2	Ref Configuration with 8 Al <sub>2</sub> O <sub>3</sub> rods	1363	1.00000		
XII_1	XII_1	15x15, UO2 pin configuration, 2.46 wt% U235 Instrumentation tubes	1340	1.00000		
XII_2	XII_1	Ref Configuration with 16 AIC rods	1264	1.00000		

**Table 13-2: B&W-1980s Critical Experiment - Reactivity Comparisons**

Configuration	Ref Configuration	Description	Boron Conc. (ppm)	Target k-eff	Calc. k-eff	C-M (pcm)
1	1	15x15, UO <sub>2</sub> pin configuration, 2.46 wt% U235 Instrumentation tube	1338	1.00000		
2	1	Ref. Configuration with 16 AIC rods	1250	1.00000		
3	1	Ref. Configuration with 8 Gd <sub>2</sub> O <sub>3</sub> rods (4 wt% / 1.94 wt% U235)	1239	1.00000		
4	1	Ref. Configuration with 8 Gd <sub>2</sub> O <sub>3</sub> rods (4 wt% / 1.94 wt% U235) + 16 AIC rods	1172	1.00000		
5	1	Ref. Configuration with 12 Gd <sub>2</sub> O <sub>3</sub> rods (4 wt% / 1.94 wt% U235)	1208	1.00000		
6	1	Ref. Configuration with 12 Gd <sub>2</sub> O <sub>3</sub> rods (4 wt% / 1.94 wt% U235) + 16 AIC rods	1156	1.00000		
7	1	Ref. Configuration with 12 Gd <sub>2</sub> O <sub>3</sub> rods (4 wt% / 1.94 wt% U235) No instrumentation tube	1209	1.00000		
12	12	15x15, UO <sub>2</sub> pin configuration, 2.46 wt% 235U outer zone and 4.02 wt% U235 inner zone	1899	1.00000		
14	12	Ref. Configuration with 12 Gd <sub>2</sub> O <sub>3</sub> rods (4 wt% / 1.94 wt% U235)	1654	1.00000		
15	12	Ref. Configuration with 12 Gd <sub>2</sub> O <sub>3</sub> rods (4 wt% / 1.94 wt% U235) + 16 B4C rods	1480	1.00000		
16	12	Ref. Configuration with 16 Gd <sub>2</sub> O <sub>3</sub> rods (4 wt% / 1.94 wt% U235)	1579	1.00000		
17	12	Ref. Configuration with 16 Gd <sub>2</sub> O <sub>3</sub> rods (4 wt% / 1.94 wt% U235) + 16 B4C rods	1432	1.00000		
18	18	16x16 CE UO <sub>2</sub> pin configuration, 2.46 wt% 235U outer zone and 4.02 wt% U235 inner zone	1777	1.00000		
20	18	Ref. Configuration with 16 Gd <sub>2</sub> O <sub>3</sub> rods (4 wt% / 1.94 wt% U235)	1499	1.00000		

**Table 13-3: KRITZ KWU Critical Experiment - Reactivity Comparisons**

Configuration	Absorbers	Temperature	Boron Conc. (ppm)	Target k-eff	Calc. k-eff	C-M (pcm)
U-WH1 22C	Empty Guide Tubes	22°C				
U-WH1 55C		55°C				
U-WH1 90C		90°C				
U-WH1 200C		200°C				
U-WH1 229C		229°C				
U-WH1 241C		241°C				
U-CR1 21C	16 AIC control rods	21°C				
U-CR1 55C		55°C				
U-CR1 91C		91°C				
U-CR1 200C		200°C				
U-CR1 225C		225°C				
U-CR1 243C		243°C				

**Table 13-4: EPICURE Critical Experiment - Reactivity Comparisons**

Configuration	Description	Boron Conc. (ppm)	Target k-eff	Calc. k-eff	C-M (pcm)
UH1.2	Homogeneous core				
UH1.2 - 30% Void	30% Void in the 7x7 central area				
UH1.2 - 50% Void	50% Void in the 7x7 central area				
UH1.2 - 100% Void	100% Void in the 7x7 central area				
UH1.4	25 Guide Tubes				
UH1.4 Pyrex	24 Pyrex rods				
UH1.4 SS&AIC	12 Stainless Steel rods and 12 AIC rods				

**Table 13-5: CAMELEON Critical Experiment - Reactivity Comparisons**

Configuration	Guide Tubes	Absorbers	Boron Conc. (ppm)	Target k-eff	Calc. k-eff	C-M (pcm)
25 Guide Tubes	25 Guide Tubes	-				
25 Guide Tubes – 12 Gd <sub>2</sub> O <sub>3</sub> Pins	25 Guide Tubes	12 Gd <sub>2</sub> O <sub>3</sub> pins (7 wt% Gd <sub>2</sub> O <sub>3</sub> and 0.25% U235)				
5 Gd <sub>2</sub> O <sub>3</sub> Pins	None	5 Gd <sub>2</sub> O <sub>3</sub> pins (3 wt% Gd <sub>2</sub> O <sub>3</sub> and 5.1% U235)				
12 Gd <sub>2</sub> O <sub>3</sub> Pins	None	12 Gd <sub>2</sub> O <sub>3</sub> pins (3 wt% Gd <sub>2</sub> O <sub>3</sub> and 5.1% U235)				
13 Gd <sub>2</sub> O <sub>3</sub> Pins	None	13 Gd <sub>2</sub> O <sub>3</sub> pins (7 wt% Gd <sub>2</sub> O <sub>3</sub> and 0.25% U235)				
24 Hf Pins	25 Guide Tubes	24 Hf pins				

**RAI 14** - Some of the fission rate results presented in Figures 12.2.1-1 through 12.2.1-6 do not agree with the results provided in Table 6.2-7. Please explain this discrepancy. If the statistics population for any critical were altered, describe the justification for this decision. (It appears that the fuel pins containing gadolinia were removed from the statistics.) [Page 6-7]

### AREVA Response

The statistics provided in Table 6.2-7 in the Topical Report only include the fuel pins with relative fission rates greater than [ ]. Since the results are presented as relative differences, the discrepancy between calculated and measured in very low fission rate pins tends to significantly skew the average results. By eliminating pins with fission rates of less than [ ], the skewing due to these low importance pins is avoided.

The fission rate results presented in Figures 12.2.1-1 through 12.2.1-6 of the Topical Report include the results for these low fission rate pins; however, the statistics presented in Table 12.2.1-2 of the Topical Report only include the pins with relative fission rates greater than [ ] as explained in Section 12.2.1 of the Topical Report.

The two different relative fission rate limits include the same pins; therefore, the results presented in Table 6.2-7 and Table 12.2.1-2 of the Topical Report are consistent.

In order to show that the low fission rate pins do not behave significantly differently from the higher fission rate pins, a summary of the statistical results for the absolute differences (C-M) of the fission rates for configurations 5, 14, and 20 with and without the inclusion of the low fission rate pins is presented in Table 14-1. Figures 14-1 and 14-2 present frequency plots of the absolute differences with and without the inclusion of the low fission rate pins, respectively.

A comparison of the statistical results with and without the inclusion of low fission rate pins clearly shows that these two sets of pins do not behave significantly differently from one another when considered on an absolute basis.

**Table 14-1. Fission Rate Comparison Statistics  
For B&W 1980's Experiments with Gadolinia**

Core	RMS (C-M)*100	
	Excluded Low Fission Rates	Included Low Fission Rates
5		
14		
20		

**Figure 14-1: Critical Experiment Frequency Distribution versus Normal Distribution (Absolute Differences with Low Fission Rate Pins)**





**Figure 14-2: Critical Experiment Frequency Distribution versus Normal Distribution (Absolute Differences without Low Fission Rate Pins)**



**RAI 15** Please provide fission rate distribution maps similar to Figure 12.2.1-1 for other criticals as well. Also please the predicted and measured peak pin fission rate locations, the peak pin fission rate differences and maximum, minimum fission rate differences in the fission rate distribution comparison in Tables 6.2-6 through 6.2-10 [Page 6-7].

### AREVA Response

Fission rate distribution maps similar to Figure 12.2.1-1 are presented for each critical configuration in Figure 15-1 through Figure 15-16. Due to their size, maps for the EPICURE and KRITZ configurations are split into smaller maps. In these cases a description of the complete map is presented first with the definition of the zones that are used for the smaller maps. The Babcock & Wilcox experiment fission rate distributions are updated as part of the response to RAI-36.

In Tables 15-1 through 15-5 (corresponding to Tables 6.2-6 through 6.2-10 of the Topical Report), in addition to the RMS, the predicted and measured peak pin fission rate values are given with their locations (using a x,y location in accordance with the Figures) and the relative errors between the predicted and measured peaks. Maximum and minimum fission rate differences in the fission rate distribution comparison are also presented in the tables. It should be noted that pins with a relative fission rate less than [ ] are excluded for the statistics in these tables as described in RAI 14.

The RMS values presented in Tables 15-1 through 15-5 show that, on average, APOLLO2-A predicts the fission rates very well. There are no configurations that exceed a [ ] difference and only one configuration, from the B&W 1970's experimental program, has a C/M comparison in which the absolute value of a single pin error exceeds [ ]. A closer evaluation of the individual pin comparisons for the fission rate distributions, presented in the figures, reveals that, although there are a few individual pins that exhibit a larger discrepancy from the measurements, most of the measurements are well within  $2\sigma$  of the measurement uncertainties presented in RAI 60.

Note : In revisiting the calculations of the critical experiments presented in the Topical Report, while responding to the RAIs, some minor errors were found in the modeling and post-processing of the fission rate distributions in the EPICURE UH1.4, KRITZ-KWU, and B&W 1980's experimental programs. Therefore, some of the RMS values presented in this response are slightly different from those presented in Section 6.2.2 of the Topical Report. All of the changes have improved the results as compared to those in the Topical Report except for Configuration 20 of the B&W criticals and the KRITZ-KWU criticals where the RMS increases slightly.

**Table 15-1: B&W-1970s Fission Rate Distribution Comparisons (TR Table 6.2-6)**

Configuration	RMS (C/M-1) in %	Peak					Differences	
		Predicted		Measured		(C/M-1) in %		
		Value	x,y	Value	x,y		Max	Min
XI_2								
XI_6								
XI_8								
XI_11								

**Table 15-2: B&W-1980s Fission Rate Distribution Comparisons (TR Table 6.2-7)**

Configuration	RMS (C/M-1) in %	Peak					Differences	
		Predicted		Measured		(C/M-1) in %		
		Value	x,y	Value	x,y		Max	Min
1								
5								
12								
14								
18								
20								

**Table 15-3: KRITZ Fission Rate Distribution Comparisons (TR Table 6.2-8)**

Configuration	RMS (C/M-1) in %	Peak					Differences	
		Predicted		Measured		(C/M-1) in %		
		Value	x,y	Value	x,y			
U-WH1								

**Table 15-4: EPICURE Fission Rate Distribution Comparisons (TR Table 6.2-9)**

Configuration	RMS (C/M-1) in %	Peak					Differences	
		Predicted		Measured		(C/M-1) in %		
		Value	x,y	Value	x,y		Max	Min
UH1.2								
UH1.2 30%								
UH1.2 50%								
UH1.2 100%								
UH1.4								
UH1.4 Pyrex								
UH1.4 SSAIC								

**Table 15-5: CAMELEON Fission Rate Distribution Comparisons (TR Table 6.2-10)**

Configuration	RMS (C/M-1) in %	Peak					Differences	
		Predicted		Measured		(C/M-1) in %		
		Value	x,y	Value	x,y		Max	Min
25GT_12GD								
13GD								
12GD								
5GD								

**Figure 15-1 - B&W 1970's Core XI\_2 Fission Rate Distribution Error (%)**



**Figure 15-2 - B&W 1970's Core XI\_6 Fission Rate Distribution Error (%)**



**Figure 15-3 - B&W 1970's Core XI\_8 Fission Rate Distribution Error (%)**



**Figure 15-4 - B&W 1970's Core XI\_11 Fission Rate Distribution Error (%)**



[x] Measurement  
 [shaded blue] Guide Tube

Red Zone  
 Blue Zone  
 Green Zone

1 2 3 4 5 6 7 8 9 10 11 12 13 14 15 16 17 18 19 20 21 22 23 24 25 26 27 28 29 30 31 32 33 34 35 36 37 38 39 40 41 42

**Figure 15-5-B – KRITZ KWU UWH1 Reference Fission Rate Distribution Error (%) –  
Red, Blue and Green Zones**

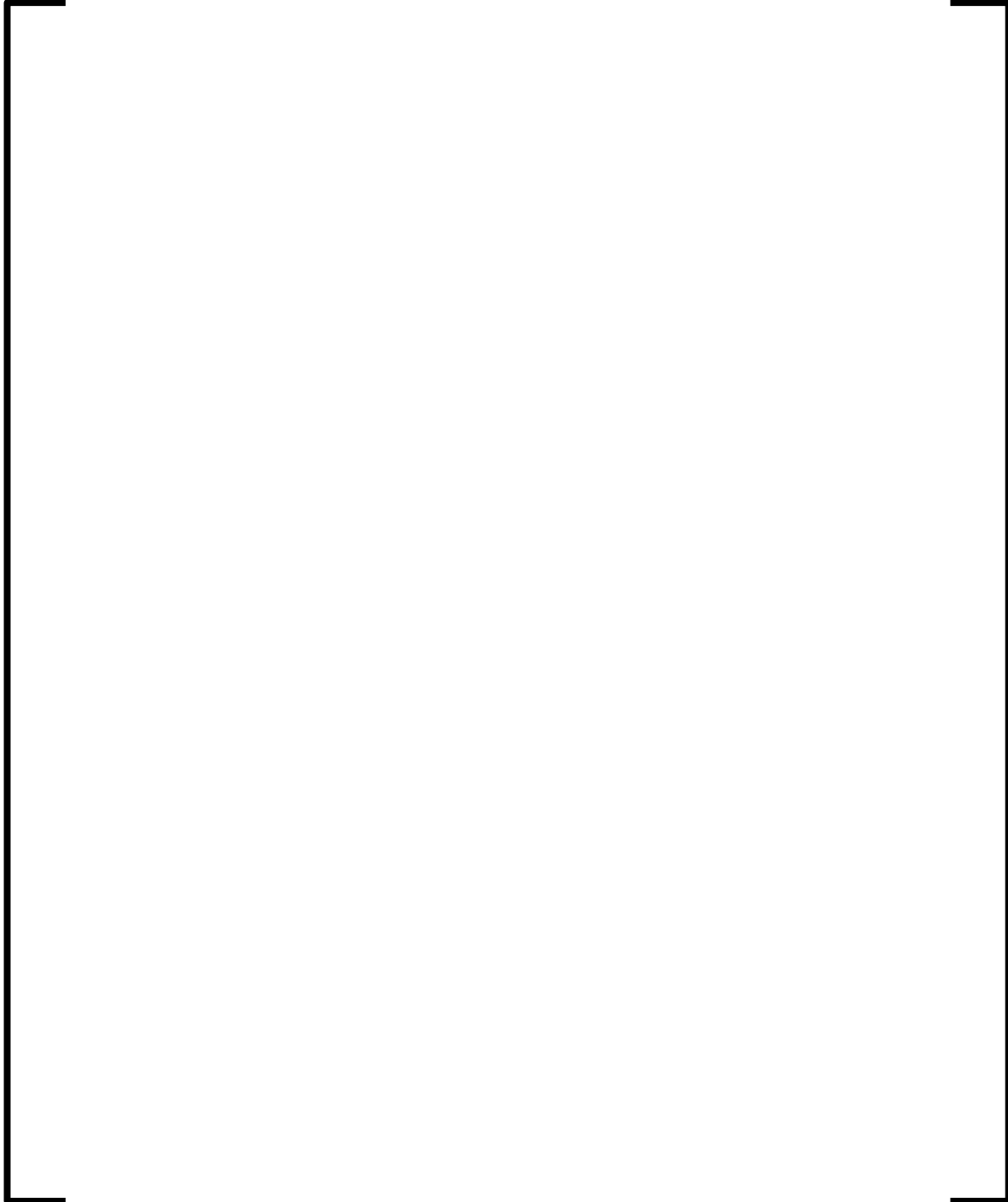
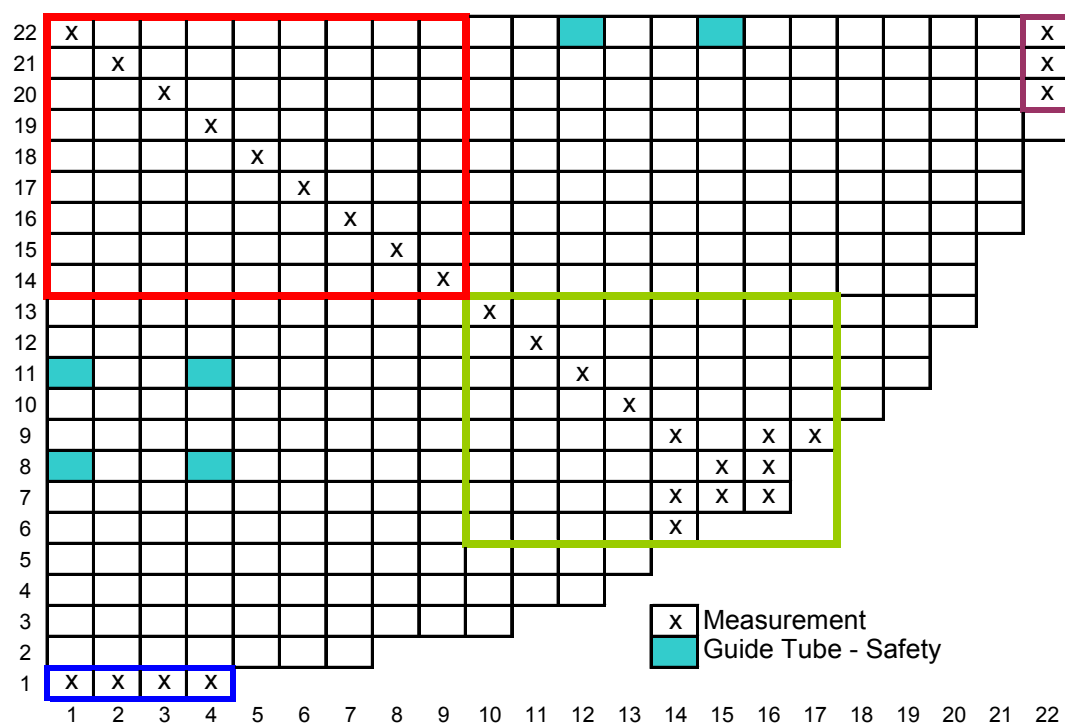




**Figure 15-6-A - EPICURE UH1.2 Reference Fission Rate Distribution**



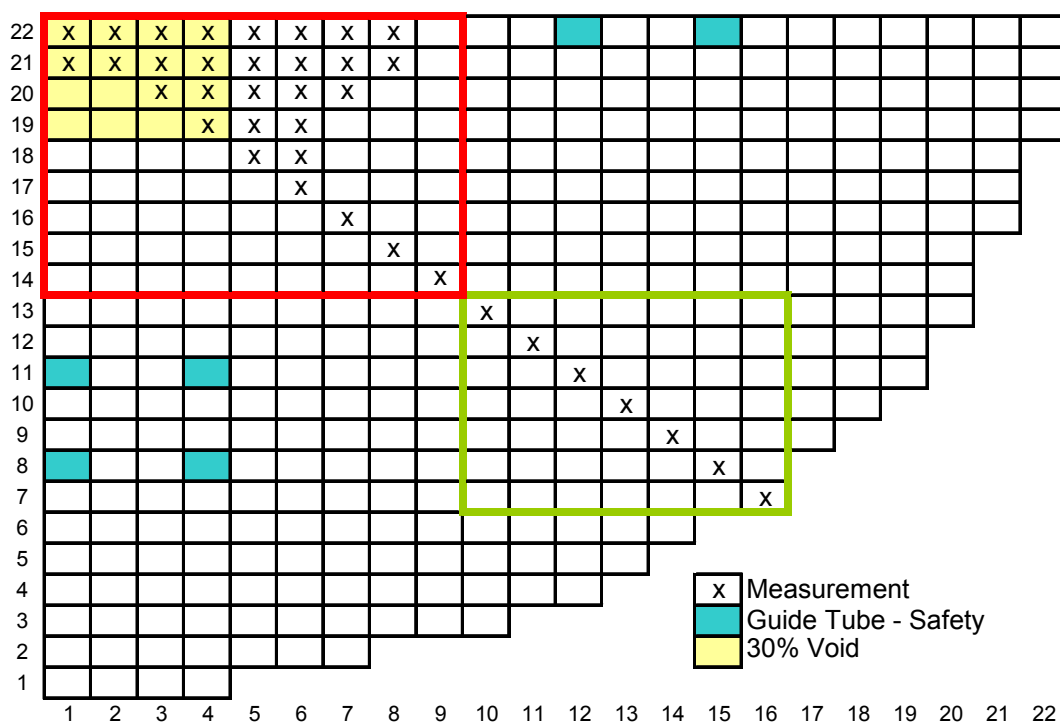
Red Zone      Green Zone      Blue Zone      Purple Zone

**Figure 15-6-B - EPICURE UH1.2 Reference Fission Rate Distribution Error (%) –  
Red Zone**



**Figure 15-6-C - EPICURE UH1.2 Reference Fission Rate Distribution Error (%) –  
Green, Blue and Purple Zone**



**Figure 15-7-A - EPICURE UH1.2 30% Void Fission Rate Distribution**

Red Zone

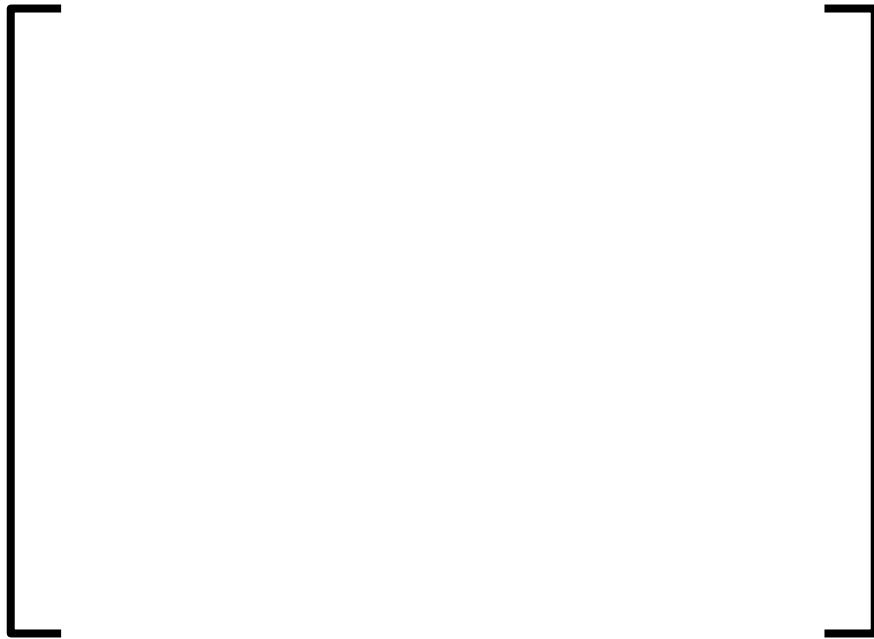


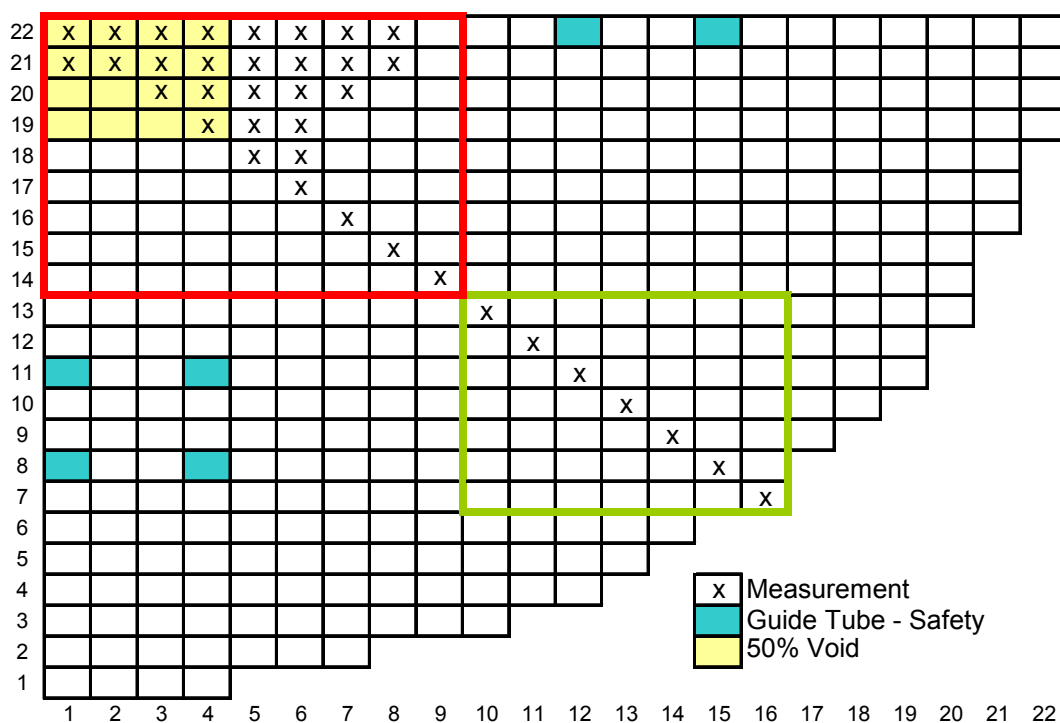
Green Zone

**Figure 15-7-B - EPICURE UH1.2 30% Void Fission Rate Distribution Error (%) –  
Red Zone**



**Figure 15-7-C - EPICURE UH1.2 30% Void Fission Rate Distribution Error (%) –  
Green Zone**



**Figure 15-8-A - EPICURE UH1.2 50% Void Fission Rate Distribution**

Red Zone



Green Zone

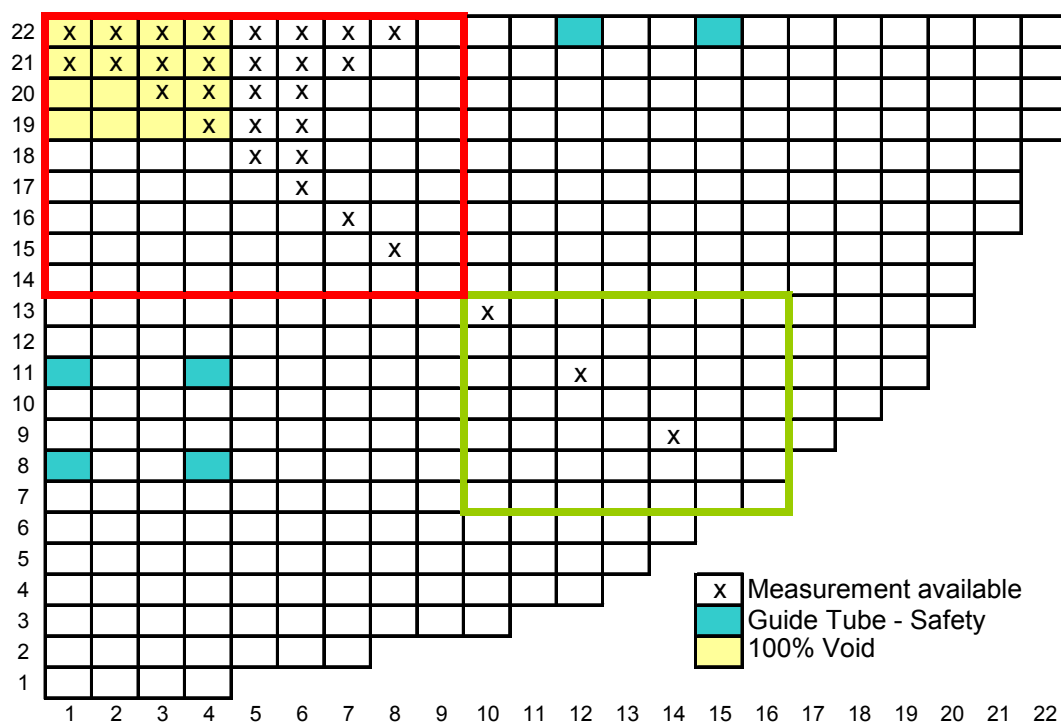
**Figure 15-8-B - EPICURE UH1.2 50% Void Fission Rate Distribution Error (%) –  
Red Zone**





**Figure 15-8-C - EPICURE UH1.2 50% Void Fission Rate Distribution Error (%) –  
Green Zone**



**Figure 15-9-A - EPICURE UH1.2 100% Void Fission Rate Distribution**

Red Zone



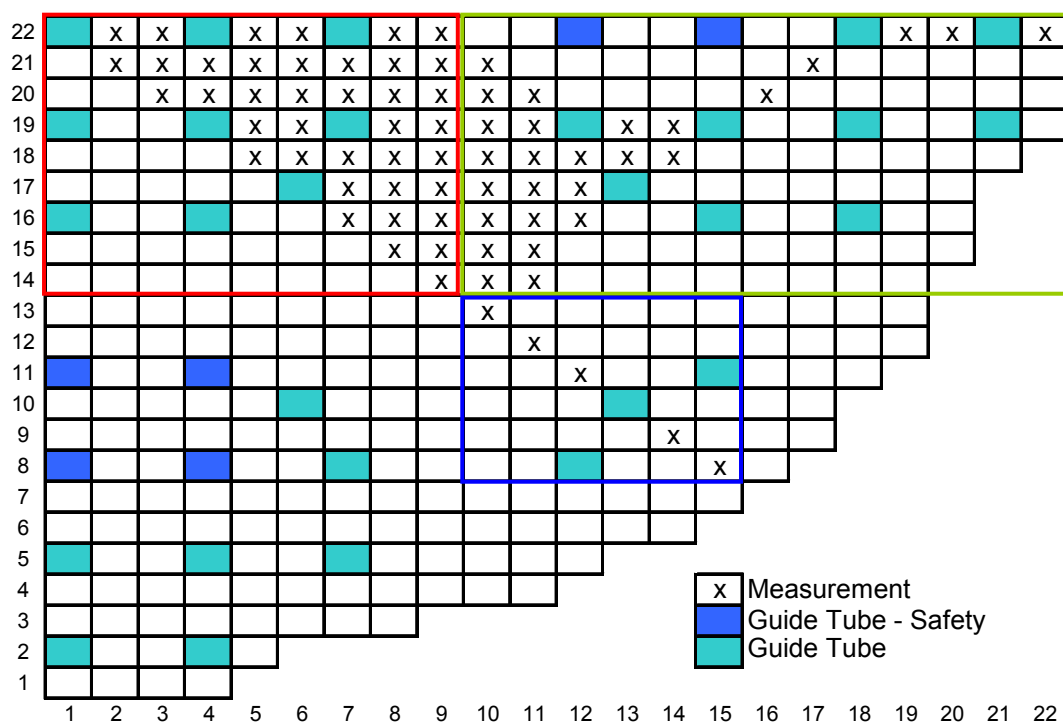
Green Zone

**Figure 15-9-B - EPICURE UH1.2 100% Void Fission Rate Distribution Error (%) –  
Red Zone**



**Figure 15-9-C - EPICURE UH1.2 100% Void Fission Rate Distribution Error (%) –  
Green Zone**



**Figure 15-10-A - EPICURE UH1.4 Reference Fission Rate Distribution**

Red Zone



Green Zone



Blue Zone

**Figure 15-10-B - EPICURE UH1.4 Reference Fission Rate Distribution Error (%) –  
Red Zone**



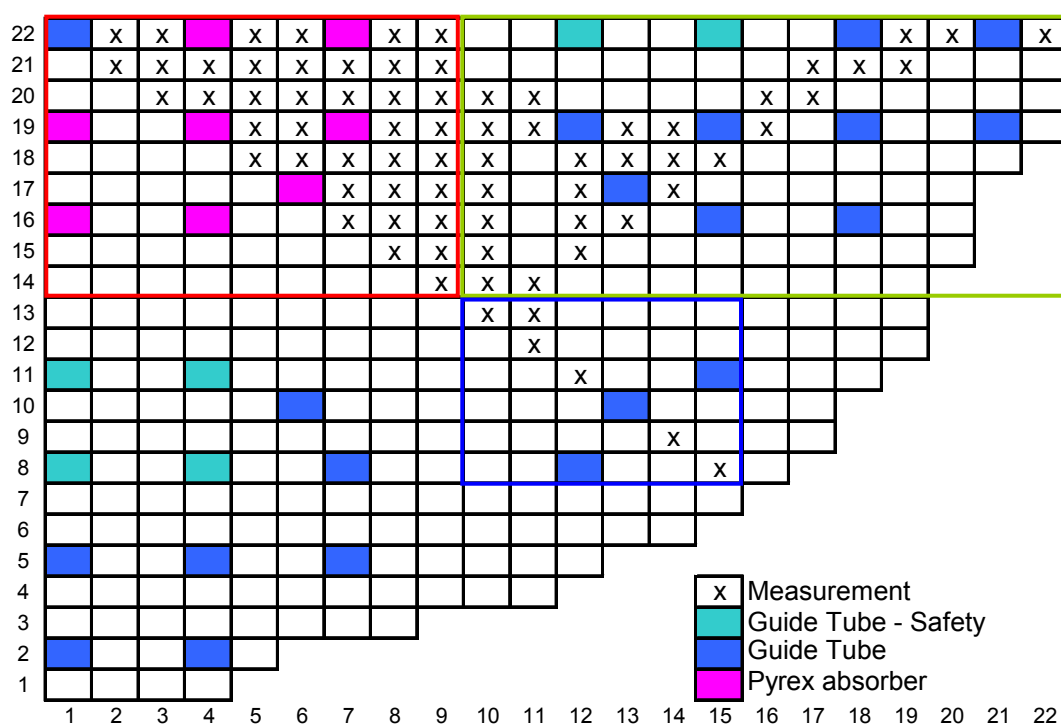
**Figure 15-10-C - EPICURE UH1.4 Reference Fission Rate Distribution Error (%) –  
Green Zone**



**Figure 15-10-D - EPICURE UH1.4 Reference Fission Rate Distribution Error (%) –  
Blue Zone**



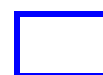


**Figure 15-11-A - EPICURE UH1.4 Pyrex Fission Rate Distribution**

Red Zone



Green Zone



Blue Zone

**Figure 15-11-B - EPICURE UH1.4 Pyrex Fission Rate Distribution Error (%) – Red Zone**

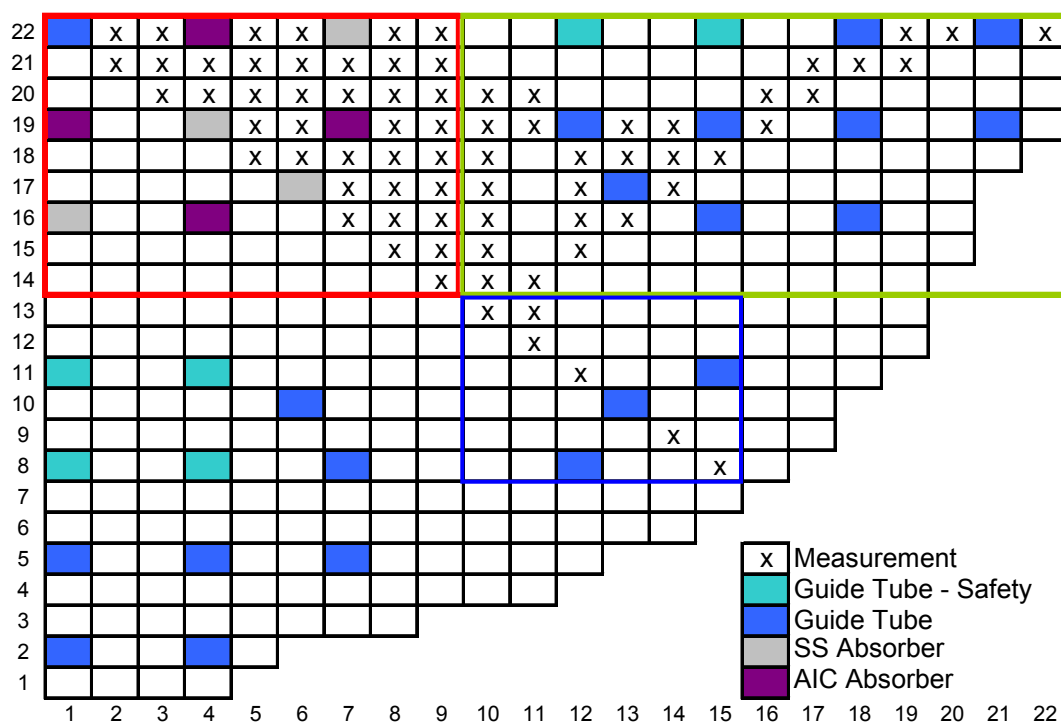


**Figure 15-11-C - EPICURE UH1.4 Pyrex Fission Rate Distribution Error (%) –  
Green Zone**



**Figure 15-11-D - EPICURE UH1.4 Pyrex Fission Rate Distribution Error (%) – Blue Zone**

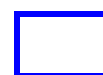


**Figure 15-12-A - EPICURE UH1.4 SS&AIC Fission Rate Distribution**

Red Zone



Green Zone



Blue Zone

**Figure 15-12-B - EPICURE UH1.4 SS&AIC Fission Rate Distribution Error (%) –  
Red Zone**



**Figure 15-12-C - EPICURE UH1.4 SS&AIC Fission Rate Distribution Error (%) –  
Green Zone**



**Figure 15-12-D - EPICURE UH1.4 SS&AIC Fission Rate Distribution Error (%) –  
Blue Zone**

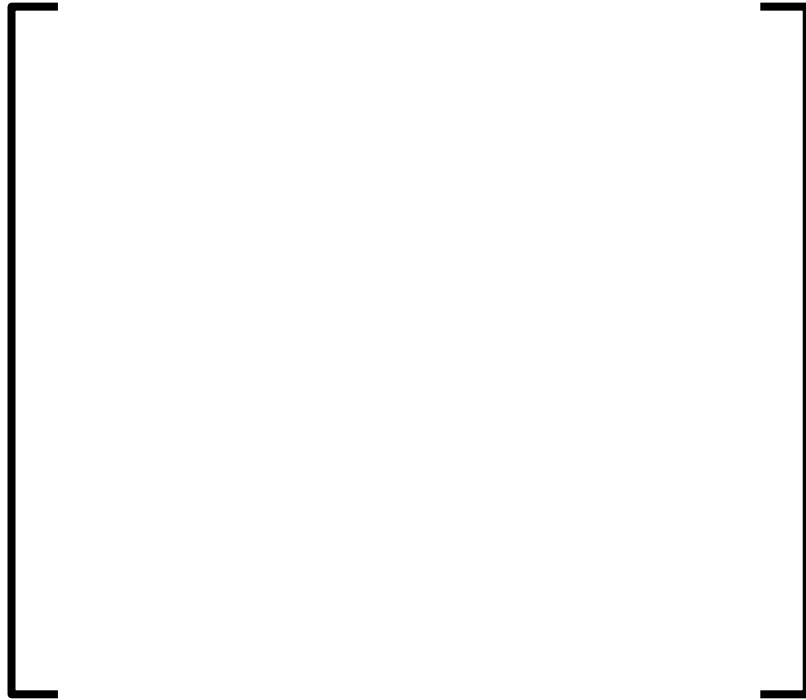




**Figure 15-13 - CAMELEON 25GT\_12GD Fission Rate Distribution Error (%)**



**Figure 15-14 - CAMELEON 13GD Fission Rate Distribution Error (%)**



**Figure 15-15 - CAMELEON 12GD Fission Rate Distribution Error (%)**



**Figure 15-16 - CAMELEON 5GD Fission Rate Distribution Error (%)**



**RAI 16** No details are provided for the gamma transport and the gamma smearing models in APOLLO2. If only the gamma smearing model is intended to be used, please provide a validation/justification for this model. Since the criticals are not considered as industry applications, it is not clear which gamma transport model was used for the criticals [Page 6-1].

### AREVA Response

As described in Section 2.9 of the Topical Report, the gamma calculation uses state of the art gamma production and transport nuclear libraries; the gamma transport equation is solved with the same Method-of-Characteristics solver and on the same detailed geometry as the neutron transport equation. This transport calculation model constitutes the best (highest order) approximation and will be considered as a reference in the following discussion.

Gamma smearing is a general term that refers to the physical process of gamma transport that tends to redistribute the gamma portion of the power distribution. This is due to the fact that most of the gamma energy is not deposited where it is produced. The smearing effect must be taken into account, especially for assemblies with strong gamma producers such as Gd pins. This effect is illustrated in Figure 16-1. It represents the pin power relative difference between a local energy deposition model (no gamma transport) and a gamma transport energy deposition model, taken as a reference, for a fresh 17x17 UOX fuel assembly (1/8 symmetry) enriched at 4.3 w/o with 20 Gadolinium pins with a Gd enrichment of 7%. [

]

Several approaches to address this issue were studied with APOLLO2-A with an increasing degree of accuracy: local gamma energy deposition (no smearing), uniform smearing of gamma energy, simplified gamma transport, and full gamma transport (regarded as the reference). The outcome of this analysis is presented here as well as the conclusion about the model to be used for industrial applications.

[

]

[

]

As for the critical experiments in Chapter 6, the measurements correspond to the fission rates (measured through fission product decay from irradiated pins) and are directly compared, through normalized distributions, to the fissions rates calculated by APOLLO2-A. Therefore, the energy deposition model does not affect the interpretation of those experiments and has no impact on the C/M comparisons on the critical experiments.

[

]

[

]

**Figure 16-1: Normalized pin power map for the local energy deposition model (upper numbers) and relative difference in % (lower numbers) with the reference gamma transport energy deposition mode**

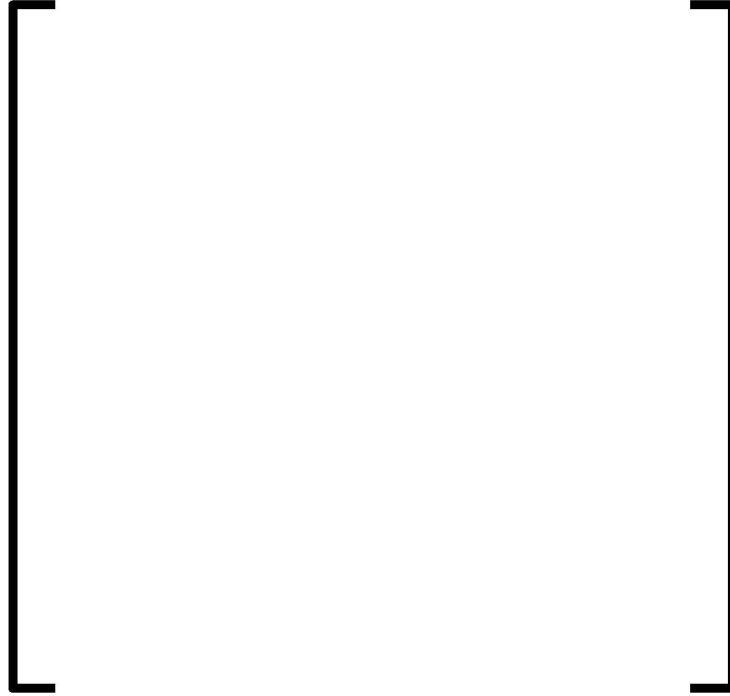


**Figure 16-2: Normalized pin power map for the uniform smearing energy deposition model (upper numbers) and relative difference (lower numbers) with the reference gamma transport energy deposition model**

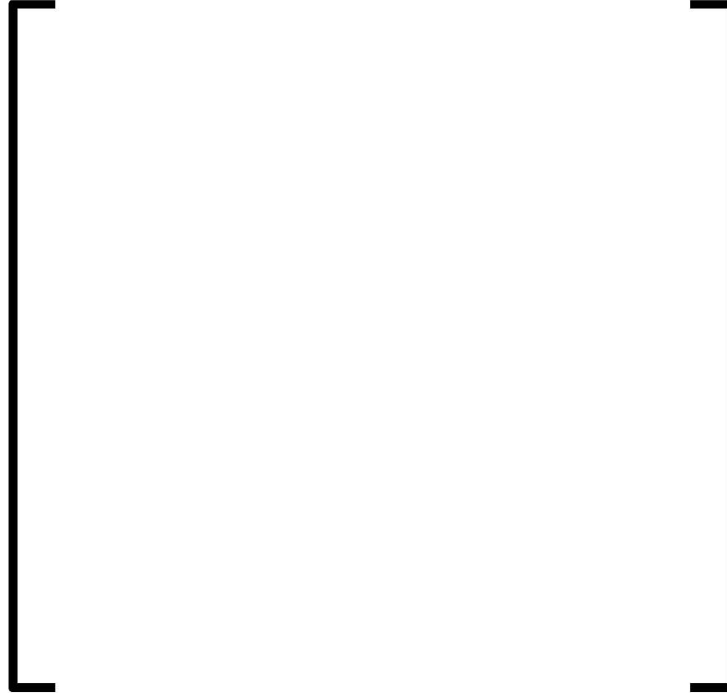


**Figure 16-3: Standard deviation of the normalized pin by pin power relative difference between various energy deposition models and explicit gamma transport model.**





**Figure 16-4: Relative difference on the assembly power peak between uniform smearing and simplified transport model and explicit gamma transport model**



**RAI 17** What is the axial buckling treatment for in APOLLO2-A? It is mentioned in the report that for the integral experiments the radial buckling is also needs to be taken into account. Please also provide details for the radial buckling treatment in the integral tests validation [Page 6-9].

### **AREVA Response**

The buckling treatment in APOLLO2-A is explained in Sections 2.2.1, 2.2.2, and 2.7 of the Topical Report. In summary, the buckling is used to perform a leakage correction on the flux. For industrial applications, this is performed as a fundamental mode calculation on a homogeneous geometry which determines a critical buckling, such that the k-effective of the assembly is unity. In this case this critical buckling accounts for all leakage in the axial and radial directions.

Aside from the fundamental mode calculation, APOLLO2-A also allows a fixed buckling to be used as input. In this case, there is no iteration to determine the critical buckling, rather, the leakage correction is simply calculated using the input value and the code calculates the appropriate k-effective.

For validation calculations, when the accuracy of the reactivity calculation is of concern, a fixed buckling is used to account for the leakage. For critical experiments, this fixed buckling consists of a measured axial buckling which is presented in the experimental reports. The radial leakage is treated explicitly using vacuum boundary conditions outside the reflector.

For the integral experiments, the experimental reports only give the pin-cell description and the total (axial and radial) measured buckling; therefore, the calculations must be performed as a single pin-cell with reflective boundary conditions in the radial directions simulating an infinite lattice with a fixed total buckling. This fixed total buckling simulates the radial and axial leakage which is present because the real experiment is a finite lattice and not an infinite lattice as modeled by the calculation.

**RAI 18** Only uranium and plutonium isotopic comparisons are presented in the spent fuel analyses. However, the fission products and other major actinides can be as important for validation of the depletion methodology and decay chains. A more extensive comparison would also show if there is a cancellation of errors due to biases to certain isotopes. Please provide isotopic comparisons for the other measured major actinides and fission products [Page 6-17].

### AREVA Response

The most important validation of the depletion methodology is the comparison of the parameters in the Appendices of the Topical Report with cycle burnup. The isotopic comparisons provide an additional validation of the depletion method. Additional comparisons for other available measured isotopes in the experimental programs are presented in Table 18-1 for UOX, ERU, and MOX fuel. In addition to uranium and plutonium, minor actinides (Np, Am, Cm) and several fission products (Cs, Nd, etc.) are included when the measurements are available.

As an indication of the neutronic importance of the presented isotopes, an estimate of reactivity worth for a 1% increase in the calculated concentration is also provided in Tables 18-1 through 18-3. This reactivity worth is assessed using the following equation:

$$\Delta K_{inf i} \approx \frac{\delta K_{inf}}{\delta N_i} \Delta N_i = \frac{\sum_p N_p \nu_p \tau_{fp}}{\sum_p N_p \tau_{ap}} \Delta N_i$$

$$= \left( \frac{\nu_i \tau_{fi}}{\sum_p N_p \tau_{ap}} - \frac{\tau_{ai} \sum_p N_p \nu_p \tau_{fp}}{\left( \sum_p N_p \tau_{ap} \right)^2} \right) \Delta N_i = \frac{\Delta N_i}{N_i} \times \left( \frac{N_i \nu_i \tau_{fi}}{A_{Tot}} - \frac{N_i \tau_{ai} P_{Tot}}{A_{Tot}^2} \right)$$

$$\Delta K_{inf i} \approx \frac{\Delta N_i}{N_i} \times \frac{P_{Tot}}{A_{Tot}} \times \left( \frac{N_i \nu_i \tau_{fi}}{P_{Tot}} - \frac{N_i \tau_{ai}}{A_{Tot}} \right)$$

Where:

$\Delta K_{inf i}$ : Variation of reactivity due to a  $\Delta N_i$  change of the concentration of isotope i

$N_i$  : Concentration of isotope i

$\frac{\Delta N_i}{N_i}$  : Fractional variation of isotopic concentration i (0.01 for this demonstration)

$\nu_i \tau_{f_i}$  : Microscopic neutron production rate of isotope i

$\tau_{a_i}$  : Microscopic absorption rate of isotope i

$\sum_p$  : Sum over all the isotopes

$P_{Tot} = \sum_p N_p \nu_p \tau_{f_p}$  : Total neutron production rate

$A_{Tot} = \sum_p N_p \tau_{a_p}$  : Total absorption rate

For this evaluation, the flux is not recalculated; therefore the values only give an approximation of the impact on reactivity of the different isotopes. The elements having the major contribution on reactivity are, as expected, Uranium and Plutonium, which were presented in the Topical Report. The results are presented in the same manner used in the Topical Report.

In general, it will be shown that high importance isotopes have errors within the expected uncertainties. Comparisons to measurements in Table 18-1 and 18-3 show quite significant discrepancies for Sm149; however, the final concentration of this isotope depends heavily on the level of flux at the end of irradiation which is not precisely known and is consequently not precisely modeled. The significant discrepancies observed for this isotope are therefore due to a lack of precision in the irradiation model.

The uncertainties associated with the following results can not be easily evaluated and are discussed in the response to RAI 60. However, as an illustration of the quality of APOLLO2-A results, the combined uncertainties for the four isotopes having the most impact on reactivity (U235, Pu239, Pu240 and Pu241) are estimated for UO2 by a square root of the sum of the squares combination of the modeling uncertainties (given versus burnup in Table 60-2) and the Malibu measurement uncertainties (given for a UO2 sample at 71 GWd/t in Table 60-4). These results are shown in Table 18-4. In all the cases, the accuracy of APOLLO2-A is within two standard deviations of the expected accuracy between the model and the measured values.

The same illustration is given for MOX fuel in Table 18-5 for the four isotopes having the most impact on reactivity (Pu239, Pu240, Pu241 and Am241). The uncertainties for MOX are estimated by a square root of the sum of the squares combination of the available modeling uncertainties (given versus burnup in Table 60-3) and the Malibu measurement uncertainties (given for a MOX sample at 68 GWd/t in Table 60-4). In all but one of the cases, the accuracy of APOLLO2-A is within two standard deviations of the expected accuracy between the model and the measured values.

Considering the importance on reactivity of the different isotopes and the uncertainties associated with the modeling of the irradiation and with the measurements (see response to RAI 60), the comparison of APOLLO2-A results to measurements are considered acceptable.

Note: Some previously presented results for actinides have been corrected as there were errors found in the original presentation of results. These changes are minor and do not affect the overall conclusions presented herein nor in Chapter 6 of the Topical Report. These changes will be incorporated into the approved version of the report.

**Table 18-1: Isotopic Burnup Analysis – UO<sub>2</sub> Concentrations Comparisons  
(C/M-1 in %) and Estimated Reactivity Weight (pcm/%)**

**Table 18-2: Isotopic Burnup Analysis – ERU Concentrations Comparisons  
(C/M-1 in %) and Estimated Reactivity Weight (pcm/%)**

--	--

**Table 18-3: Isotopic Burnup Analysis – MOX**  
**Concentrations Comparisons (C/M-1 in %) and Estimated Reactivity Weight**  
**(pcm/%)**



**Table 18-4: Isotopic Burnup Analysis – UO<sub>2</sub>**  
**APOLLO2-A Results (C/M-1 in %) versus Estimated Uncertainties**

--

**Table 18-5: Isotopic Burnup Analysis – MOX**  
**APOLLO2-A Results (C/M-1 in %) versus Estimated Uncertainties**

--

**RAI 19** Explain why the isotopic comparison of the  $\text{UO}_2\text{Gd}_2\text{O}_3$  results was changed to an absolute difference relative to  $\text{Gd}_{\text{Tot}}$  rather than a relative error normalized to final  $\text{U}^{238}$ ? Is the  $\text{Gd}_{\text{Tot}}$  concentration calculated or measured? If the  $\text{Gd}_{\text{Tot}}$  is the calculated concentration than the values in Table 6.4.3 do not represent the relative error. Please provide a more consistent comparison by calculating isotope-by-isotope relative error normalized to  $\text{U}^{238}$  final value [Page 6-17].

### AREVA Response

In the  $\text{UO}_2\text{-Gd}_2\text{O}_3$  Gedeon 1 and 2 experimental programs, the available measurements for the  $\text{UO}_2\text{-Gd}_2\text{O}_3$  samples are the ratio of each Gd isotope over total Gd. Therefore the C/M comparisons are presented in the same manner in order to be consistent with the measurement values. The  $\text{U}^{238}$  concentration was not measured on these samples, so providing a result normalized to  $\text{U}^{238}$  final value is not possible.

The  $\text{Gd}_{\text{Tot}}$  concentration is not measured for each irradiated sample. The initial composition of the fuel is given and is used as an input to APOLLO2-A. The  $\text{Gd}_{\text{Tot}}$  concentration used in the comparisons to measurements is identical to the initial  $\text{Gd}_{\text{Tot}}$  concentration, since the  $\text{Gd}_{\text{Tot}}$  concentration remains relatively constant throughout the irradiation (absorbent Gd isotopes primarily remain Gd after absorption of a neutron, and the amount of Gd created by fission is negligible).

The results are presented in terms of absolute differences since relative differences are not pertinent when low concentration ratios are considered; for example, for a 12 GWd/t sample of the Gedeon 2 experimental program, the ratio of  $\text{Gd}^{155}$  over  $\text{Gd}_{\text{Tot}}$  is [ ] and the ratio of  $\text{Gd}^{157}$  over  $\text{Gd}_{\text{Tot}}$  is [ ] so presenting comparisons in terms of relative differences would indicate that significant differences exist, but are actually insignificant since these isotopes have almost completely been depleted.

**RAI 20** It would be useful to display the post-gad burnout agreement on non-gad isotopes. This provides a measurement validation of the behavior of gadolinia fuel after the gad is predominantly depleted. [Page 6-17].

### AREVA Response

In the  $\text{UO}_2\text{-Gd}_2\text{O}_3$  Gedeon 1 and 2 experimental programs, measurements of actinide concentrations were only performed up to approximately [                      ]. This is at a burnup prior to gad burn-out. Therefore, there are no measurements available after the gadolinia is burned-out.

**RAI 21** Section 7.3.1 states that “Generally, the cross-sections for the ARTEMIS reflector model are transformed into microscopic cross sections.” Please explain under which conditions this transformation is done and why? Please clarify which model is used for the benchmarks [Page 7-3].

**AREVA Response**

The microscopic representation of the reflector cross sections is the standard model. All calculations in the Topical Report were performed using the standard model. The macroscopic model is available in ARTEMIS for internal comparisons with other AREVA codes. It is not AREVA’s intent to use the macroscopic reflector cross section representation.

The advantage of the microscopic representation is a more explicit treatment of the non-linearity of the moderator density.

**RAI 22** For “heavy reflectors”, (reflectors comprised of a thick steel shroud and low moderation inside the core barrel), the water scattering cross sections are calibrated with factors “deduced from the comparison of the 2D power density distribution calculated by ARTEMIS with the corresponding reference MCNP result”. The methodology used to “deduce” these factors should be documented and some justification should be made as to the application of the modified scattering cross section to other plant/fuel types. A quantification of the magnitude of the calibration should also be provided. [Page 7-4]

### AREVA Response

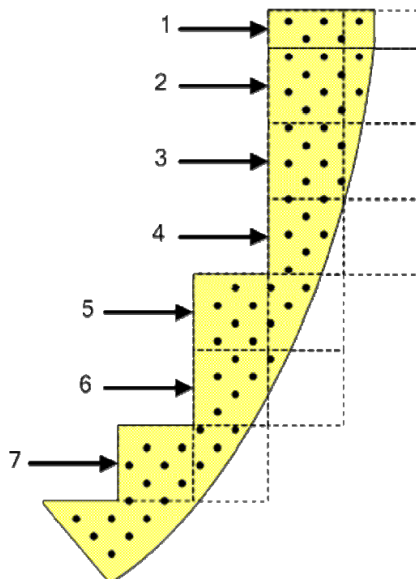
The 1D spectral geometries with reflective boundary conditions used for deriving the cross sections for the radial reflector neglect transverse leakage (2D) effects. For the heavy reflector this leads to discrepancies between ARTEMIS and MCNP reactor calculations when using non-adapted reflector cross sections.

An iterative procedure, a variant of the simulated annealing algorithm, was developed for the purpose of deriving adaptation factors for the heavy reflector cross sections. The procedure adapts the microscopic slowing-down cross section of H<sub>2</sub>O until spread and standard deviation of the differences of the normalized core wide power density distribution of ARTEMIS and the fission rate distribution of MCNP are minimized. In ARTEMIS the normalized power density and fission rate distribution is consistent.

Two types of adaptation factors were found to be sufficient for avoiding heavy reflector induced in/out or azimuthal trends, one for non in-side (edge) and one for re-entrant (corner) reflector nodes. The classification of the heavy reflector nodes is (see Figure 7.3-2 of the Topical Report):

reflector nodes 1, 2, 3, 4, 6 → edge  
reflector nodes 5, 7 → corner

Figure 7.3-2: Heavy Reflector Geometry



Copy of Topical Report Figure  
7.3-2

---

The resulting adaptation factors are 3.02 for the edge reflector nodes and 4.01 for the corner reflector nodes.

The qualification of the derived heavy reflector cross sections is shown in Figure 7.3-3 of the Topical Report. For this qualification a significant number of core calculations with varying state parameters (variation of boron concentration and moderator temperature) were calculated with ARTEMIS and MCNP and the results compared. In addition these reflector cross sections were applied to an independent core loading pattern. As can be seen in the figure there is no dependence of the spread and the standard deviation on these parameters. The deviations are of the same size as for the cases with standard shroud/water reflector. The variation of the deviations is in the order of magnitude of the Monte Carlo calculation.

**RAI 23** The report states that, regarding power distribution comparison against MCNP, “no in/out or azimuthal trends of the error distribution can be identified”. However, both Figures 7.3-4 and 7.3-5 display clear trends with distance from the reflector (in/out). In both cases, ARTEMIS under-predicts all peripheral assemblies (those next to reflector) and over-predicts most of the assemblies within 2-4 assemblies from the reflector. Furthermore, the case of the heavy reflector significantly under-predicts the power in the center of the core. A very clear radial pattern exists in both figures. [Page 7-6]

### **AREVA Response**

In the view of comparing results from two independent code systems with very different geometry and energy group representation of the reactor problem the agreement demonstrated in Figures 7.3-4 and 7.3-5 is quite satisfactory. The radial reflector determines the core wide in-out tilt of the fast flux and the very local flux shape at the core/reflector interface by the reflection of thermal neutrons. The representation of the radial reflector is not responsible for deviations in individual fuel assembly types or local core regions as long as the differences of the power densities in the core center and at the core periphery are of the same order of magnitude and of the same direction (negative in these cases).

For both sample problems no significant azimuthal variation of the differences can be observed. This confirms the applicability of the corrections for the re-entrant reflector corners for either a “normal” steel/shroud or a heavy reflector as described in the Topical Report.

**RAI 24** Figures 7.3-4 and 7.3-5 look like full core but the documentation states that MCNP was run with octant symmetry. Why are full core results provided?  
[Page 7-5]

**AREVA Response**

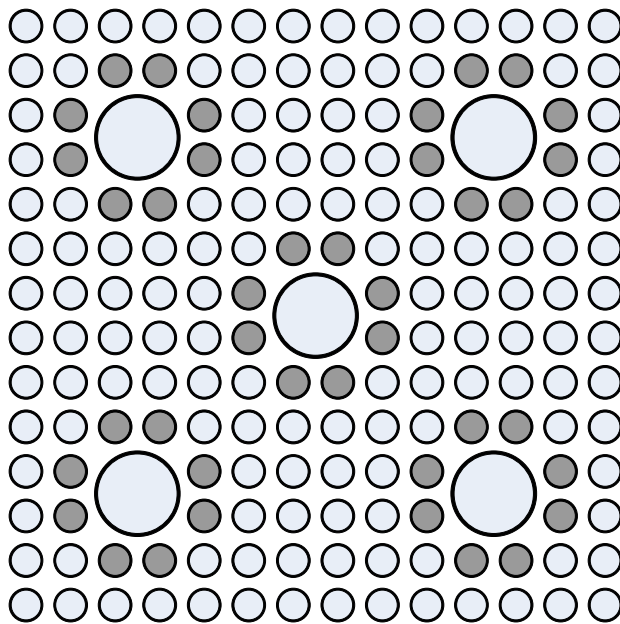
The represented cores are octant symmetric. Nevertheless, the ARTEMIS Calculations were performed in full core geometry. For direct application of existing scripts the MCNP results were unfolded to full core geometry.




**RAI 25** The descriptor “zone-loaded” is used frequently in the benchmarking results section of the report. This term should be defined in the document, possibly with an example image of what it means in terms of lattice enrichment. [Page 10-9]

### AREVA Response

Zone loading of fuel pins is common in CE type assemblies. The zone loaded fuel pins are pins with a lower enrichment that are inserted adjacent to the guide tubes and the instrument tube to reduce power peaking in these locations. A typical zone loaded assembly lattice is shown below:



Rod Type	# of Rods	Rod Description
	136	High Enriched
	40	Low Enriched

**RAI 26** For startup physics test results, the “measured data has been adjusted to reflect the ARCADIA delayed neutron parameters”. This adjustment should be provided in more detail and some quantification or magnitude should be provided in order to assess the impact on the calculation uncertainty. [Page 10-30]

### AREVA Response

Plant measurements are made using a reactivity computer where a calculated set of delayed neutron factors and prompt neutron lifetimes are input. These parameters vary based on the reference data used and the process used to generate these parameters. To compensate for this, an approximation is used to adjust the measured data to be consistent with the ARTEMIS generated delayed neutron fractions and prompt neutron lifetimes. This correction is determined as the ratio of the effective delayed neutron fraction from ARTEMIS ( $\beta_{eff \text{ ARTEMIS}}$ ) to the effective delayed neutron fraction from the measurement ( $\beta_{eff \text{ meas}}$ ). The adjustment is made as

$$\beta_{eff \text{ adjustment}} = \frac{\beta_{eff \text{ Artemis}}}{\beta_{eff \text{ meas}}}$$

The  $\beta_{eff}$  adjustments for Plants A, C, S1 and S2 are provided in the following table to illustrate the typical range for this adjustment.

Cycle	$\beta_{eff}$ adjustment			
	Plant A	Plant C	Plant S1	Plant S2
1				
2				
3				
4				
5				
6				
7				
8				
9				
10				
11				
12				
13				
14				
15				
16				
17				
18				

**RAI 27** The exclusion of Bank D from the startup physics summary for Plant A Cycle 11 is not justified. The fact that the bank met the criterion in previous and subsequent cycles does not prove a measurement anomaly, especially without a detailed analysis of other plant differences (core design, flow conditions, rod shadow, etc). Data should not be manipulated to support the desired conclusions. [Page 10-30 ]

### AREVA Response

The referenced paragraph did not provide enough detail in what the context of “not considered” means. The current pass/fail criterion of 15% or 100 pcm are review criteria for the plant during startup and is being used as a screening criterion for ARCADIA. If all values are less than 15%, then the plant cycles would have passed the startup criteria using ARCADIA. With this screening criterion, one measurement was found that exceeded this criterion with ARCADIA. So the failure rate by ARCADIA for single bank worth comparisons leads to a failure rate of 0.4%. This level of failure rate is reasonably expected. In addition, if we calculate a 95/95 limit for single bank worths for all the plants, it would lead to an uncertainty of less than 15% (see table 27-1). Hence, the ARCADIA prediction for bank D in Plant A Cycle 11 is not considered a failure of ARCADIA. This worth is included in the calculation of total worth.

**Table 27-1, Statistics for Single Bank Worths**

Individual Bank Worth	Mean (%)	Standard Deviation (%)	K factor 265 pts	95/95 Tolerance limit
All plants and cycles	[			]
				<15% criterion

**RAI 28** Plant G1 Cycle's 27 and 28 had a BOC B10 abundance of 19.2%. Also, Cycle's 29 and 30 used enriched B10 at about 30%. The report states that the Cycle 26 HZP boron measurement "may be suspect because of the B10 isotopic abundance was not measured". However, there are no unexpected comparisons at BOC HFP, which indicates that no additional B10 correction should be necessary at HZP. The report does not clearly describe which boron measurements are adjusted for B-10 content, and which are not. B10 corrections, both at HZP and HFP (i.e. B-10 depletion, if included) should be applied consistently for all cycles and should be clearly documented. [Page 10-31,1035]

### AREVA Response

For Cycle 26 of plant G1 the B-10 abundance was not measured, but the measured B-10 abundances are known for Cycles 27 to 30. These abundances are provided below:

Cycle	B-10 Abundance (a/o B-10)
27	19.20
28	19.25
29	31.61
30	31.55

The measured B-10 abundances from Cycles 27 to 30 were used to adjust the respective measured boron concentrations such that they are relative to natural boron.

For Cycle 26, where no measured B-10 abundance is available, an assumed boron abundance of 19.2 a/o B-10 (Cycle 27 value) is used.

Erroneously the critical boron adjustment in Table G1 10.3.4-1 and in Figure G1 10.4.4-1 of the Topical Report for Cycle 26 was applied to the calculated values to make them relative to the measured B-10 abundance instead of using the assumed measured B-10 abundance to adjust the measured critical boron concentrations such that they are relative to concentrations with natural boron. The values have been updated and are presented in Table 28-G1-1 and Figure 28-G1-1 (see below).

Moreover, in the Tables and Figures of Appendices G1 and G2 an inconsistency in the results has been corrected. The B-10 abundance of natural boron was assumed to be 19.74 a/o when adjusting the measured values, whereas ARTEMIS uses the value 19.9 a/o. To compare boron concentrations directly it is necessary that the adjusted measured boron concentrations correspond to the ARTEMIS B-10 abundance, so in the following tables and figures the measured boron concentrations have been adjusted to correspond to a B-10 abundance of 19.9 a/o.

These corrections have been applied and are shown in Table 28-G1-1, Table 28-G2-1, Figures 28-G1-1 through 28-G1-5 and Figures 28-G2-1 through 28-G2-5.

Plant/Cycle	Measured (ppm)	Calculated (ppm)	Difference C-M (ppm)
G1 Cycle 26	1628	1596	-32
G1 Cycle 27	1764	1757	-7
G1 Cycle 28	1638	1593	-45
G1 Cycle 29	1689	1648	-41
G1 Cycle 30	1760	1716	-44

**Table 28-G1-1: Plant G1 Hot Zero Power All Rods Out Critical Boron Concentrations for Cycles 26-30**

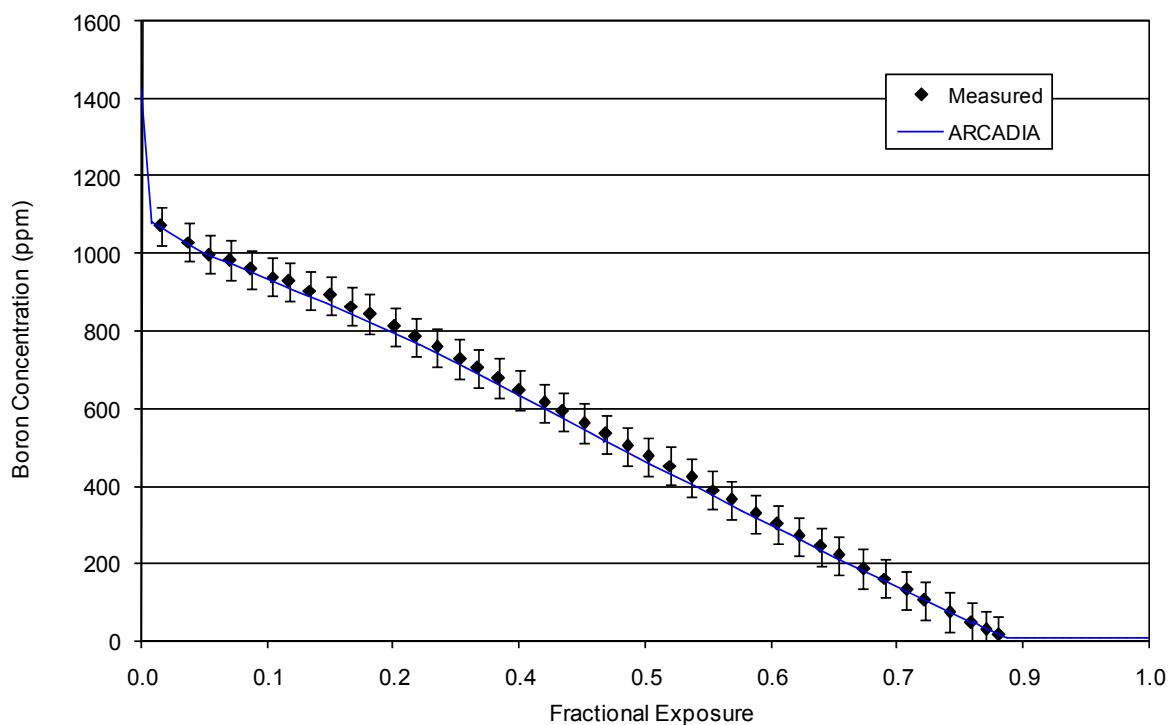


**Figure 28-G1-1: Plant G1 Cycle 26 Critical Boron Concentration vs. Burnup**

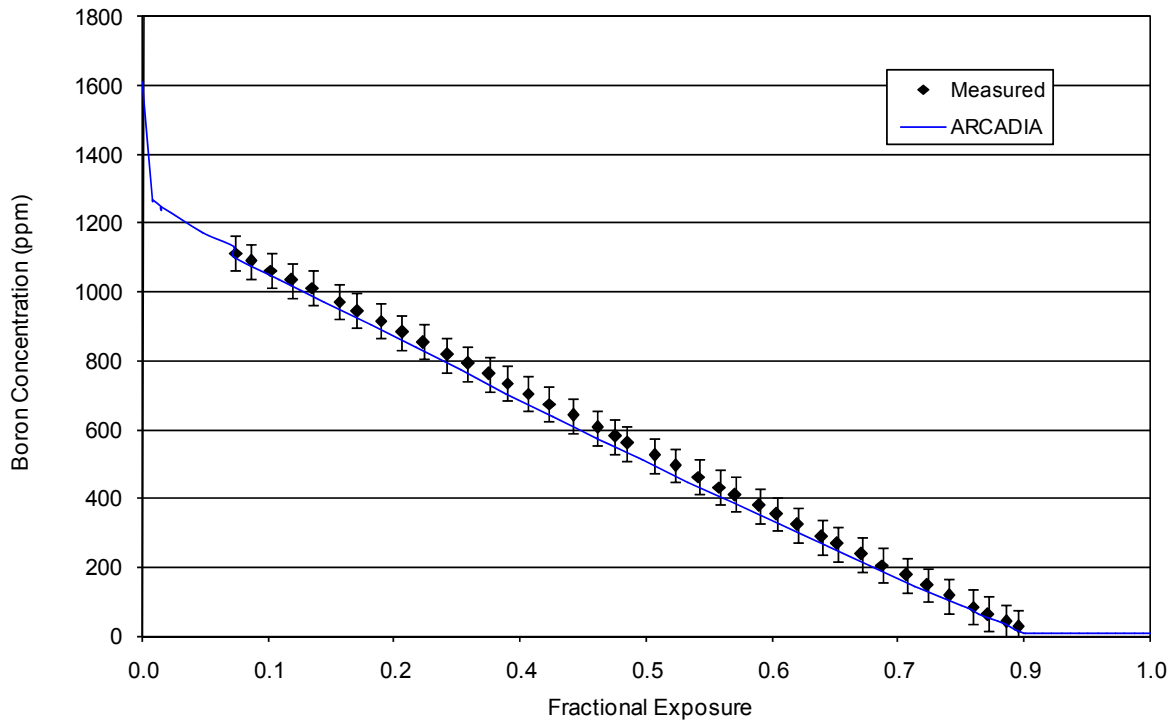


**Figure 28-G1-2: Plant G1 Cycle 27 Critical Boron Concentration vs. Burnup**

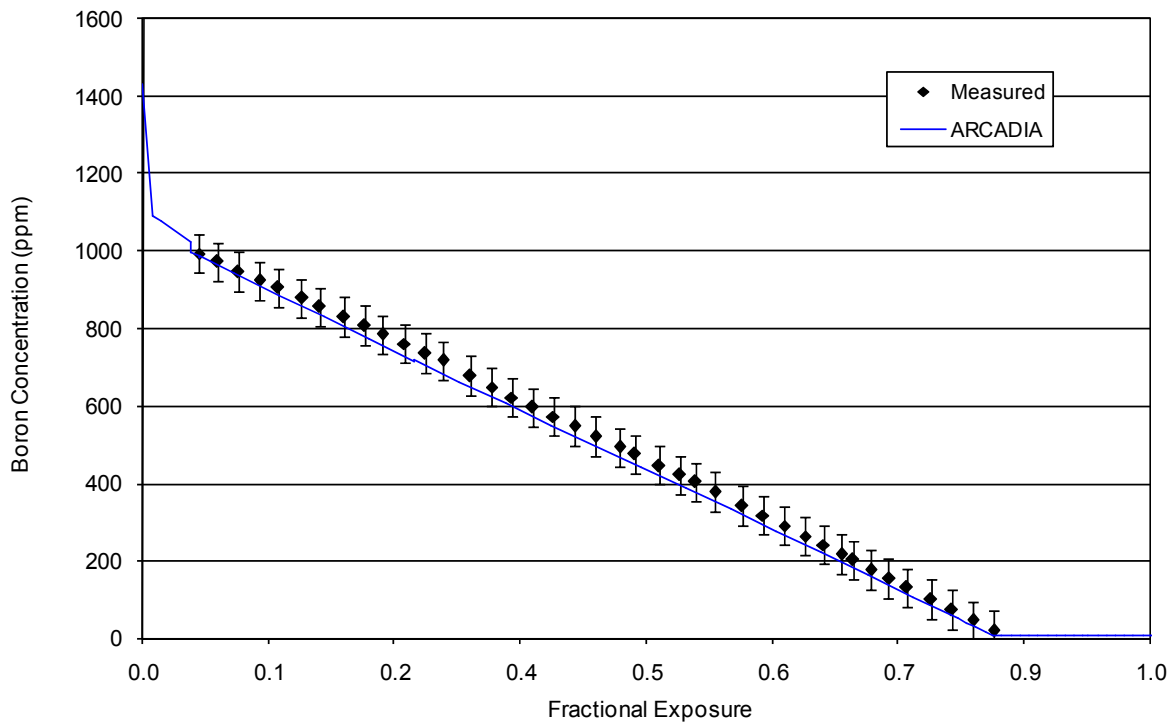


**Figure 28-G1-3: Plant G1 Cycle 28 Critical Boron Concentration vs. Burnup**

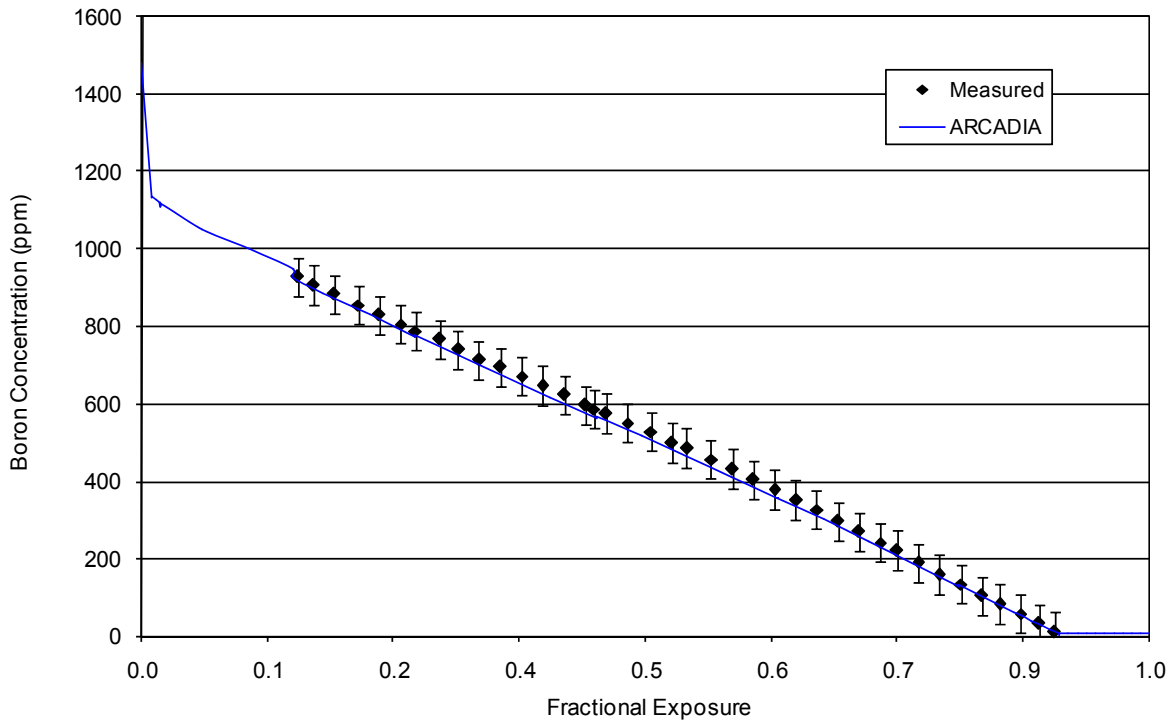


Figure 28-G1-4: Plant G1 Cycle 29 Critical Boron Concentration vs. Burnup

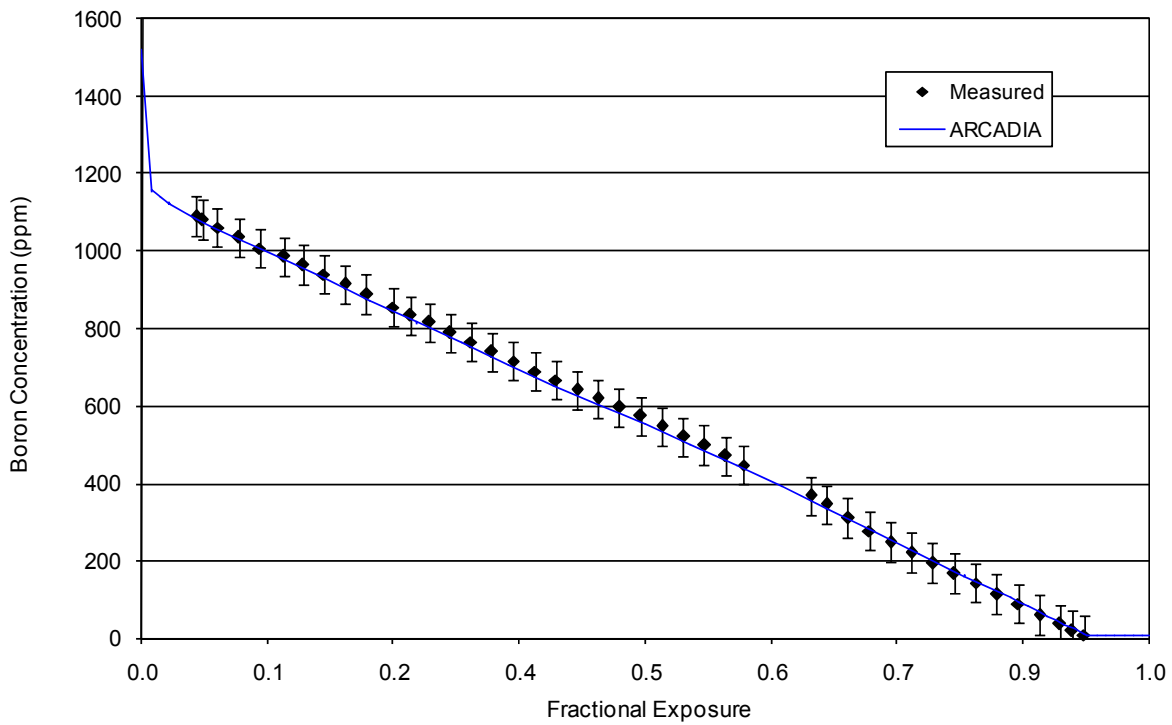
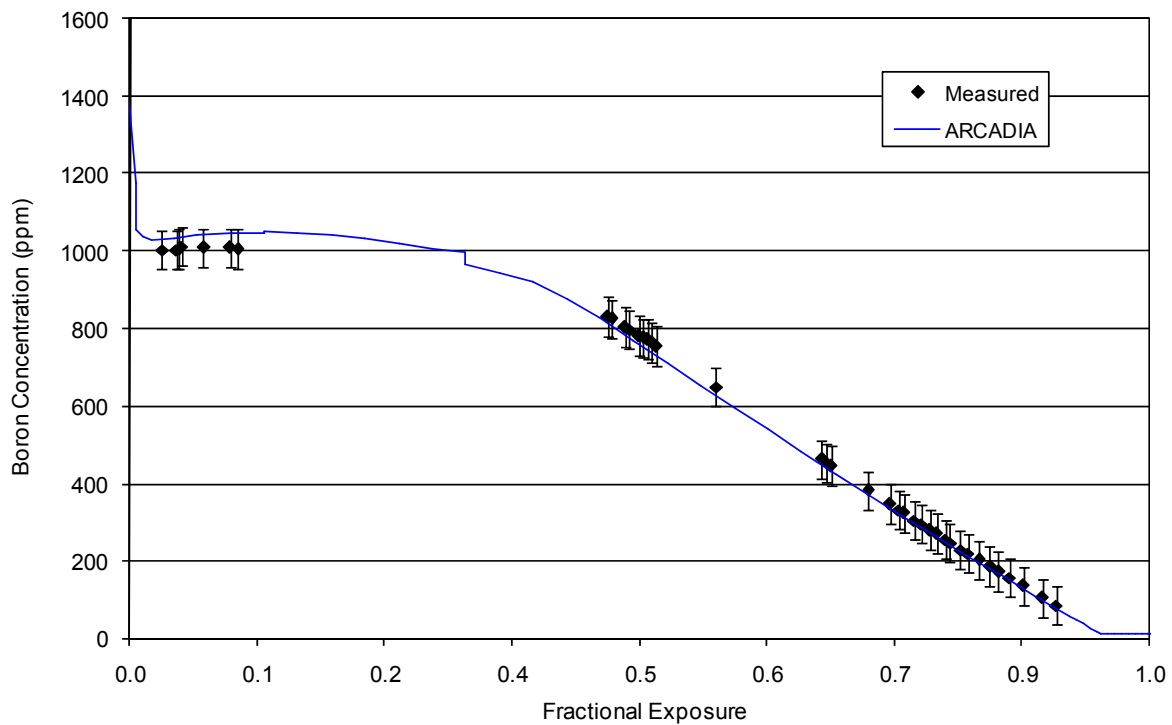


Figure 28-G1-5: Plant G1 Cycle 30 Critical Boron Concentration vs. Burnup

Plant/Cycle	Measured (ppm)	Calculated (ppm)	Difference C-M (ppm)
G2 Cycle 1	1426	1445	19
G2 Cycle 2	1407	1383	-24
G2 Cycle 3	1543	1520	-23
G2 Cycle 4	1396	1381	-15
G2 Cycle 5	1528	1499	-29

**Table 28-G2-1: Plant G2 Hot Zero Power All Rods Out Critical Boron Concentrations for Cycles 1-5**



**Figure 28-G2-1: Plant G2 Cycle 1 Critical Boron Concentration vs. Burnup**



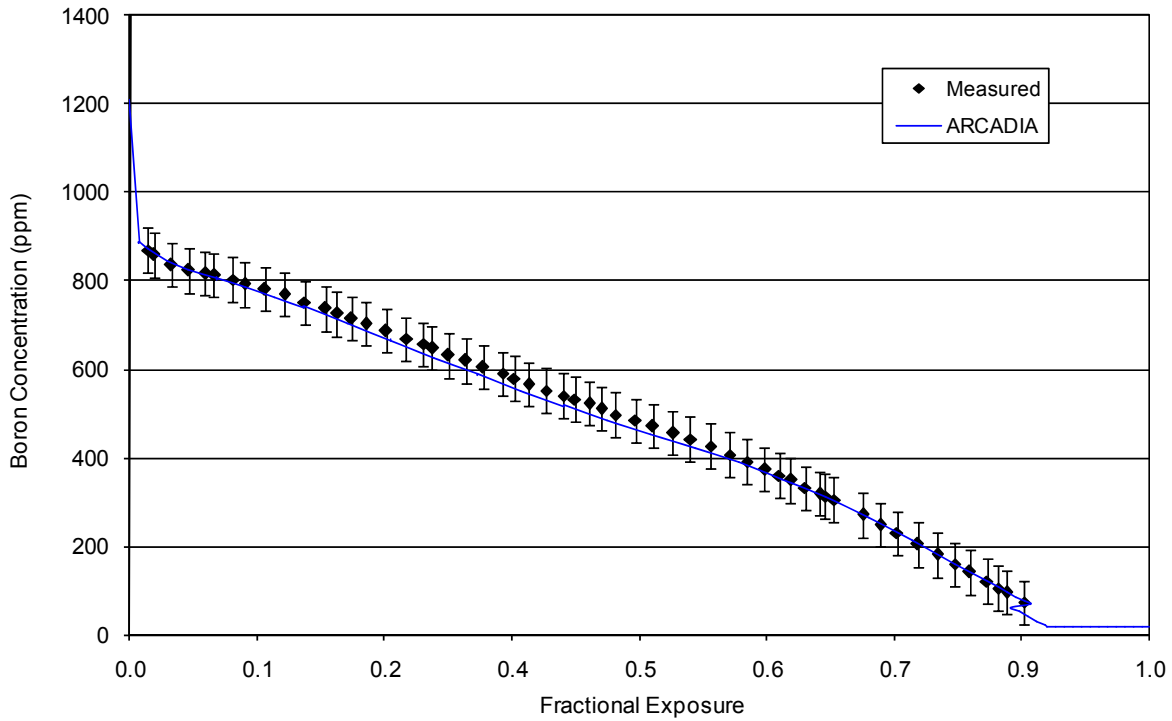


**Figure 28-G2-2: Plant G2 Cycle 2 Critical Boron Concentration vs. Burnup**

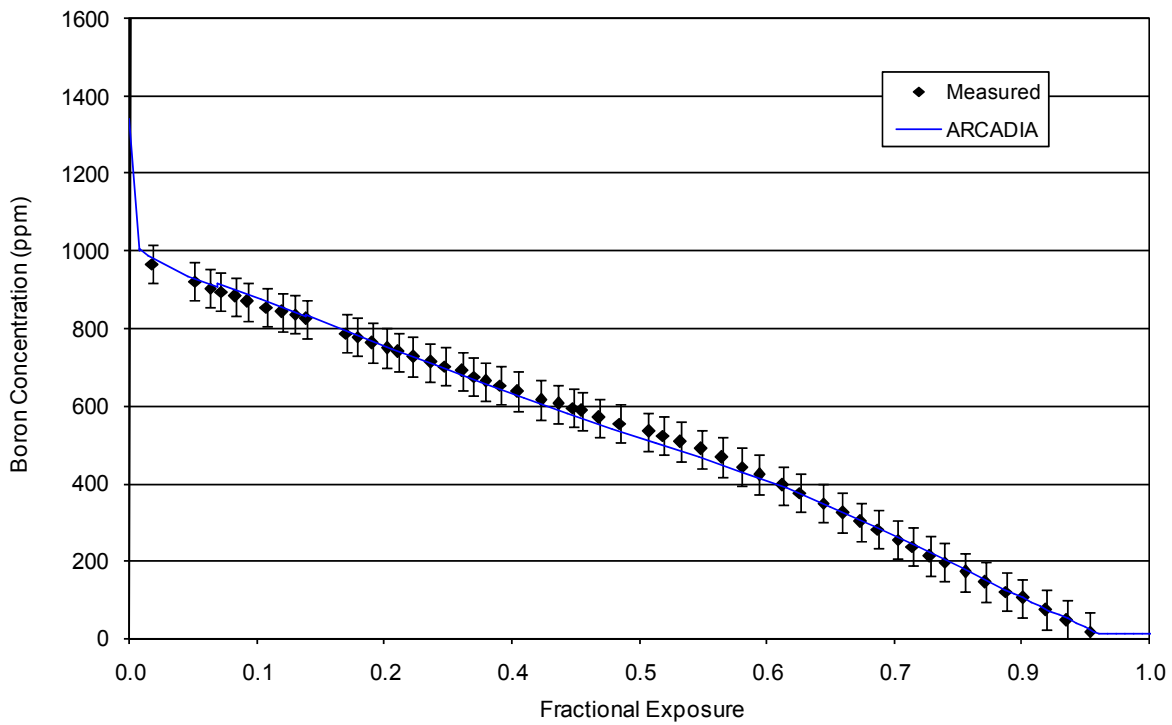


**Figure 28-G2-3: Plant G2 Cycle 3 Critical Boron Concentration vs. Burnup**

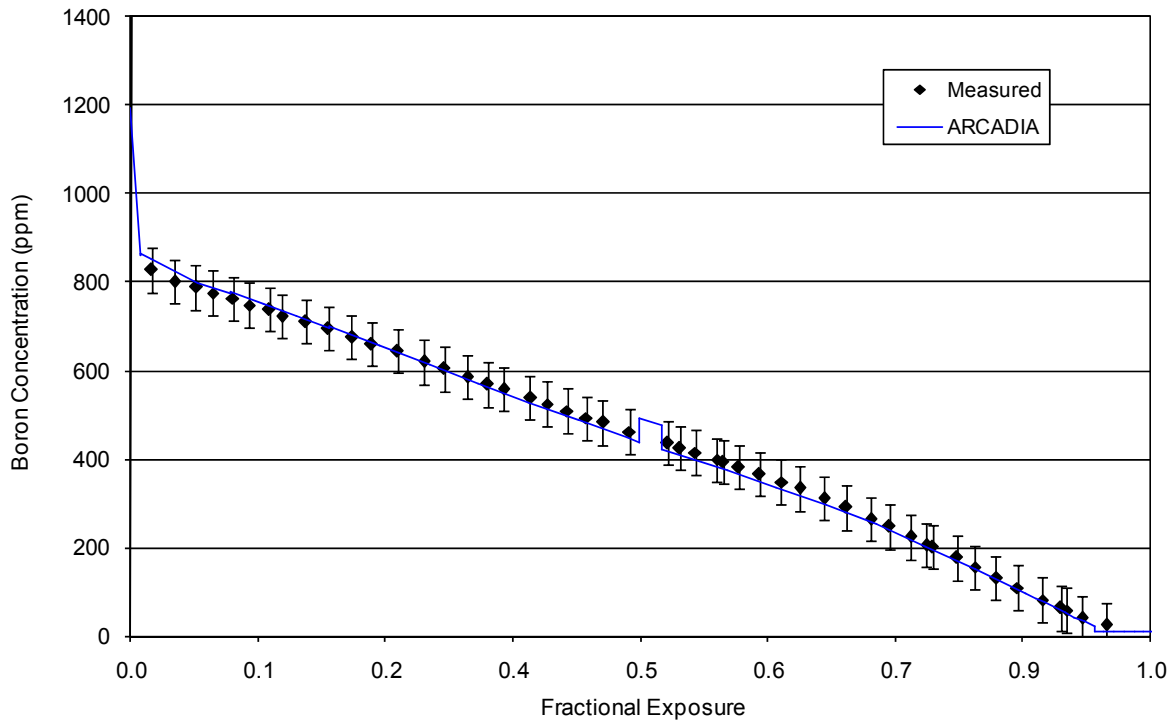


**Figure 28-G2-4: Plant G2 Cycle 4 Critical Boron Concentration vs. Burnup**

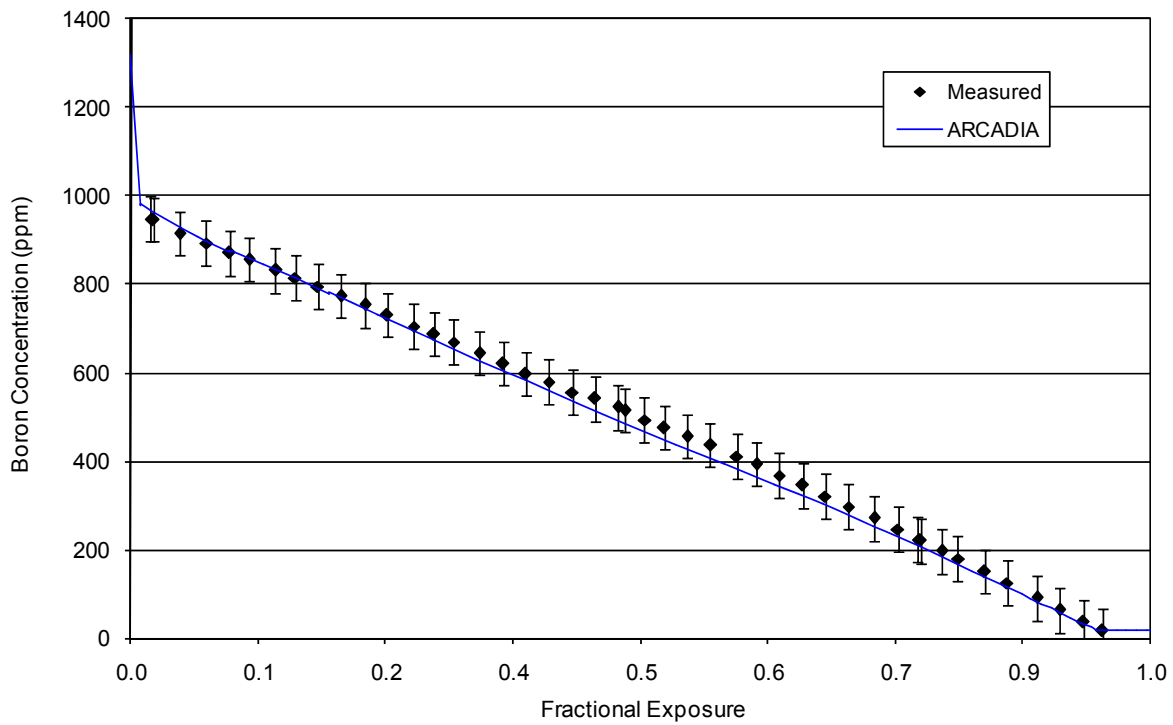


**Figure 28-G2-5: Plant G2 Cycle 5 Critical Boron Concentration vs. Burnup**

**RAI 29** The reference to 9 cycles cannot be located. Is this intended to be nine cycles per plant (for a typical licensee/operator)? This may have been removed in the latest version of the referenced ANSI/ANS standard. [Page 10-32]

### AREVA Response

A review of the ANSI/ANS-19.6.1-2005 standard does not specify a requirement for a specific number of cycles to be considered. Supplying a reference for this criterion was unintentional. Also Reference 10.6-2 should have specified the 2005 standard (Reference 1) and not the 1995 standard. Reference 10.6-2 will be corrected in the approved version of the ARCADIA® topical report. It is proposed that the wording of the paragraph in question be changed as follows:

*Core follow comparisons include two different plant/fuel types with additional data, as available from Siemens type reactors. A minimum of nine cycles of operation should be considered with at least three cycles of operations per plant type. Core follow predictions are compared to the available data measured at, or near, hot full power for each cycle of each plant/fuel type. The parameters compared are...*

### Reference

1. Reload Startup Physics Tests for Pressurized Water Reactors, ANSI/ANS-19.6.1-2005, American Nuclear Society, 2005.

**RAI 30** In support of the global peak statistics, more core maps displaying the radial distribution of the total (3d) peaking differences would be beneficial. Currently only distributions for the radial and axial core averages are displayed. [Page 12-25]

### AREVA Response

Core maps of peak power comparisons are provided. For each detector location, the measured peak power value within the assembly was determined and compared with the corresponding calculated peak power at that node. The difference between measured and calculated peak power values is given as  $(\text{calculated} - \text{measured}) * 100$ .

[

]

The power maps provided support the conclusion and the uncertainties generated for the ARCADIA® system.



Figure 30-A-1: BOC 11 Peak Power Comparison

Figure 30-A-2: MOC 11 Peak Power Comparison

Figure 30-A-3: EOC 11 Peak Power Comparison

Figure 30-A-4: BOC 12 Peak Power Comparison



Figure 30-A-5: MOC 12 Peak Power Comparison

Figure 30-A-6: EOC 12 Peak Power Comparison

Figure 30-A-7: BOC 13 Peak Power Comparison

Figure 30-A-8: MOC 13 Peak Power Comparison

Figure 30-A-9: EOC 13 Peak Power Comparison

Figure 30-A-10: BOC 14 Peak Power Comparison

Figure 30-A-11: MOC 14 Peak Power Comparison

Figure 30-A-12: EOC 14 Peak Power Comparison



Figure 30-C-1: BOC 14 Peak Power Comparison

Figure 30-C-2: MOC 14 Peak Power Comparison

Figure 30-C-3: EOC 14 Peak Power Comparison

Figure 30-C-4: BOC 15 Peak Power Comparison

Figure 30-C-5: MOC 15 Peak Power Comparison

Figure 30-C-6: EOC 15 Peak Power Comparison

Figure 30-C-7: BOC 16 Peak Power Comparison

Figure 30-C-8: MOC 16 Peak Power Comparison



Figure 30-C-9: EOC 16 Peak Power Comparison

Figure 30-C-10: BOC 17 Peak Power Comparison

Figure 30-C-11: MOC 17 Peak Power Comparison

Figure 30-C-12: EOC 17 Peak Power Comparison

Figure 30-C-13: BOC 18 Peak Power Comparison

Figure 30-C-14: MOC 18 Peak Power Comparison

Figure 30-C-15: EOC 18 Peak Power Comparison

Figure 30-G1-1: BOC 26 Peak Power Comparison



Figure 30-G1-2: MOC 26 Peak Power Comparison

Figure 30-G1-3: EOC 26 Peak Power Comparison

Figure 30-G1-4: BOC 27 Peak Power Comparison

Figure 30-G1-5: MOC 27 Peak Power Comparison

Figure 30-G1-6: EOC 27 Peak Power Comparison

Figure 30-G1-7: BOC 28 Peak Power Comparison

Figure 30-G1-8: MOC 28 Peak Power Comparison

Figure 30-G1-9: EOC 28 Peak Power Comparison



Figure 30-G1-10: BOC 29 Peak Power Comparison

Figure 30-G1-11: MOC 29 Peak Power Comparison

Figure 30-G1-12: EOC 29 Peak Power Comparison

Figure 30-G1-13: BOC 30 Peak Power Comparison

Figure 30-G1-14: MOC 30 Peak Power Comparison

Figure 30-G1-15: EOC 30 Peak Power Comparison

Figure 30-G2-1: BOC 3 Peak Power Comparison

Figure 30-G2-2: MOC 3 Peak Power Comparison



Figure 30-G2-3: EOC 3 Peak Power Comparison

Figure 30-G2-4: BOC 4 Peak Power Comparison

Figure 30-G2-5: MOC 4 Peak Power Comparison

Figure 30-G2-6: EOC 4 Peak Power Comparison

Figure 30-G2-7: BOC 5 Peak Power Comparison

Figure 30-G2-8: MOC 5 Peak Power Comparison

Figure 30-G2-9: EOC 5 Peak Power Comparison

Figure 30-S1-1: BOC 12 Peak Power Comparison



Figure 30-S1-2: MOC 12 Peak Power Comparison

Figure 30-S1-3: EOC 12 Peak Power Comparison

Figure 30-S1-4: BOC 13 Peak Power Comparison

Figure 30-S1-5: MOC 13 Peak Power Comparison

Figure 30-S1-6: EOC 13 Peak Power Comparison

Figure 30-S1-7: BOC 14 Peak Power Comparison

Figure 30-S1-8: MOC 14 Peak Power Comparison

Figure 30-S1-9: EOC 14 Peak Power Comparison



Figure 30-S2-1: BOC 12 Peak Power Comparison

Figure 30-S2-2: MOC 12 Peak Power Comparison

Figure 30-S2-3: EOC 12 Peak Power Comparison

Figure 30-S2-4: BOC 13 Peak Power Comparison

Figure 30-S2-5: MOC 13 Peak Power Comparison

Figure 30-S2-6: EOC 13 Peak Power Comparison

Figure 30-S2-7: BOC 14 Peak Power Comparison

Figure 30-S2-8: MOC 14 Peak Power Comparison



Figure 30-S2-9: EOC 14 Peak Power Comparison

Figure 30-T1-1: BOC 12 Peak Power Comparison

Figure 30-T1-2: MOC 12 Peak Power Comparison

Figure 30-T1-3: EOC 12 Peak Power Comparison

Figure 30-T1-4: BOC 13 Peak Power Comparison

Figure 30-T1-5: MOC 13 Peak Power Comparison

Figure 30-T1-6: EOC 13 Peak Power Comparison

Figure 30-T1-7: BOC 14 Peak Power Comparison



Figure 30-T1-8: MOC 14 Peak Power Comparison

Figure 30-T1-9: EOC 14 Peak Power Comparison

Figure 30-T1-10: BOC 15 Peak Power Comparison

Figure 30-T1-11: MOC 15 Peak Power Comparison

Figure 30-T1-12: EOC 15 Peak Power Comparison

Figure 30-V1-1: BOC 18 Peak Power Comparison

Figure 30-V1-2: MOC 18 Peak Power Comparison

Figure 30-V1-3: EOC 18 Peak Power Comparison



Figure 30-V1-4: BOC 19 Peak Power Comparison

Figure 30-V1-5: MOC 19 Peak Power Comparison

Figure 30-V1-6: EOC 19 Peak Power Comparison

Figure 30-V1-7: BOC 20 Peak Power Comparison

Figure 30-V1-8: MOC 20 Peak Power Comparison

Figure 30-V1-9: EOC 20 Peak Power Comparison

Figure 30-V1-10: BOC 21 Peak Power Comparison

Figure 30-V1-11: MOC 21 Peak Power Comparison



Figure 30-V1-12: EOC 21 Peak Power Comparison

Figure 30-V1-13: BOC 22 Peak Power Comparison

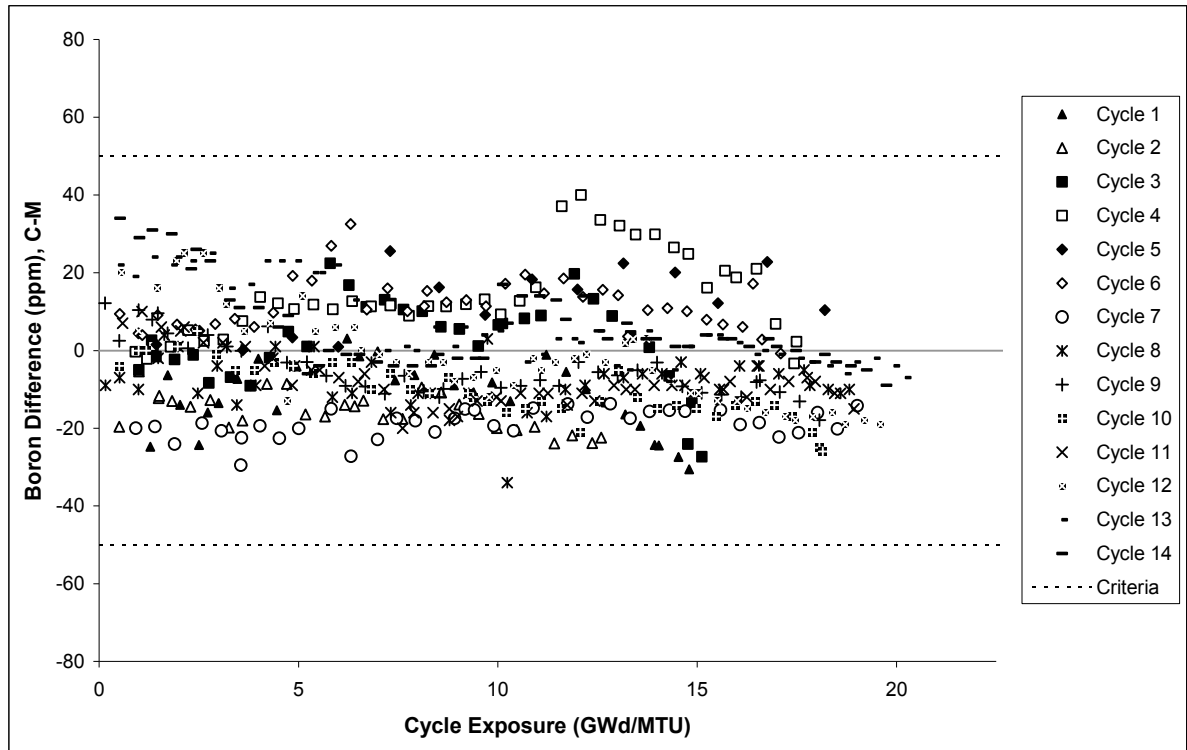
Figure 30-V1-14: MOC 22 Peak Power Comparison

Figure 30-V1-15: EOC 22 Peak Power Comparison

**RAI 31** The boron letdown curves are presented for each cycle individually as a function of fractional cycle length. This scale is confusing because it prevents some comparisons from cycle to cycle, and inhibits the ability to approximate cycle length-based effects, such as gadolinia depletion, B-10 depletion, and design implications for 24 vs 12 month cycles, etc. Furthermore, the letdown curves are presented on an absolute value scale, which makes individual deviations very hard to discern. A summary plot of boron difference for all cycles (to compare against each other, potential by plant), plotted versus a non-relative scale such as cycle exposure would be useful. [Page A-9+]

### AREVA Response

Summary plots of the boron deviations are provided. These plots use an absolute scale for burnup and present the boron deltas for all cycles by plant.



**Figure 31-A-1: Boron Differences**

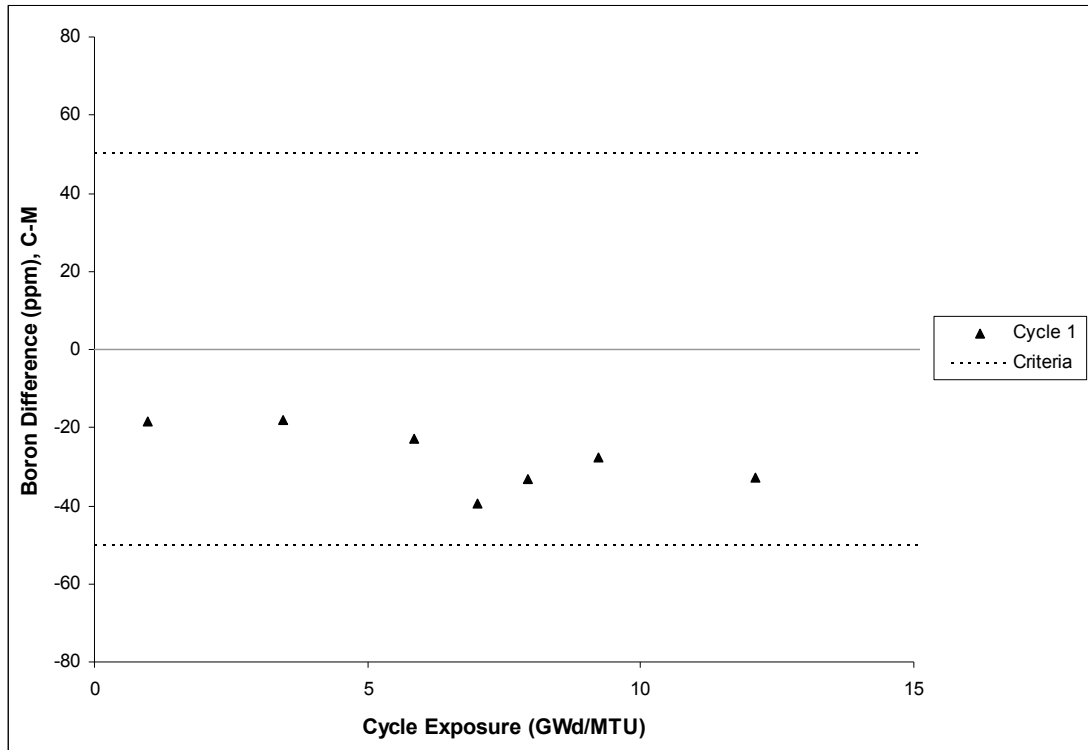


Figure 31-B-1: Boron Differences

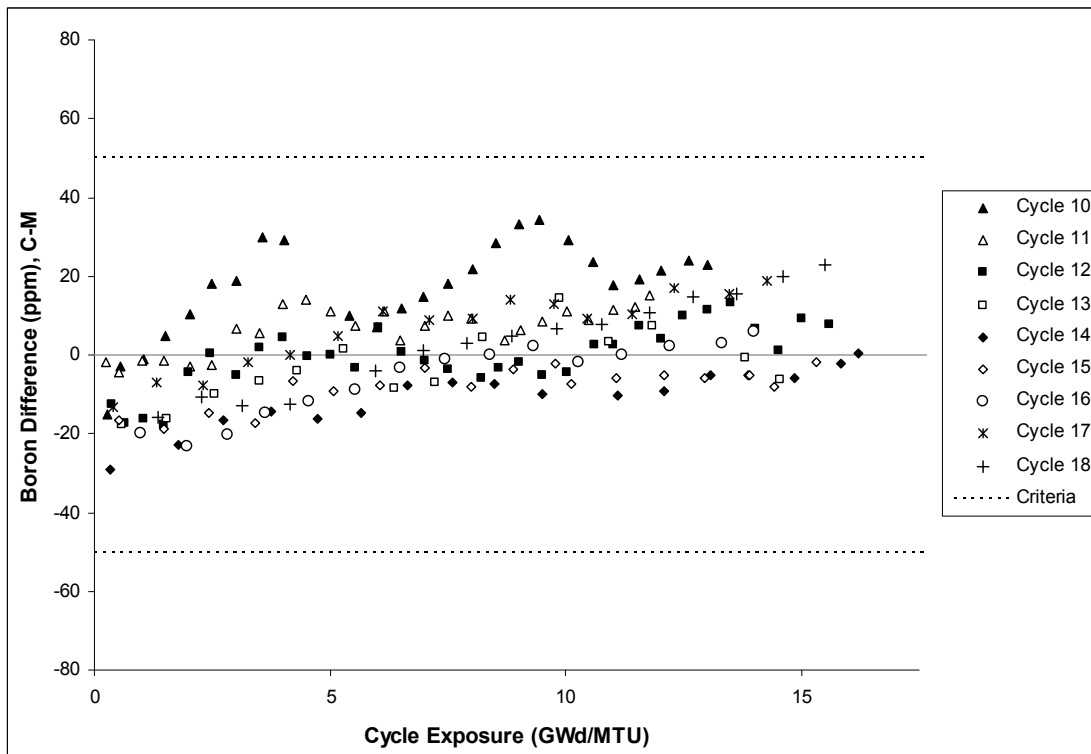


Figure 31-C-1: Boron Differences

Responses to Requests for Additional Information for the Review of THE ARCADIA®  
Reactor Analysis System for PWRs Methodology Description and Benchmarking Results  
Topical Report

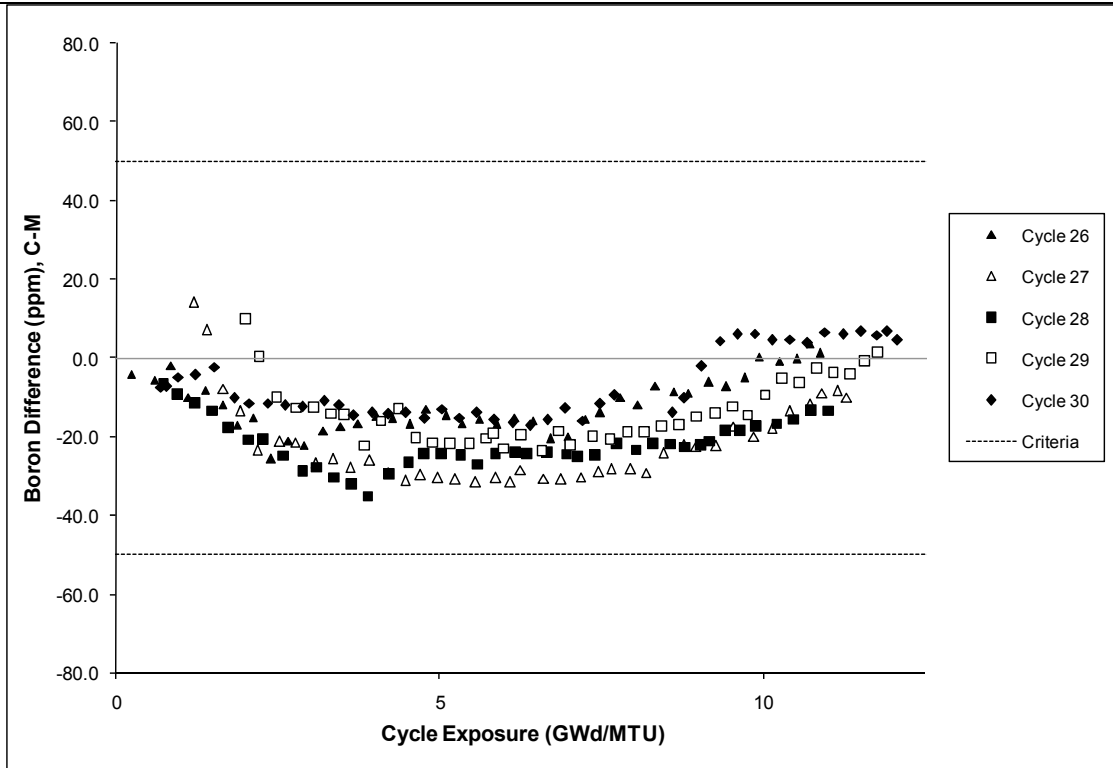


Figure 31-G1-1: Boron Differences

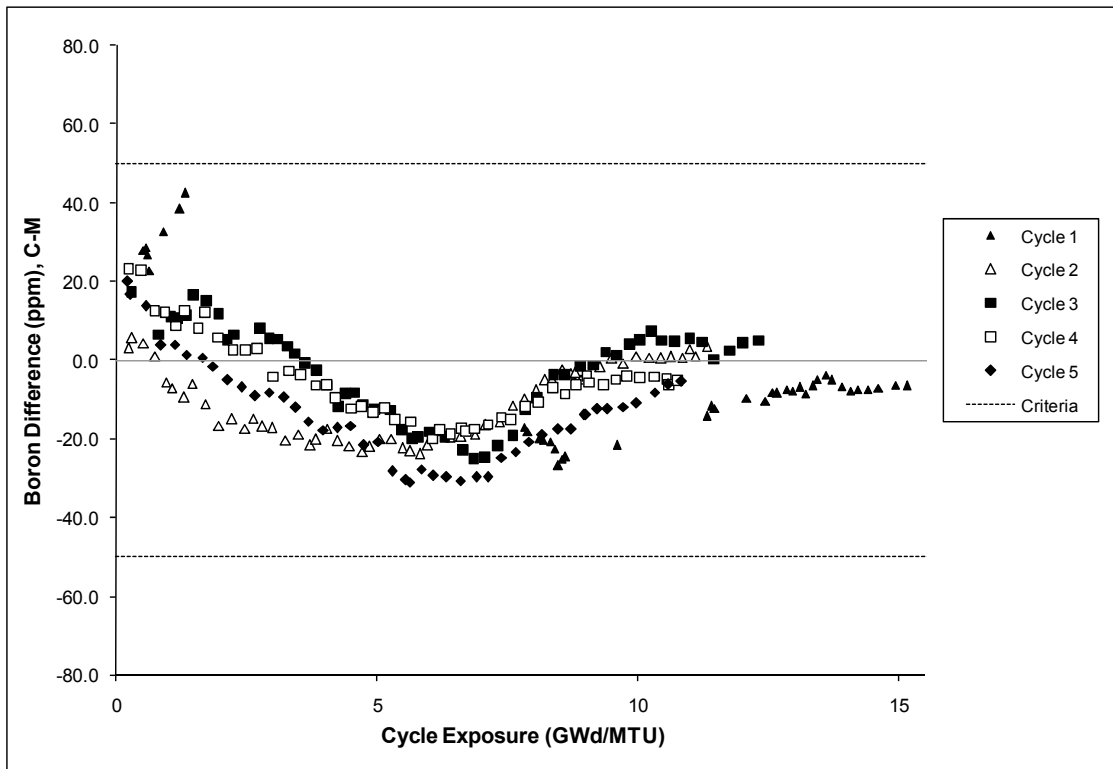


Figure 31-G2-1: Boron Differences

Responses to Requests for Additional Information for the Review of THE ARCADIA<sup>®</sup>  
Reactor Analysis System for PWRs Methodology Description and Benchmarking Results  
Topical Report

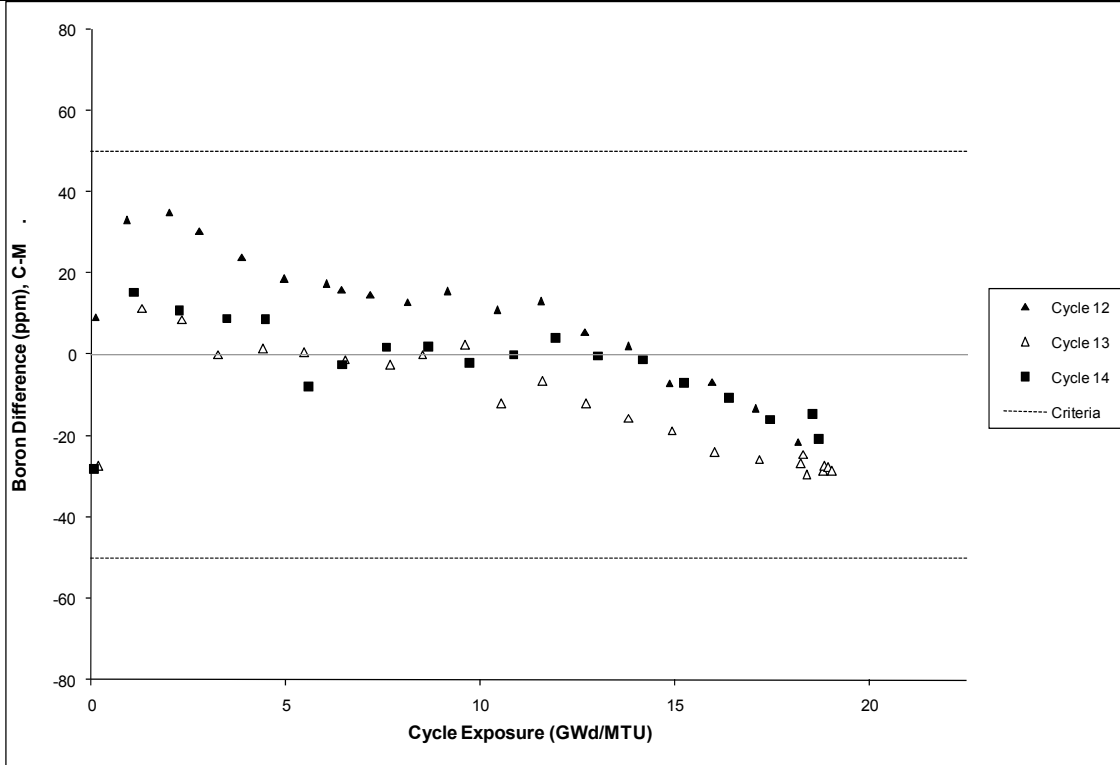


Figure 31-S1-1: Boron Differences

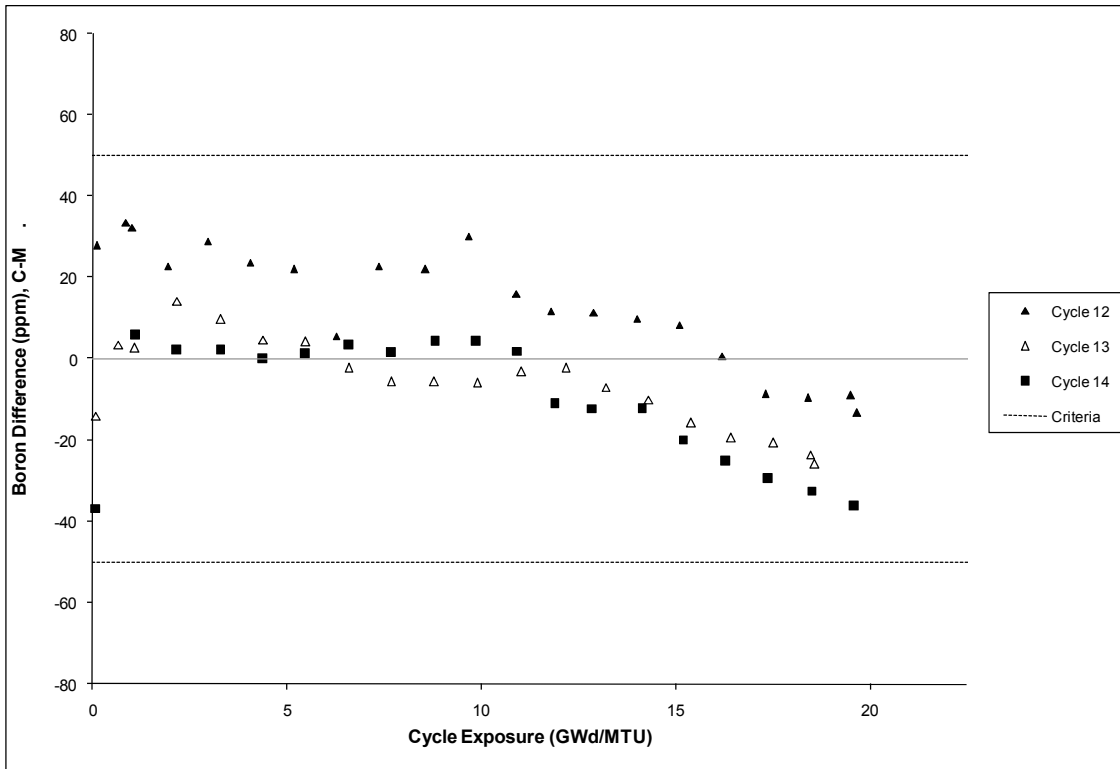


Figure 31-S2-1: Boron Differences



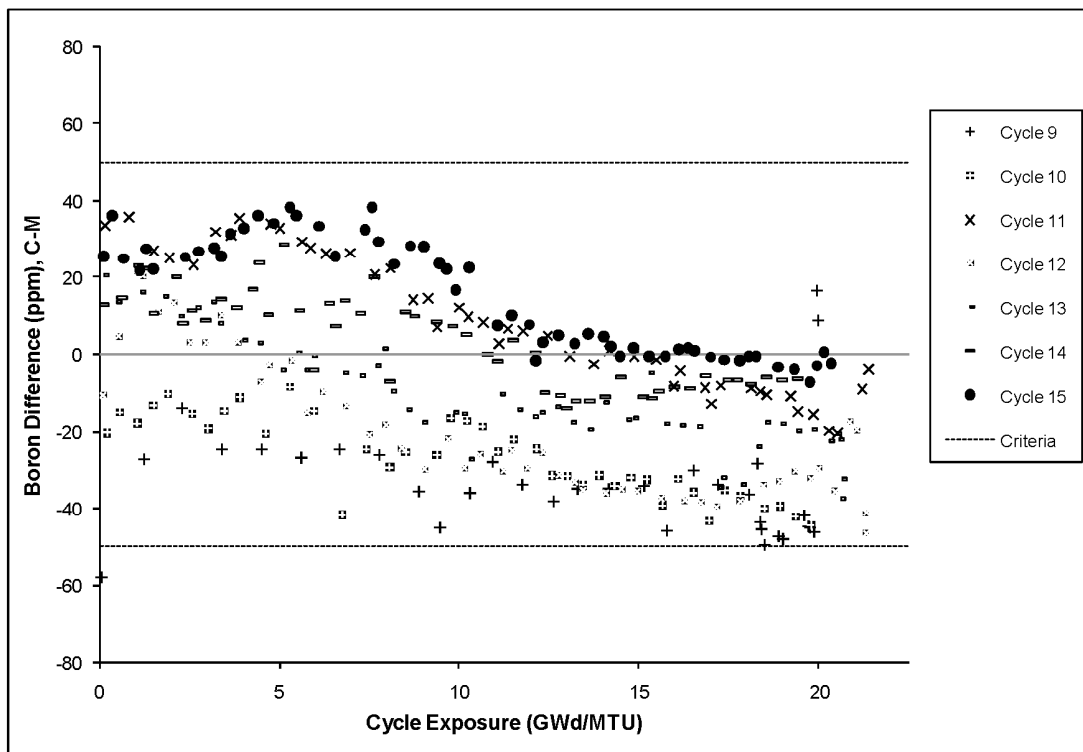


Figure 31-T1-1: Boron Differences

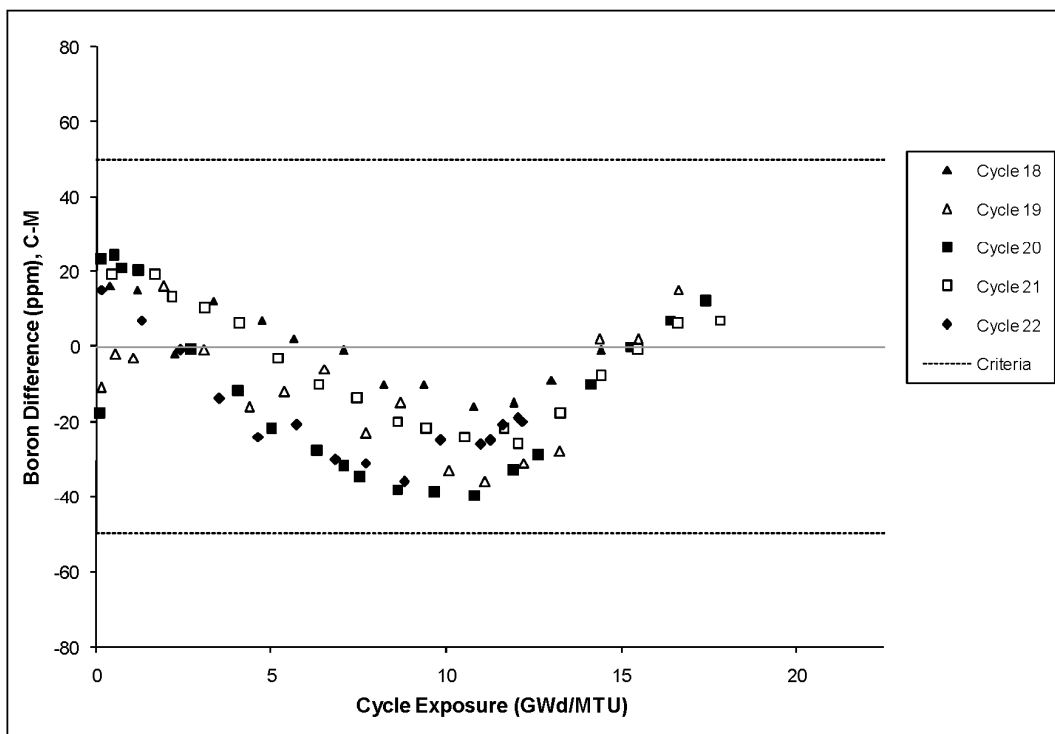


Figure 31-V1-1: Boron Differences

**RAI 32** For the boron comparison cases where the 50 ppm B criteria was not met, a less conservative 500 pcm criteria was selected? Was measured or calculated boron worth used, or predicted differential boron worth? For the cycles with known differences in B- 10 isotopic abundance, was the boron worth used (if predicted) adjusted to account for the different B-10 content? [Page 10-29, 10-30, etc]. if the calculated boron worth is used , justify using the calculated boron worth when the error in the calculated boron concentration exceed the first criteria ?

### AREVA Response

The HZP boron concentration differences (C-M) for Cycles 7 and 8 of Plant A and Cycle 10 of Plant T1 exceed the 50 PPM criterion. No measured boron worths were available for Plant A. Therefore, the respective calculated boron worths were used to make the adjustments for Cycle 7 and 8 of Plant A. A measured boron worth was available for Cycle 10 of Plant T1 and this measured boron worth was used to make the adjustment.

In all cycles of plant A, the measured boron concentrations were adjusted to account for the measured B-10 content. The boron worth calculation is based on the ARTEMIS B-10 content of 19.9 at%. Boron worth measurements are available for some of the benchmark cycles. Therefore, boron worth predictions were made for these cycles and compared to the measured values. Comparisons for plants A, S1 and S2 are shown in the following tables:

Cycle	Measured (pcm/ppm)	Calculated (pcm/ppm)	Difference (C-M) (pcm/ppm)
1	-10.5	-10.43	0.07
2	-8.29	-8.268	0.02
3	-7.67	-7.944	-0.27
4	-7.86	-7.697	0.16
9	-6.42	-6.519	-0.10

**Table 32 -1, Plant A Boron Worth Comparisons**

<b>Cycle</b>	<b>Measured (pcm/ppm)</b>	<b>Calculated (pcm/ppm)</b>	<b>Difference (C-M) (pcm/ppm)</b>
S1, 12	-7.18	-6.93	0.25
S1, 13	-6.88	-6.93	-0.05
S1, 14	-7.04	-6.88	0.16
S2, 12	-7.05	-6.70	0.35
S2, 13	-6.99	-6.72	0.27
S2, 14	-6.92	-6.75	0.17

**Table 32-2, Plant S1 and S2 Boron Worth Comparisons**

These comparisons show good agreement between the predicted and measured boron worths and justify the use of a calculated boron worth to make the adjustment between boron and reactivity.

The response to RAI 28 shows that after the data were properly adjusted for plant G1 that all data met the 50 ppm criterion. Therefore, this question no longer applies to G1.

**RAI 33** For critical boron concentration comparisons, the differential boron worth (DBW) is used to adjust the measured concentration to ARO conditions. It would be prudent to compare measured and predicted boron worths from each cycle's ZPPT, if available. If the predicted boron worth is used to convert the 500 pcm criteria to boron concentration, then the DBW validation may be more important. [Page 10-3]

**AREVA Response:**

See the response to RAI 32.

**RAI 34** Rod worth results may have different uncertainties and biases for different measurement techniques (i.e. rod swap may be more accurate than boron swap). It would be beneficial to provide the rod worth measurement technique with each set of results and attempt to provide a conclusion about the accuracy of the methods vs. each technique. [A-1]

**AREVA Response:**

The table below shows the rod worth measurement technique used for each of the benchmarked plants and cycles. Plants G1 and G2 are not included because bank worth measurement are not performed for these plants.

Cycle	Plant						
	A	B	C	S1	S2	T1	V1
1	Boron Swap	Rod Swap					
2	Rod Swap						
3	Rod Swap						
4	Rod Swap						
5	Rod Swap						
6	Rod Swap						
7	Rod Swap						
8	Rod Swap						
9	Rod Swap					Boron Swap	
10	Rod Swap					Boron Swap	
11	Rod Swap					Boron Swap	
12	Rod Swap					Boron Swap	
13	Rod Swap					Boron Swap	
14	Rod Swap					Boron Swap	
15						Boron Swap	
16						Boron Swap	
17							
18							Boron Swap
19							Boron Swap
20							Boron Swap
21							Boron Swap
22							Boron Swap

The rod swap measurement technique has been employed by the nuclear industry to help reduce the time required for startup physics testing. The boron swap method has fewer predictions/uncertainties associated with it. The rod swap method has uncertainties associated with the prediction of the reference bank position, the actual measured reference bank position, the test bank position, the measured reference bank worth, and the rod shadowing factors. The boron swap has uncertainties associated with the positions of the individual banks, boron measurements and the shadowing effects of other rods present in the core. However, in the boron swap method it can be difficult to control the dilution and rod pulls to ensure that overshoots or undershoots on reactivity do not occur which can add to the uncertainty of this method.

Since measurements were performed using both techniques, a statistical comparison can be performed. The statistics for the differences in total bank worth  $((C-M)/M*100)$  for the boron swap, rod swap techniques and the combined measurements are provided below:

Boron Swap				
Rod Swap				
Combined				

The above statistics show that the two measurement techniques used are consistent for the cycles analyzed. The boron swap method does produce a lower standard deviation but has a higher bias. Both methods are statistically within the  $\pm 10\%$  criterion on total rod worth. This is also consistent with the ANSI standard (which uses the same criterion for both rod swap and boron swap).

**RAI 35** For the power uncertainty statistics, the normality of each population of interest should be stated along with the mean and standard deviation. For normal distributions, it is beneficial to also provide the tolerance factors used for the uncertainty calculations. [12-24,12-25]

**AREVA Response:**

The technique does not require normality since the more limiting uncertainty of either a normal or non-parametric uncertainty is used. The frequency distributions are provided to show that the statistical sampling is visually Gaussian (nearly normal) and not too abnormal (no double peaks or large skews). The statistics for the uncertainty calculations are shown in Table 35-1.

**Table 35-1: Uncertainties Assuming Normality\***

	FΔH	FQ
Critical Experiments Mean/Standard Deviation /df		
Multi-assembly Mean/Standard Deviation /df		
Core Mean/Standard Deviation /df		
Total Standard Deviation		
Combined Degrees of Freedom		
95/95 K Factor		
Uncertainty (rounded up) Assuming Normality		

\* Values for mean, standard deviation , and uncertainty are in percent.

**RAI 36** For local peaking uncertainty, the report states that “No biases are observed around water holes or poisons.” However, in most of the cases (Cores 4, 5, 12, 14, 18), the fuel rod next to the instrument tube has a much higher error than most or all of the other fuel rods. In Core 18, another rod next to the large water hole also has a much higher error. Final, the gadolinia fuel pins in Cores 5, 14, and 20 clearly demonstrate a substantial bias (up to 6% deviation) as compared to non-gadolinia fuel rods. [Page 12-3]

### AREVA Response

Each of the statements in this request is addressed below. The statement “No biases are observed around water holes or poisons” is made relative to biases that have been seen with previous methods that are no longer seen with APOLLO2-A. [

] APOLLO2-A uses Method of Characteristics with neutron transport and does not exhibit this behavior.

The bias around the instrument cell is [

] The overall statistics in Table 36-1 [ ] improves over the standard deviation used for the uncertainty analysis in Section 12.

In Core 18, the average and standard deviation of all the pins around the water hole in Figure 12.2.1-5 is [

] Hence, this higher deviation around the water hole in Core 18 is seen as a normal variation that is not statistically significant.

The % bias in the Gadolinia pins is discussed. The absolute error as described in response to RAI 14 is similar for all the pins indicating that the error is related to the physical measurement accuracy of the system and is not related to the accuracy of the prediction. Alternatively, if the large power prediction bias is caused by the strong



absorptions of the Gd isotopes, the power is low and the bias in the power prediction is of no safety significance. Once the Gd155 and Gd157 isotopes are depleted, the power in the pin approaches the UO<sub>2</sub> power and the cause of the bias no longer exists. Hence, the bias in the Gad pins observed in these critical experiments is not applicable to high powered Gad pins.

Nonetheless, it is worthwhile to examine the biases to determine if there could be a systematic bias in the predicted or measured results for these very low powered Gad pins. From a methods standpoint [

Responses to Requests for Additional Information for the Review of THE ARCADIA®  
Reactor Analysis System for PWRs Methodology Description and Benchmarking Results  
Topical Report

[

]

In conclusion, the bias seen in these results for the Gad pins is more indicative of the ability to measure the power of the low powered Gad fuel pin than the ability of APOLLO2-A to predict the power.

**Table 36-1. Statistics with Rh Modeled.**

Core	Number of Samples	Observed Mean	Observed Deviation	Measured Deviation	Estimated Calculated Deviation
Core 1					
Core 12					
Core 18					
All Non-Gad					
Core 5					
Core 14					
Core 20					
Gad Cores					
All Cores					

**Table 36-2. Test Rod Physical Properties**

	Gad Rod	2.46 w/o rod	4.02 w/o rod
Clad OD, in	0.475	0.4748	0.4755
Clad Thickness, in	0.032	0.032	0.016
Clad Material	Al 6063	Al 6061	SS 304
Fuel Form	Pellet	Pellet	Powder
Fuel OD	0.4055	0.4054	0.444
Fuel Density	9.99	10.24	9.46

### Figures 36-1 Core 1



**Figure 36-2 Core 5**



**Figure 36-3 Core 12**



**Figure 36-4 Core 14**



**Figure 36-5 Core 18**





**Figure 36-6 Core 20**



**Figure 36-7. Decay Heat Between Gad and UO2 Rod for Same Initial Power  
[(G-U)/U]\*100%**



**RAI 37** A cumulative standard deviation is provided for the Global Radial Statistics in Table 12.4.1-1, but not for the Global Peak Statistics in Table 12.4.1-2. [Page 12-25]

**AREVA Response:**

As described in the text, the cumulative statistics for this table are not provided because each plant can have a bias relative to the measurement of the grid depressions which does not reflect the calculational accuracy. The text on page 12-13 contains the combined statistics with a mean of [ ] and a standard deviation of [ ] after the bias is removed for each plant.

**RAI 38** The local peaking uncertainty analyses exclude fuel pins with relative power less than 0.8, including gadolinia rods. For Cores 5, 14, 20, the non-gad pin power standard deviation is approximately the same as the experiments without gad, Cores 1, 12, and 18. [Page 12-16] However, the application range states that the comparisons included “Gadolinium poison up to 10 weight percent in U fuel.” The report does not calculate the uncertainty of the fuel rods which contain gadolinia (which is calculated with up to 6% error), and does not by any other means justify the use of a power-producing gadolinia rod within the application range. [Page 13- 2]

### AREVA Response

The apparent bias in the Gad pins as described in the response to RAI 36 is believed to be related to characterization of the measurement rather than the accuracy of the code. Even if the strong absorption in the Gad rod created a prediction bias, the powers are so low (<0.8) that an increased uncertainty has no real impact on the safety significance of the plant. In addition, after the parasitic isotopes are depleted, the prediction bias is removed from the calculation and no longer affects the ability to predict the resultant power of the pins. Hence, the ability of the code to predict the neutronic behavior of the burned Gad pin is similar to that of the UO<sub>2</sub> pin and a different uncertainty is not needed. The ability of ARTEMIS to predict the Gad powers relative to APOLLO2-A is included in the multi-assembly calculations.

The 10 wt% Gad is based upon Plant V1 Cycles 18 through 22 where fresh fuel assemblies containing 10 wt% Gad pins were loaded. The global peak and global radial statistics for the V1 plant are within the range of those calculated for the other plants as shown in Table 38-1. Therefore, the fuel with 10 wt% Gad in UO<sub>2</sub> has similar statistics to other cores and the conclusions of this Topical Report are also valid for this fuel.

**Table 38-1. Comparison of Plant V1 (contains fuel with 10% Gad) with other plants**

	Low	Plant V1	High
Global Radial mean			
Global Radial $\sigma$			
Global Peak mean*			
Global Peak $\sigma$			

\* This value is strongly dependent upon the grid type and measurement system and the results for those plants with the same type of measurement system and grid type are listed.

**RAI 39** Gadolinia rod power comparison in the multi-assembly calculations with APOLLO2-A and ARTEMIS demonstrate that the agreement gets better as the gadolinium isotopes deplete, but it shows that the uncertainty at 10 GWd/mtU may be as high as the uncertainty at 0.1 GWd/mtU. [Page 12-37]

**AREVA Response:**

Your observation is correct. The errors look similar to the low burnup case. The peaking in the Gad pins is still below 0.8 power at 10.0 GWd/mtU and the parasitic Gadolinium isotopes are not completely depleted. These cases are being pooled with the low burnup cases and discarded as not limiting. The statistics of the Gad pins for powers less than 0.8 are a mean of [ ] and a standard deviation of [ ] which is slightly worse than the statistics for all pins with powers over 0.8 (mean of [ ] and a standard deviation of [ ] ).

**RAI 40** Please provide more detail about how the “grid bias” is calculated and removed from each plant. [Page 12-13]

**AREVA Response:**

The grid bias is seen in many of the Average Axial Power Distribution Figures in the appendix. For those plants with fine axial measurements with grid depressions, the measured result between the grids is generally higher than the calculated result with homogenized grid model. Figure S2 10.47-13 on page S2-15 illustrates this effect for a moveable incore measurement system. In addition, this effect depends upon the grid type and the type of measurement system. In Figure C 10.4.3-55 on page C-62, the measurement system uses fixed incores which are discrete and incapable of measuring the grid depressions. Plants G1 and G2 have an Aeroball system which does not have as fine of an axial resolution as the moveable detectors and the grid depressions are more spread out. Inconel grids with more parasitic properties than Zirconium alloys would have deeper depressions and higher measured peaks than a calculation that homogenizes the grids. For calculational models with homogenized grids, a power peaking bias or uncertainty is applied to account for the grid. As an example, the Inconel grid factor for B&W plants prior to introduction of Zirconium alloy grids was 1.026 multiplier (2.6%) and the Zirc4 grid factor was 1.01 (1%). To estimate the calculational error of a model that is independent of the grid type and measurement system, the bias of the results is removed by multiplying the results by the bias calculated for each plant. These bias adjustments are very close to the grid multipliers for the respective grid type and are a reasonable approach.

**RAI 41** Please provide Multi-Assembly summary statistics at the bottom of Table 12.2.2-2. [Page 12-18].

**AREVA Response:**

The term “color set” in Section 2 is synonymous with “Multi-Assembly” in Section 12. The mean and standard deviation is [                      ], respectively and are listed in Table 12.3.1-2 under the label colorsets.

**RAI 42** Please provide more details in Figures 12.2.2-1 to 12.2.2-6. What are the units of the values shown? Is it C-M or M-C, for instance? [Page 12-33 to 12-38]

**AREVA Response:**

These are the percent differences between ARTEMIS and APOLLO2 {(ARTEMIS – APOLLO2) / ARTEMIS\*100%}.



**RAI 43** The error bars on the boron letdown curves appear to be the +/-50 ppm criteria. They are too big to be measurement uncertainty.

**AREVA Response:**

It is correct that the error bars on the boron letdown curves indicate the  $\pm 50$  ppm criterion and not a measurement uncertainty.

**RAI 44** The average axial power shapes of plants C & T appear to be smooth extrapolations of fixed incore detectors. The type of detectors should be provided for each plant, and if the measured axial distribution is calculated from a limited number of fixed signals, the method used for performing the extrapolation should be documented. [Page 10-33]

**AREVA Response:**

The measurement systems used in the benchmarked plants are included in the following table:

Plant	Measurement System
A	Moveable Fission Detector
B	Moveable Fission Detector
C	Fixed Rhodium Detector
G1	Moveable Vanadium Aeroballs
G2	Moveable Vanadium Aeroballs
S1	Moveable Fission Detector
S2	Moveable Fission Detector
T1	Fixed Rhodium Detectors
V1	Moveable Fission Detector

The generation of the “measured axial power shape” from a limited number (N) of axially fixed incore detectors is defined by the following process (Reference [1]):

Predicted (ARTEMIS) power distributions are generated at each axial detector level by axially integrating the predicted axial power distribution over the axial segment of the core corresponding to the detector height. Predicted detector signals are similarly generated at each axial detector level. The ratio of the predicted powers to the predicted signals is used to convert measured signals to measured/inferred powers at each axial detector level.

The above inferred power distribution, corresponding to the N axial detector levels, is expanded into 24 equidistant axial nodes as follows: A predicted 24 equidistant node axial power distribution is generated by axially integrating the predicted axial power distribution over 24 equidistant axial nodes. For each axial detector level, the ratio of the inferred axial power and the calculated axial power is calculated in order to convert the predicted 24 equidistant node axial powers to the measured/inferred 24 equidistant node axial powers.

For equidistant nodes whose centerline lies within a detector span, the ratio from that detector level is used. For nodes below the bottom detector level, the ratio from the bottom detector level is used. For equidistant nodes above the top detector level, the ratio from the top detector level is used. For equidistant nodes whose centerline lies between 2 detector spans, the ratio is determined by linearly interpolating the values from the 2 adjacent detector segments.

The 24 equidistant axial node powers in the detected locations is then expanded to the undetected locations in the same manner as used for INPAX-W. The inferred distribution is then renormalized to an average value of 1.0 to produce the final three dimensional nodal power distribution.

#### Reference

1. AREVA NP Document, XN-NF-83-01(P), EXXON Nuclear Analysis of Power Distribution Measurement Uncertainty for St. Lucie Unit 1, January 1983

**RAI 45** A summary plot of the difference between calculated and measured axial offset, by cycle, would be beneficial. This may help to discern if the core average axial shape is contributing to the peak assembly power deviations.

**AREVA Response:**

Summary plots showing the calculated to measured AO differences at the points in cycle that are consistent with the core average power maps. This was done so that the measured AO values are consistent with the predicted values. The plots of showing the AO differences are given below:

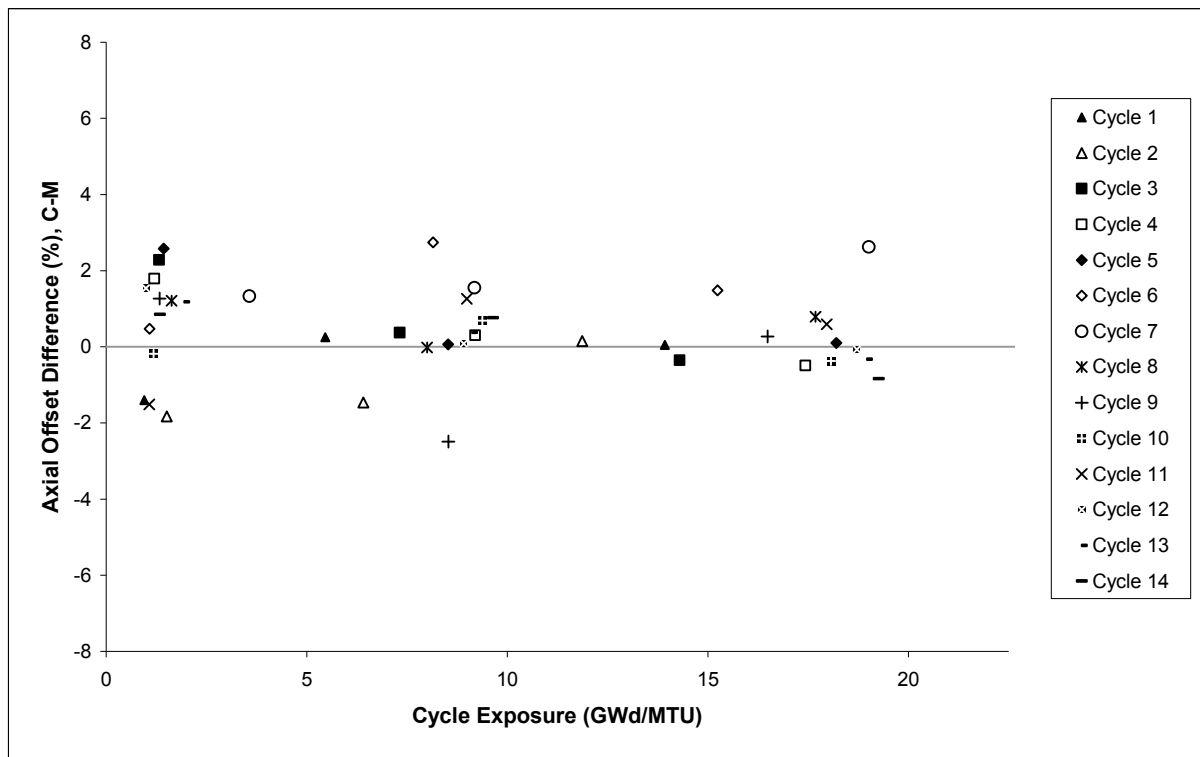


**Figure 45-A-1: AO Comparisons**

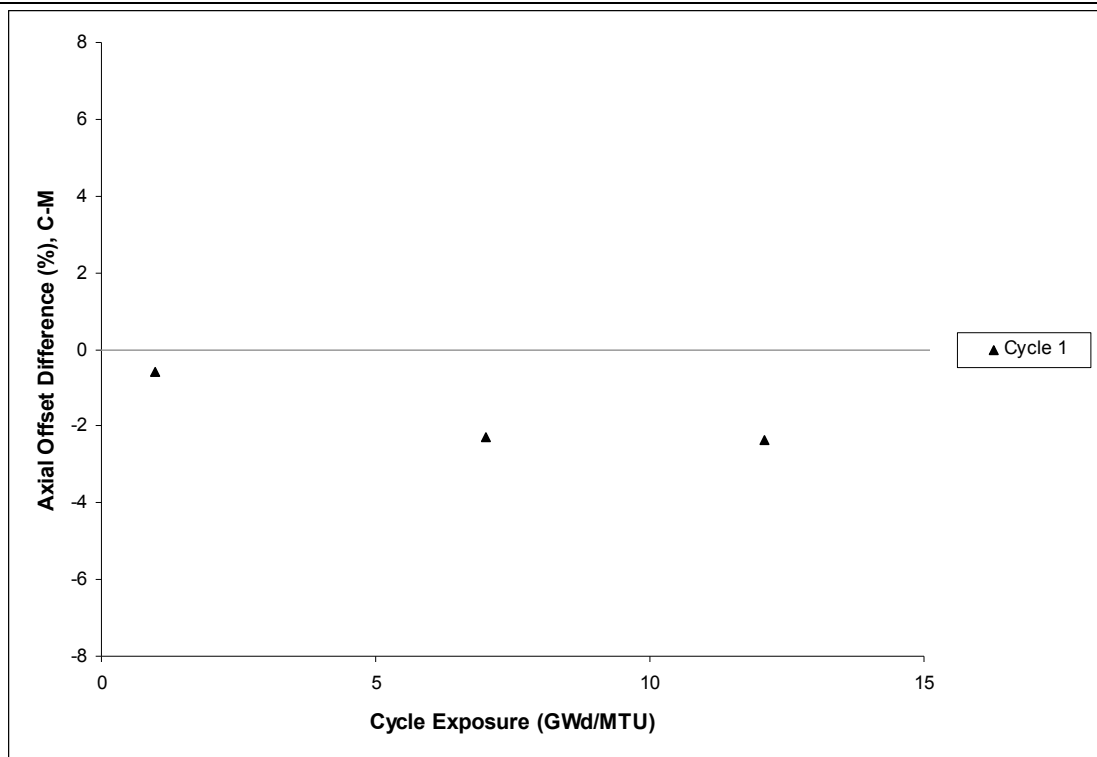


Figure 45-B-1: AO Comparisons

Figure 45-C-1: AO Comparison

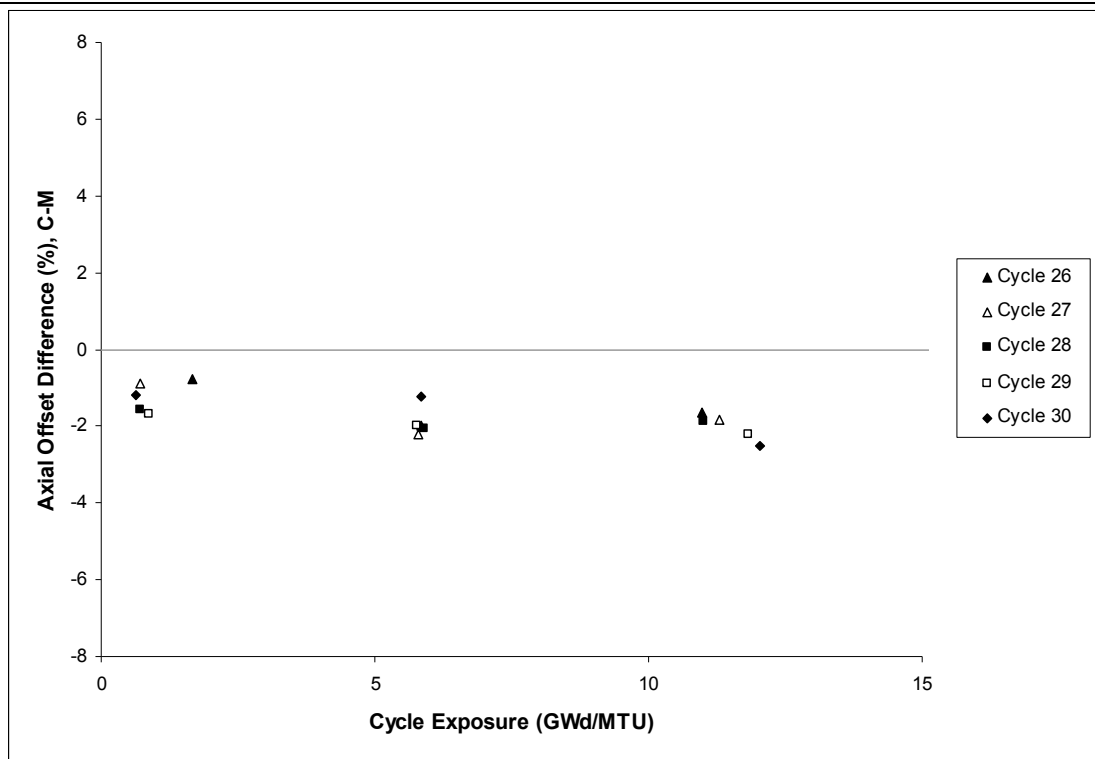


Figure 45-G1-1: AO Comparisons

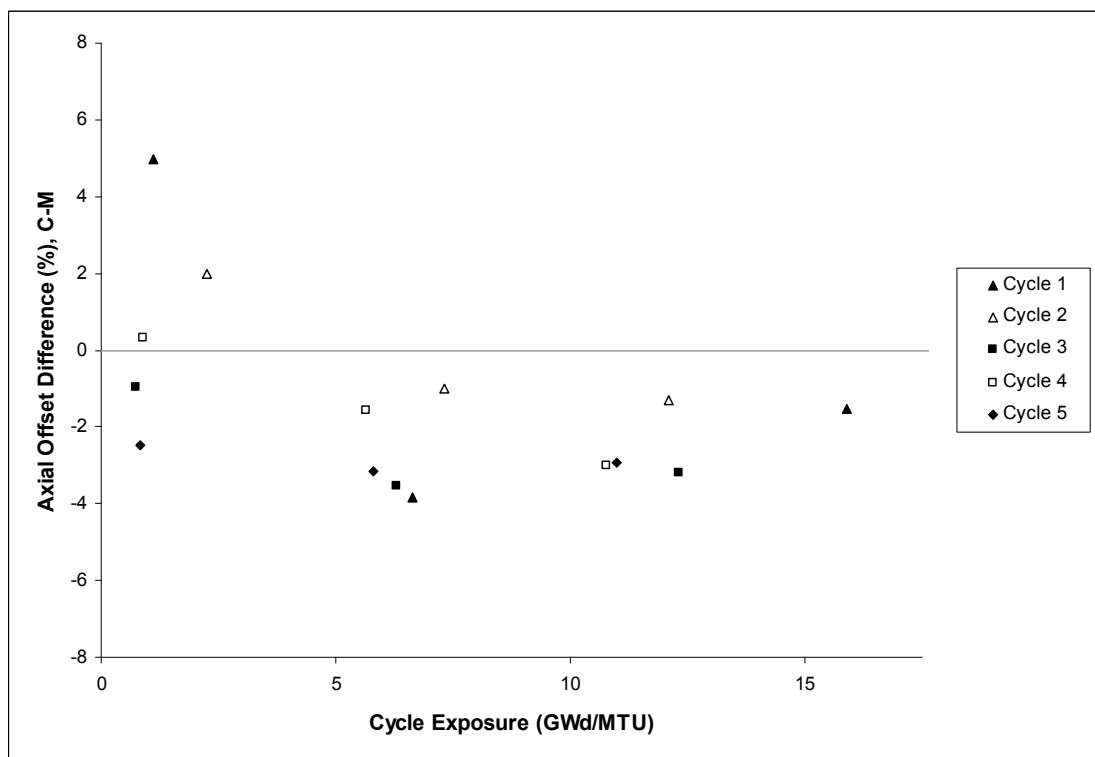


Figure 45-G2-1: AO Comparison

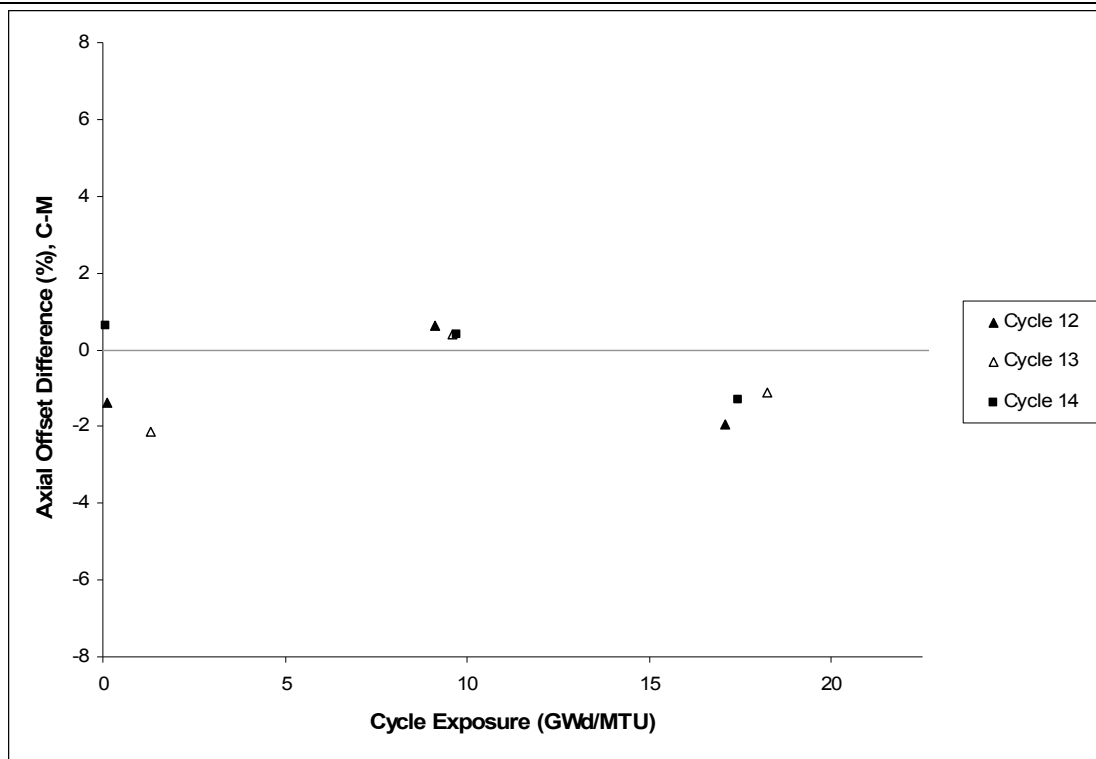


Figure 45-S1-1: AO Comparisons

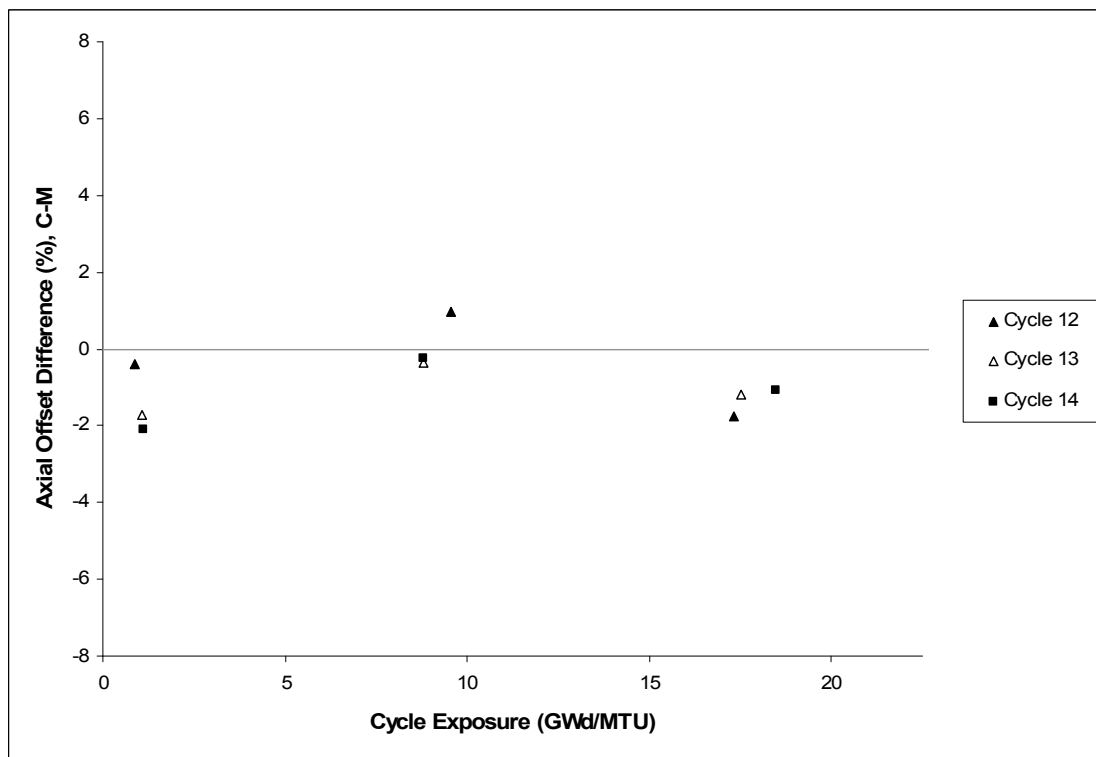


Figure 45-S2-1: AO Comparisons

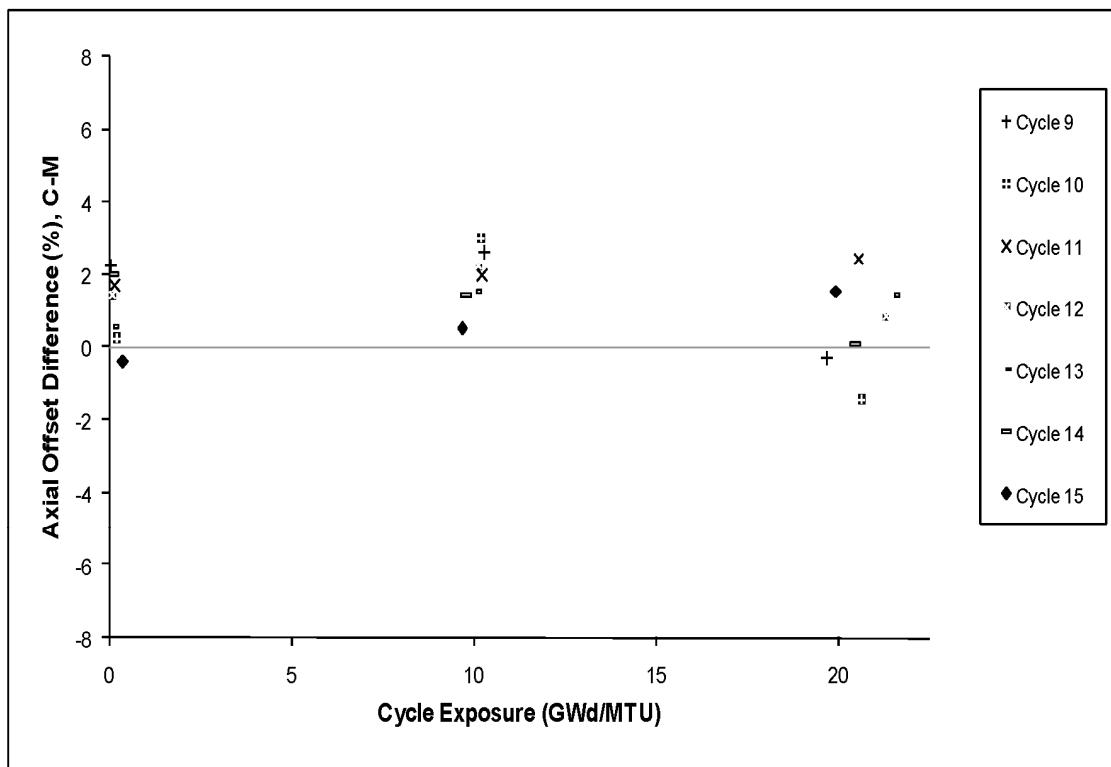


Figure 45-T1-1: AO Comparisons

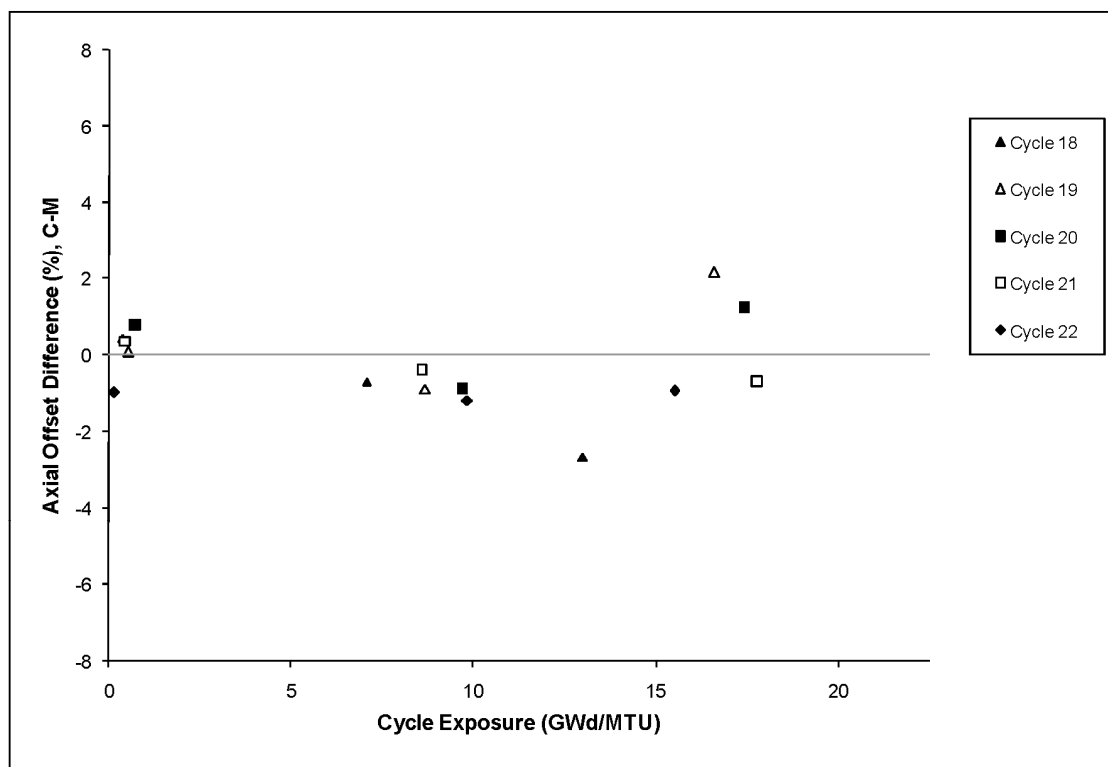


Figure 45-V1-1: AO Comparisons



**RAI 46** The report states that plant G1 has a 2% bias for the peak assemble power comparison. The context of this statement is the discussion of grid depressions (or lack thereof). However, analysis of the average axial power plots for G1 indicates this deviation is possibly due to an increased difference in core average axial offset and not the lack of compensation of an explicit grid flux depression effect. [Page 12-12]

**AREVA Response:**

The context of the discussion on Page 12-12 is that the bias for plant G1 is higher than the expected Zr grid bias. The cause of the larger bias was not identified in the topical. The report identified what would be done if a larger bias was found for a plant that implemented these uncertainties with ARCADIA. It states, "The G1 plant does not currently use this uncertainty method but if it did, either the reason for the higher bias would need to be resolved or a higher grid bias would be applied." From a visual inspection of the core average axial power comparisons, the increased bias above the grid bias in plant G1 could be a difference in axial offset prediction. Any consistent axial offset shift could cause an increase in the bias and would always be super imposed upon the grid bias. On an analytical basis, the "lack of compensation of an explicit grid flux depression effect" should always result in an underprediction of the peak of the magnitudes as stated. In practice, there could be other effects that add or subtract from this grid effect.

**RAI 47** Section 12 in general lacks equations describing the uncertainty analysis process and statistical calculations. Please provide equations for the calculated total inferred and NRF uncertainties. Define each contributing factor to the total uncertainty such as observed variance and measured variance. Although, the standard definitions for FDH and FQ are assumed, these terms are not defined in the report explicitly, please also provide definitions for these terms. It would also be helpful if the references or relevant sections of the references 12.6-1 and 12.6-2, 12.6-6 and 12.6-7 can be provided [Page 12-1].

### AREVA Response

The relevant sections of the requested references are provided. The equations and methods are provided for continuity.

#### Definition of Terms

Although typically the Fdh and Fq terms typically represent a single maximum value for the core, this same term is defined for each assembly.

Fdh(n) = The enthalpy rise hot channel factor is the ratio of the integral of the linear power along the rod with the highest integrated power in assembly n to the average rod power in the core.

Fq(n) = The heat flux hot channel factor is the ratio of the maximum local heat flux on the surface of a rod in assembly n to the average rod heat flux in the core.

#### Statistical Methodology

For a particular uncertainty parameter, whether for inferred measured uncertainties or calculated power uncertainties, the basic process and equations are the same. The only difference would be in the definition of the global term which is the value of the plant database contribution(s). For illustration, the Fq uncertainty calculations for the (1) INPAX-W reconstruction methodology and (2) the calculated NRF will be presented that are used to generate Tables 12.3.1-3 and 12.4.1-4. Two approaches are considered to bound either the distribution assuming normality or the actual distribution with nonparametric statistics.

#### Databases:

As explained in the topical there are three databases, the Criticals data (a local peaking component), the Multi-assembly data (a local peaking component), and the plant data (a global peaking component). The equations used for each are described below.

B&W Criticals Database: 183 data points from 6 critical experiments (CX).

[

]

Colorset/Multi-Assembly (MA) Database: 6766 data points

There are 6765 degrees of freedom. [

]

Plant Database

The plant data has different definitions depending upon whether it is an inferred measured error or a calculational error (NRF). These different definitions are described below for Fq and are similar for Fdh.

INPAX-W Fq

[

]

[

]

NRF Fq

[

]

### Uncertainty Assuming Normality

In this section, the equations are given for the determination of the uncertainties from the three error components for the inferred measured uncertainty for Fq. The IP subscript is used for the inferred global errors. For the NRF Fq uncertainty, the process is repeated by substituting subscript CP for IP. For Fdh, the process is repeated with observed plant data for Fdh in place of Fq.

The one-sided 95/95 tolerance limits can be determined from the above relative standard deviations assuming that the errors are normally distributed. The uncertainty factors for the inferred measured powers are calculated from the equation  $(1 + x + K \cdot S_0)$ . The one-sided 95/95 tolerance factor, K, is a function of the number of degrees of freedom associated with the relative standard deviation.

Where:

$x$  = The absolute value of the sum of the negative means. (A positive mean is conservatively set to zero.)

The total variance ( $S_0^2$ ) is defined as:

$$S_0^2 = a_{CX} S_{CX}^2 + a_{MA} S_{MA}^2 + a_{IP} S_{IP}^2$$

[ ]

The degrees of freedom (df) is calculated from Satterthwaite's formula, given below:

$$df_0 = S_0^4 / (a_{CX}^2 S_{CX}^4 / df_{CX} + a_{MA}^2 S_{MA}^4 / df_{MA} + a_{IP}^2 S_{IP}^4 / df_{IP})$$

The one-sided tolerance factor,  $K^1$ , may be computed by:

$$K = \frac{z_p + \sqrt{z_p^2 - ab}}{a}$$

where

$$a = 1 - \frac{z_\gamma^2}{2(n-1)}$$

$$b = z_p^2 - \frac{z_\gamma^2}{n}$$

For a 95/95 tolerance factor, both  $z_\gamma$  and  $z_p$  are equal to 1.645.

<sup>1</sup> The equation for the tolerance confidence limit (K) in References 12.6-2 and 12.6-6 contains a typo. The correct equation for K has been used in the results and is provided in this response.

### Uncertainty Examples assuming Normality

The results are provided for both the inferred measurement error for INPAX-W Fq and the NRF for Fq (calculational error).

#### INPAX-W Fq

[

]

#### NRF Fq

[

]

### Uncertainty Assuming Nonparametric

[

]

[ ]

Reference: “Experimental Statistics”, Mary Gibbons Natrella, US Department of Commerce,, National Bureau of Standards Handbook 91, Issued August 1, 1963.

### Non-Parametric Uncertainty Examples

The results are provided for both the inferred measurement error for INPAX-W Fq and the NRF for Fq (calculational error).

#### INPAX-W Fq

[

]

#### NRF Fq

[

]

### Uncertainty

The uncertainty reported is the higher of the Normal or Non-Parametric uncertainty.

**RAI 48** As explained in section 12.1, the inferred uncertainties are based on the ability of ARCADIA to predict the powers in uninstrumented assemblies. Later in section 12.3 the total inferred uncertainties are defined as the sum of the power uncertainty at the uninstrumented assemblies plus the local uncertainties which include the pin power uncertainties from APOLLO2-A and the pin power reconstruction uncertainties from ARTEMIS-APOLLO2-A comparisons. However, it is not clear how the ARCADIA simulation of the plant cycles are used in this process? [Page 12-7]

**AREVA Response:**

References 12.6-1, 12.6-2, and 12.6-6 include detailed descriptions of three different measurement processing systems that include how the core neutronic simulator is used to generate a full core power distribution map from instrumented locations. To perform this calculation, a neutronic core simulator is needed to produce predicted signals, relationships between those signals and power in the assembly for both the measured and unmeasured locations. ARCADIA is used to generate this information for these plants and cycles. In a general sense, the INPAX-W, INPAX-CE, and MEDIAN methods use the calculated power shape to propagate the differences seen between the measured and predicted powers in the measured locations to the unmeasured locations. The global error component of the inferred uncertainty has not been greatly affected by the evolution of core simulators which indicates that the error is dominated by the measurement errors.



**RAI 49** Three measurement systems, INPAX-W, INPAX-CE and MEDIAN AMS, are evaluated for the inferred power distribution uncertainties. The ARCADIA application range statement should mention these systems specifically [Page 13-1].

**AREVA Response:**

The sentence “The three measurement systems evaluated are the INPAX-W system, the INPAX-CE system (also known as INPAX-II), and the MEDIAN AMS.” from page 12-7 does not fully describe the process. There are three types of physical measurement systems, moveable incore, Rh fixed incore, and Aeroball detector systems. Each of these systems uses processing algorithms/software to convert the raw measured data to measured power distributions. The algorithms are the INPAX-W system, the INPAX-CE system (also known as INPAX-II), and the MEDIAN AMS systems, respectively.

The following wording is proposed to be added in the middle of section after the phrase “Framatome designed reactors.” in section 13.1 in the approved version of the topical report.

*These benchmarks include uncertainty verification for plants that use moveable incore, Rh fixed incore, and Aeroball incore detectors.*

The following wording is proposed to replace section 13.3 in the approved version of the topical report.

*AREVA will continue to monitor its methods with respect to current cycle designs for its licensing applications. Prior to licensing a new contract, AREVA will evaluate at least three cycles of data relative to these criteria prior to licensing the first cycle with AREVA fuel with ARCADIA. This includes verification of their measurement uncertainties and/or calculational uncertainties by using the appropriate method presented in Section 12.*

**RAI 50** Please explain how the FSA component of the uncertainty is calculated in Section 12.3.2 [Page 12-9].

**AREVA Response:**

The FSA uncertainty component is calculated in a similar manner as the 2D relative power uncertainty component is calculated for the INPAX-W reconstruction methodology. Rather than being the average relative power over the entire length of the fuel (INPAX-W), FSA represents the average relative power over the 4 (for CE reactors) axial heights of the fixed incore detectors.

At each of the 4 axial detector levels, the detector signals are converted to powers and expanded radially to all assembly locations. These 4 x N (# of assy.) powers are then normalized to an average value of 1.0. For a given assembly the FSA term is the average of the 4 normalized values (since all detector lengths are the same). The process to determine the uncertainty of FSA is as described in the first part of Section 12.3. In the 2nd paragraph of Section 12.3, the sentence could read “For a given parameter of interest, e.g. FSA, the methodology...”.

**RAI 51** In section 12.3.2 FR and FZ components of the uncertainty analysis for plant C (INPAX-CE) are calculated using S1, S2 and A plant detector measurements (INPAX-W system). Please justify calculating FR and FZ uncertainties in INPAX-W system and using them in INPAX-CE system [Page 12-9]

**AREVA Response:**

Definitions:

FSA = Average segment power

FR = Ratio of average assembly power to average segment power. The average assembly power is obtained by integrating the power over the entire length of the assembly.

FZ = Ratio of the peak planar power in an assembly to the assembly relative power.

Discussion

The FR and FZ uncertainties represent the ability of the INPAX-CE methodology to reconstruct detailed axial information from the coarse measured information available in the fixed incore detector system. [

[

]

**RAI 52** Since the Inconel grids are eliminated from uncertainty analysis due to large grid depressions and only used in the old fuel assemblies, it should be mentioned in the application statement [Page 12-13].

**AREVA Response:**

The qualification of ARCADIA is not impacted by the exclusion of the peak statistics for Inconel grids. Rather, the uncertainty section identifies that grid type and other aspects of plant types could affect the bias of the peak prediction and needs to be addressed for each plant and grid type. This is evidenced by both the Inconel grid discussion and the bias discussion on the G1 plant on page 12-13. The process to define such biases occurs in the implementation phase of the code or fuel contract and could be a simple adjustment of the uncertainty or peaking allowances used in the safety analyses. The following wording is proposed to be added at the end of the replacement for section 13.3 from the response to RAI 49 and included in the approved version of the topical report.

*During the verification of uncertainties, any peaking biases due to grid type or other plant effects will be quantified and accounted for in the uncertainties and/or peaking allowances in the licensing calculations.*

**RAI 53** Section 12.3 states that “data reduction and statistical treatment techniques” are used to drive one-sided 95/95 relative uncertainties. Please provide more information about these techniques [Page 12-7].

**AREVA Response**

The data reduction techniques are listed in the text following the statement. The statistical treatment techniques are those defined in the references which are described in response to RAI 47

**RAI 54** For multi assembly calculations in Section 12.2.2, provide lattice description (type, enrichment) and lattice combinations used in the 20 multi assembly calculations.

**AREVA Response:**

No response is provided for this RAI. It is expected that this RAI will not be part of the final set of requests.

**RAI 55** Figures 12.2.2-1 through 12.2.2-6 show burnable poison location with no data. Does it mean the relative difference in those pin locations were rejected because of their low power?

**AREVA Response:**

No, these pin locations are guide tube locations filled with rods containing only Al<sub>2</sub>O<sub>3</sub>-B<sub>4</sub>C pellets and have no fission power.



**RAI 56** Provide peak to peak pin power relative difference statistics (maximum, average, std deviation) and peak pin power location comparisons for APOLLO2 validation in Section 6.

### AREVA Response

Peak to peak pin relative difference statistics are presented in Table 56-1

Peak pin power location comparisons for APOLLO2-A validation are provided in the response to RAI 15 in Tables 15-1 through 15-5.

**Table 56-1: Predicted and Measured Peak Statistical Analysis**

(C/M-1) in %		Average in %	Standard Deviation in %
Max	Min		

**RAI 57** The report states that 15x5 and 16x16 fuel lattices from B&W 1980 criticals were used in local peaking factor uncertainties in Section 12.2.1. However, the B&W 16x16 fuel lattice criticals are not mentioned in APOLLO2 validation in Section 6.2.1.1. Why is this set eliminated from the statistics in APOLLO2 validation?

### **AREVA Response**

The 16x16 fuel lattices from the B&W 1980 experiments are included in the statistics of the APOLLO2-A validation in Section 6.2 of the Topical Report as well as the local peaking factor uncertainties in Section 12.2. The sentence in Section 6.2.1.1 in question is confusing because of a typographical error. The sentence should read as follows:

The geometrical pin arrangement was modeled after realistic PWR reactors, with 14x14 Siemens, 15x15 B&W, 16x16 Combustion Engineering, and 17x17 Westinghouse type assembly designs.

This change will be made to the approved version of the Topical Report.

**RAI 58** It is not clear why statistics of criticals other than a portion of B&W 1980 experiments are eliminated from local uncertainty analysis in Section 12. The report states that B&W 1980 criticals are more recent and found to have a low measurement uncertainty. If that is the justification for selecting B&W 1980 criticals, please justify elimination 14x14 and 17x17 lattice results from the uncertainty analysis.

### AREVA Response

To answer this request, first the rationale for selecting the B&W 1980 criticals is provided and the other critical results are reviewed. The B&W 1980 criticals have been used in the past for the validations performed in References 12.6-1, 12.6-2, 12.6-5, and 12.6-6. Also, Reference 12.6-7 uses these experiments in its validation for Gad fuel. To remain consistent with past code verifications, these criticals are used. Core XI Loading 2 from Reference 6.5-1 is the identical critical experiment to Core 1 from Reference 12.6-4 except that Core 1 contains a fixed incore detector in the central water hole. The critical facility, the fuel pins, and the measurement apparatus description are the same. In reference 12.6-4 for Core 1, the measurement description includes two other techniques not mentioned in Reference 6.5-1.

- 1) The fuel pins were rotated during the gamma counts to remove any gradient effects.
- 2) Three distinct reactor runs were counted for each experiment. Taking three counts from the same irradiation would take three times as long and would reduce counting efficiency of the last pins sampled.

The measurement error for Core XI Loading 2 is 1.0% and for Core 1 is 0.3%. This significant uncertainty reduction is likely the result of rotating the pins to obtain a pin average value. This is the basis for the statement in the topical, "These experiments are some of the most recent experiments and are found to have a low measurement uncertainty and are sufficient to determine the accuracy of APOLLO2-A to predict pin powers within the assembly with no burnup."

The other critical measurements are reviewed for applicability and the B&W 1980 criticals are shown to be representative of all the appropriate critical results. The coverage area for the pin power uncertainty is defined as the central assembly. The reported data for the B&W-1980 critical experiments are for the central assembly region only. The RMS comparisons for the KRITZ (14x14) and EPICURE (17x17) critical experiments are based on all the measured pins in the entire core not just the central assembly zone. The statistics for the entire core would include the local and global component of the uncertainty which is not a consistent comparison. In addition, the KRITZ, several of the EPICURE, and CAMELEON (17x17) experiments do not measure the entire central assembly zone so it does not provide an entire map of the assembly pin powers and is not consistent with the B&W-1980 critical experiments. The statistics

(mean and standard deviation) for the central assembly for these experiments are listed in Table 58-1.

When these cases are examined on a similar basis, B&W 1980 critical experiments are now more typical of the other comparisons. The standard deviations for the critical experiments typical of PWR configurations are consistent with the statistics for all the configurations from the B&W 1980 critical experiments. Those values that are significantly higher are configurations that are not typical of PWR conditions. Even for those configurations outside typical PWR conditions, the standard deviation remains less than or equal to 1.6 which illustrates the robustness of the APOLLO2-A solution in extreme conditions. Those configurations outside PWR conditions are the EPICURE UH1.2 / 50% void and EPICURE UH1.2 / 100% void (PWRs even in accident conditions do not approach 50-100% voids), and the EPICURE UH1.4 SSAIC (peaks also do not occur in assemblies that contain control rods). The CAMELEON 13G, 12G, and 5G cases are under review. These experiments are being reviewed for applicability. They have no water holes and have different structural materials that may affect the measured definition. In addition, the documentation does not state whether the pins were rotated. If the applicable critical benchmarks and the CAMELEON suspect configurations are statistically combined, the standard deviation is [ ] which is the same as combined B&W 1980 critical experiments. Based on this comparison, the B&W 1980 critical experiments are representative of the appropriate test results and the uncertainty determination remains valid.

In addition, these results show that the predictive capability of APOLLO2-A is not affected by the central fuel lattice type.

**Table 58-1. Statistics for Central Assembly Region**

Configuration	Mean	$\sigma$	Number of Pins measured in central assembly / Number of measured pins for the RMS in section 6.2.2.2	Assembly Type / Number of unique pins in an 1/8 assembly
<b>Typical PWR Configurations</b>				
B&W 1980 Core 1			32 / 32	15x15 / 32
B&W 1980 Core 5			32 / 32	15x15 / 32
B&W 1980 Core 12			32 / 32	15x15 / 32
B&W 1980 Core 14			32 / 32	15x15 / 32
B&W 1980 Core 18			32 / 32	16x16 / 32
B&W 1980 Core 20			32 / 32	16x16 / 32
<b>All B&amp;W 1980 Criticals</b>			<b>32 / 32</b>	
KRITZ			12 / 20	14x14 / 25
EPICURE UH1.2			8 / 29	17x17 / 39
EPICURE UH1.2 / 30% void			29 / 37	17x17 / 39
EPICURE UH1.4			39 / 71	17x17 / 39
EPICURE UH1.4 Pyrex			39 / 75	17x17 / 39
CAMELEON 25GT_12GD			15 / 15	17x17 / 39
<b>Measurements Under Review</b>				
CAMELEON 13GD			15 / 15	17x17 / 39
CAMELEON 12 GD			15 / 15	17x17 / 39
CAMELEON 5GD			13 / 13	17x17 / 39
<b>Outside PWR Application</b>				
EPICURE UH1.2 / 50% void			30 / 37	17x17 / 39
EPICURE UH1.2 / 100% void			27 / 30	17x17 / 39
EPICURE UH1.4 SSAIC			39 / 75	17x17 / 39

**RAI 59** Results of the B&W 1980 criticals do not exhibit the typical results from the other criticals. If a selective set of criticals are intended to be used for the uncertainty analysis, then a more representative set of the typical pin power uncertainties should be selected.

#### **AREVA Response**

See the response to RAI 58.

**RAI 60** Please include the measurement uncertainties for the criticals in Chapter 6, Section 12.2.1 and spent fuel isotopic measurement uncertainties in the relevant chapters and tables.

## AREVA Response

### **Critical Experiments**

The measurement uncertainties for the critical experiments consist of uncertainties related to the reactivity and uncertainties related to the fission rate distributions.

The uncertainty related to the reactivity (k-effective) is difficult to assess properly because it is the product of several measurement uncertainties (boron concentration, buckling measurement, approach to criticality, etc.) and engineering uncertainties (fuel composition, pin dimensions, etc).

The Commissariat à l'Energie Atomique (CEA) has, however, performed several sensitivity calculations for the EPICURE and CAMELEON critical configurations considering each of the related uncertainties. The result of this study has shown that the experimental uncertainty (which is the combination of both measurement and engineering uncertainties) for UO<sub>2</sub> fueled critical experiments is [ ]

There was no evaluation of the uncertainty on reactivity given for the Babcock and Wilcox, and KRITZ-KWU configurations. However, because of the similar nature of the experimental configurations (array size, pin size, fuel composition, etc), it can be assumed that the EPICURE experimental uncertainty is valid also for the Babcock and Wilcox, and KRITZ-KWU configurations.

The uncertainty related to the fission rate measurements is reported differently for each experimental program.

For the Babcock and Wilcox 1980's experiments, the individual rod scan data is provided for each experimental run in the experimental report. This allows the uncertainty related to using the given fission rate values to be assessed statistically. For the Babcock and Wilcox 1970's experiments, the standard deviation is given for each rod based on "two or more measurements." It is not clear from the report if the same number of measurements were used for each rod and/or if this was two or more experimental runs or two gamma scanning measurements. From these values, however, an overall uncertainty on the fission rate measurements is approximated for each configuration.

For the EPICURE, CAMELEON, and KRITZ-KWU experiments, the uncertainties reported for the fission rates are given as a single value for all configurations.

The uncertainties related to the fission rate measurements for the Babcock and Wilcox 1970's and 1980's experimental fission rate measurements are presented in Table 60-1.

The experimental uncertainties for the EPICURE and CAMELEON experiments are provided by CEA and include both the measurements and the engineering uncertainties within the experiments. This experimental uncertainty is estimated at [ ] for EPICURE and CAMELEON.

For the uncertainty on the KRITZ-KWU configuration, it is unclear whether the stated uncertainty on the fission rates of [ ] is a pure measurement uncertainty or whether it is an experimental uncertainty. Due to the elevated value compared to the other experimental programs, AREVA considers it as an experimental uncertainty.

## Spent Fuel Analysis

There are two types of uncertainties related to the spent fuel isotopic analyses:

- Uncertainties associated with the modeling of the irradiation (modeling uncertainties)
- Uncertainties associated with the chemical analyses of a sample (measurement uncertainties)

It is important to consider the modeling uncertainties as well as the measurement uncertainties because, for some isotopes, the modeling uncertainties can be significant in comparison to the measurement uncertainties.

### Modeling Uncertainties

The different origins of the modeling uncertainties are the following:

- Engineering uncertainties (especially the initial fuel composition)
- Operational uncertainties
  - Evaluation of the fuel temperature during irradiation
  - Evaluation of the moderator temperature during irradiation
  - Power history
  - Boron letdown
  - Surrounding assemblies and water gap width

Sensitivity studies conducted by CEA estimated the Modeling Uncertainties for U, Pu, Np, Am, and Cm isotopes and are presented in Table 60-2 for UOX fuel as a function of burnup ( $1\sigma$ ), and in Table 60-3 for MOX fuel as a function of burnup ( $1\sigma$ ).

The similar combined modeling uncertainties for fission products or for other fuel types like ERU, or UO<sub>2</sub>- Gd<sub>2</sub>O<sub>3</sub> are not available.



---

### Measurement Uncertainties

The second type of uncertainties concern the process of the chemical analyses of an irradiated sample.

[

]

[

]

**Table 60-1: Measurement Uncertainties for the Babcock and Wilcox Fission Rate Distributions**

Configuration	Measurement Uncertainty (1 $\sigma$ )
Core 1	
Core 5	
Core 12	
Core 14	
Core 18	
Core 20	
XI_2	
XI_6	
XI_8	
XI_11	

**Table 60-2: Isotopic Burnup Analysis –  
 Modeling Uncertainties for UOX (in %)**

Burnup	20 GWd/t	40 GWd/t	50 GWd/t	60 GWd/t	70 GWd/t
U234/U238					
U235/U238					
U236/U238					
Pu238/U238					
Pu239/U238					
Pu240/U238					
Pu241/U238					
Pu242/U238					
Np237/U238					
Am241/U238					
Am242m/U238					
Am243/U238					
Cm242/U238					
Cm243/U238					
Cm244/U238					
Cm245/U238					
Cm246/U238					
Cm247/U238					

**Table 60-3: Isotopic Burnup Analysis –  
Modeling Uncertainties for MOX (in %)**

Burnup	50 GWd/t	60 GWd/t
U234/U238		
U235/U238		
U236/U238		
Pu238/U238		
Pu239/U238		
Pu240/U238		
Pu241/U238		
Pu242/U238		
Np237/U238		
Am241/U238		
Am242m/U238		
Am243/U238		
Cm243/U238		
Cm244/U238		
Cm245/U238		
Cm246/U238		
Cm247/U238		

**Table 60-4: Isotopic Burnup Analysis –  
 Malibu Measurements Uncertainties (in %)**

Isotope	UOX	MOX	Isotope	UOX	MOX
U234/U238			Ce144/U238		
U235/U238			Nd142/U238		
U236/U238			Nd143/U238		
Np237/U238			Nd144/U238		
Pu238/U238			Nd145/U238		
Pu239/U238			Nd146/U238		
Pu240/U238			Nd148/U238		
Pu241/U238			Nd150/U238		
Pu242/U238			Pm147/U238		
Pu244/U238			Sm147/U238		
Am241/U238			Sm148/U238		
Am242m/U238			Sm149/U238		
Am243/U238			Sm150/U238		
Cm242/U238			Sm151/U238		
Cm243/U238			Sm152/U238		
Cm244/U238			Sm154/U238		
Cm245/U238			Eu151/U238		
Cm246/U238			Eu153/U238		
Cs133/U238			Eu154/U238		
Cs134/U238			Eu155/U238		
Cs135/U238			Gd155/U238		
Cs137/U238					

**Table 60-5: Malibu Isotopic Analyses –  
 Measurements comparisons between laboratories (in %)**

<b>Burnup</b>	<b>UOX Sample (PSI / CEA) - 1</b>	<b>MOX Sample (PSI / CEA) - 1</b>	<b>MOX Sample (SCK / CEA) - 1</b>
U234/U238			
U235/U238			
U236/U238			
Pu238/U238			
Pu239/U238			
Pu240/U238			
Pu241/U238			
Pu242/U238			
Np237/U238			
Am241/U238			
Am242M/U238			
Am243/U238			
Cm242/U238			
Cm243/U238			
Cm244/U238			
Cm245/U238			
Cm246/U238			
Nd142/U238			
Nd143/U238			
Nd144/U238			
Nd145/U238			
Nd146/U238			
Nd148/U238			
Nd150/U238			
Cs133/U238			
Cs134/U238			
Cs135/U238			
Cs137/U238			
Pm147/U238			
Sm147/U238			
Sm148/U238			
Sm149/U238			
Sm150/U238			
Sm151/U238			
Sm152/U238			
Sm154/U238			
Eu151/U238			
Eu153/U238			
Eu154/U238			
Eu155/U238			

**RAI 61** In Table 12-5.1 Inferred FDH and FQ uncertainties for various power reconstruction methods are compared to the uncertainty criteria. Although it is not clear in the report, based on the references it assumed that these criteria are based on the uncertainties of the previous code systems. Please provide justification for these criteria.

**AREVA Response:**

For the inferred uncertainty verification, the criteria are based on the measurement uncertainty and not on a previous code system. As stated on page 12-6, "Hence, the inferred uncertainty includes the effects of both calculated and measured powers and results in an uncertainty that can be compared to the measurement system uncertainty." The inferred uncertainties are used to estimate the measurement system uncertainty for FΔH and FQ in the specific plant Technical Specifications using AREVA methods. The criteria provided in this Topical are the typical measurement uncertainties encountered for each type of measurement system. Because there can be plant to plant variations of these uncertainties, the process to implement AREVA fuel and methods validates these uncertainties on a plant by plant basis as noted in Section 13.3.

This method has been used by AREVA to validate the application of the INPAX-W, INPAX-CE, MEDIAN, and neutronic core simulators to be used for plant Technical Specification Monitoring. For example, Section 3.3 of the Technical Evaluation Report of the INPAX-W method in Reference 12.6-2 contains the following statement, "It is concluded that the SPC determination of the EMF-93-164(P) uncertainty limits provides a reliable estimate of the INPAX-W calculational uncertainty and is therefore acceptable."

For Nuclear Reliability Factors in Section 12.4 which are not the same error estimates as the inferred errors, the criteria are obtained from a previous code package (Reference 12.6-7) and are currently used in several plants for licensing calculations. Section 12.4 demonstrates that continued use of these uncertainties is conservative for ARCADIA.



**RAI 62** TYPO: Subscripts in Table 6.2-5 are sized inconsistently (Gd3O3). [Page 6-7].

**AREVA Response:**

This issue will be fixed in the approved version of the topical report.

**RAI 63** The transverse-integrated precursor concentration is denoted as  $\xi$  above and below Equation 3-27 instead of  $\varsigma$  [Page 3-10]

**AREVA Response:**

This issue will be fixed in the approved version of the topical report.

**RAI 64** Zircaloy is misspelled (as Zircalloy). [Page 6.12]

**AREVA Response:**

This issue will be fixed in the approved version of the topical report.